

**Development of Antimicrobial Thin-Film Composite Forward Osmosis Membranes by  
Using Silver Nanoparticles and Graphene Oxide Nanosheets**

Adel Soroush

A Thesis

In

The Department of

Building, Civil and Environmental Engineering

Presented in partial fulfillment of the requirement

For the Degree of Master of Applied Science (Civil Engineering) at

Concordia University

Montreal, Quebec, Canada.

September 2015

© Adel Soroush, 2015

**CONCORDIA UNIVERSITY**  
**School of Graduate Studies**

This is to certify that the thesis prepared

By: Adel Soroush

Entitled: Conductive Ultrafiltration Membrane Fabrication via a Novel Vacuum-Assisted Layer-by-Layer Assembly of Functionalized Carbon Nanotubes

and submitted in partial fulfillment of the requirements for the degree of

**Master of Applied Science (Civil Engineering)**

complies with the regulations of the University and meets the accepted standards with respect to originality and quality.

Signed by the final Examining Committee:

\_\_\_\_\_ Chair  
*Dr. Catherine Mulligan*

\_\_\_\_\_ Examiner  
*Dr. Fuzhan Nasiri*

\_\_\_\_\_ Examiner  
*Dr. Ali Dolatabadi*

\_\_\_\_\_ Supervisor  
*Dr. Saifur Rahaman*

Approved by \_\_\_\_\_  
*Dr. Fariborz Haghighat*

2015 \_\_\_\_\_ *Dr.* \_\_\_\_\_ *Amir* \_\_\_\_\_ *Asif*

## **Abstract**

# **Development of Antimicrobial Thin-Film Composite Forward Osmosis Membranes by Using Silver Nanoparticles and Graphene Oxide Nanosheets**

Adel Soroush

Membrane filtration has been gaining great attention in water and wastewater treatments processes because of its high-performance efficacy, modular design, and smaller physical footprint. Thanks to special membrane materials and structure, osmosis processes are widely used in water desalination and water reuse processes. Aside from their high performance of osmosis processes, they inevitably do suffer from membrane fouling and biofouling during treatment processes that significantly decrease water treatment performance and final product quality.

Two different biocidal nanomaterials and their combinations were used in this project for the modification of membrane surfaces and the development of biocidal membranes: silver nanoparticles (AgNPs) and graphene oxide nanosheets (GO).

GO/Ag nanocomposite functionalization of TFC FO membranes provides an efficient antimicrobial surface that has more desirable characteristics than those with only GO or Ag NPs. Also, the higher hydrophilicity of the resulting membranes, the low material cost, and the ease of preparation (dip coating method) offer a more efficient approach than other modification methods. In comparison to the formation of AgNPs on pristine TFC FO membranes, the in situ formation of AgNPs on the GO-modified membrane surface resulted in greater silver loading, higher and longer lasting ion-release, and more effective antimicrobial properties.

The regeneration of GO-Ag-modified membranes was also examined. Modified membranes were kept in DI water for seven days to emulate depletion. AgNPs were successfully formed using an in-situ procedure on the surface of the membranes, identical to the initial membrane formation. Results show that membrane hydrophilicity and its antimicrobial ability decreased after the releasing process, however, the regeneration process allowed the membrane

to nearly regain the properties seen in the freshly modified membrane. The simple regeneration method developed in this study will allow on-site modification and regeneration of different types of industrial membrane modules (hollow fiber, spiral wound).

## **Acknowledgments**

I would like to acknowledge and extend my heartfelt gratitude to my supervisor, Dr. Saifur Rahaman, for granting me an opportunity to pursue my graduate studies at Concordia University, as well as for his continuous inspiration and guidance in this research. I really appreciate his vast arena of knowledge, his expertise and his patience during correcting my writing. His encouraging words always cheered me up in difficult times of problem solving.

## **Dedication**

To my lovely parents for their love and support.

## Table of Contents

Table of Contents .....	vii
List of Figures .....	x
List of Tables .....	xii
List of Abbreviations .....	xiii
1 INTRODUCTION .....	1
1.1 Motivation .....	1
1.1.1 Water Scarcity throughout the World .....	1
1.2 Osmosis-Based Membrane Processes for Water Desalination and Reuse .....	2
1.3 Fouling and Biofouling Mitigation through Surface Modification .....	7
1.4 Biocidal Nanomaterials .....	7
1.4.1 Silver Nanoparticles .....	7
1.4.2 Graphene Oxide Nanosheets .....	13
1.5 Objective .....	19
1.6 Organization of Dissertation .....	19
2 SURFACE MODIFICATION OF THIN FILM COMPOSITE FORWARD OSMOSIS MEMBRANE BY SILVER-DECORATED GRAPHENE-OXIDE NANOSHEETS .....	20
2.1 Introduction .....	20
2.2 Materials and Methods .....	22
2.2.1 Materials .....	22
2.2.2 Synthesis and Characterization of AgNPs and GO/Ag Nanocomposites .....	22
2.2.3 Surface Modification and Characterization of TFC FO Membranes .....	23
2.2.4 Antimicrobial Activity of GO/Ag Functionalized Membranes .....	26
2.2.5 Silver Release Experiments .....	27

2.3	Results and Discussion.....	27
2.3.1	Successful Graphene Oxide/ Silver Nanocomposite Synthesis Confirmed by UV-Vis, TEM, TGA and XRD Analyses .....	27
2.3.2	Graphene Oxide/ Silver Nanocomposites were Covalently Bonded to the Surface of the TFC Polyamide Membrane.....	28
2.3.3	Membrane Transport Properties were not Significantly Affected by GO/Ag Functionalization.....	31
2.3.4	The Functionalized Membrane Exhibited Strong Antimicrobial Activity .....	33
2.3.5	Silver Ion Release Behavior was Different for Composite and only AgNP Modified Membranes.....	36
2.4	Conclusions .....	36
2.5	Supporting Information.....	38
2.5.1	Materials and Methods.....	38
2.5.2	Nanoparticles and Nanocomposites Characterization .....	39
3	IN SITU SILVER DECORATION ON GRAPHENE OXIDE-TREATED THIN FILM COMPOSITE FORWARD OSMOSIS MEMBRANES: BIOCIDAL PROPERTIES AND REGENERATION POTENTIAL.....	47
3.1	Introduction .....	47
3.2	EXPERIMENTAL .....	48
3.2.1	Materials .....	48
3.2.2	Surface modification with GO nanosheets .....	48
3.2.3	In situ Ag NP formation on GO modified membranes.....	49
3.2.4	Membrane characterization.....	49
3.2.5	Anti-microbial properties of modified membranes.....	50
3.2.6	Loading, stability and release of Ag NPs.....	50
3.2.7	Regeneration of Ag NPs on the membrane surfaces .....	50

3.3	Results and Discussion.....	51
3.3.1	Ag NPs were formed successfully and their loading increased in the presence of GO nanosheets .....	51
3.3.2	Membrane surface hydrophilicity changed after modification while performance remained unchanged .....	53
3.3.3	Bacterial growth inhibition increased in the presence of GO nanosheets .....	56
3.3.4	Ag NP regenerated successfully on the surface of GO-Ag-modified membranes .	58
3.4	Conclusion.....	60
3.5	Supporting Information .....	60
3.5.1	TFC membrane modification.....	60
3.5.2	Scanning Electron Microscopy.....	61
3.5.3	Contact Angle Measurements .....	61
3.5.4	Membrane Performance Evaluation .....	62
3.5.5	Antimicrobial Evaluation of Membranes.....	63
4	CONCLUSION and RECOMMENDATIONS .....	70
5	REFERENCES .....	72

## List of Figures

Figure 1: The schematic picture of pore size range for different pressure-driven membranes .....	3
Figure 2: Schematic picture of the reverse osmosis process used for seawater desalination .....	5
Figure 3: Schematic picture of FO and PRO systems for water treatment .....	6
Figure 4: Schematic illustration of the 4-step silver formation mechanism .....	8
Figure 5: Diagram summarizing nanoscaled silver interaction with bacterial cells .....	9
Figure 6: Chemical and 3D structures of GO nanosheets .....	15
Figure 7: Mechanisms of cellular inactivation of graphene nanomaterials with bacteria .....	16
Figure 8: Surface functionalization of membranes with graphene nanomaterials .....	18
Figure 9: covalently bonded AgNP-decorated GO nanosheets through click chemistry .....	26
Figure 10: Characterization of the GO/Ag nanocomposite .....	30
Figure 11: FESEM images of pristine and functionalized TFC membranes .....	30
Figure 12: Surface characterization of pristine and functionalized TFC FO membranes .....	33
Figure 13: Membrane properties before and after modification .....	35
Figure 14: Colony-forming units (CFU) after E. coli cells had been in contact with the control and GO/Ag functionalized membranes for 1 h at room temperature .....	37
Figure 15: FE-SEM images and backscatter electron imaging for functionalized membranes .....	39
Figure 16: TEM images of (A) GO, (B) Ag NPs, (C) GO/Ag nanocomposite .....	41
Figure 17: ATR-FTIR spectra of (A) GO nanosheets and GO/Ag nanocomposite, and (B) ControlTFC and GO/Ag nanocomposite functionalized TFC membranes .....	42
Figure 18: Zeta potential of the surface of the pristine and functionalized membranes .....	43
Figure 19: XPS results for pristine membrane and cysteamine treated TFC FO membranes .....	44
Figure 20: XPS results showing physical stability of silver NPs .....	46
Figure 21: In situ Ag NP formation on the surface of GO-modified membranes .....	49
Figure 22: BSE-SEM and AFM images of pristine and functionalized membranes .....	53
Figure 23: XPS spectra of pristine (A) and modified membranes (B). ICP-MS results of loading and stability (C) as well as releasing behavior (D) of functionalized membranes .....	54
Figure 24: Water contact angle and surface energy, drop shape and performance of pristine and modified membranes .....	55
Figure 25: The number of live cells on the pristine, Ag, GO and GO-Ag-modified surfaces over 1 hr contact with E. coli D21f2 bacterial suspension .....	57

Figure 26: Normalized silver content on the surface of membranes (A), antimicrobial properties of pristine and modified membranes (B), and XPS spectra for Ag (3d) (C), Raman shift of pristine and modified membranes (D) before and after regeneration. ....	59
Figure 27: Images of pristine, TFC-GO, TFC-Ag and TFC-GO-Ag-modified membranes. ....	64
Figure 28: FE-SEM images of pristine and modified membranes .....	65
Figure 29: Physical stability of Ag NPs on the surface of modified membranes after 7 minutes of bath sonication .....	66
Figure 30: XPS peak analysis for TFC and modified membranes before and after regeneration	67
Figure 31: SEM images of cells (E. coli D21f2) after contacting with pristine and modified membranes for 1 h .....	68

### **List of Tables**

Table 1: Surface roughness properties of the pristine and the GO/Ag functionalized TFC FO membranes .....	43
Table 2: Elemental composition by XPS analysis of the membrane surface of pristine and functionalized membranes, before and after sonication. ....	45
Table 3: Surface roughness properties of the pristine and functionalized TFC FO membranes. .	69

### List of Abbreviations

WHO	World Health Organization
UNICEF	United Nations Children's Emergency Fund
RO	Reverse Osmosis
MF	Microfiltration
UF	Ultrafiltration
NF	Nanofiltration
ED	Electrodialysis
FO	Forward Osmosis
PRO	Pressure Retarded Osmosis
TFC	Thin Film Composite
CTA	Cellulose Triacetate
Ag	Silver
NPs	Nanoparticles
GO	Graphene Oxide
PVP	Polyvinylpyrrolidone
ATP	Adenosine Triphosphate
DNA	Deoxyribonucleic acid
ROS	Reactive Oxygen Species
PEI	Polyethyleneimine
EDC	N-Ethyl-N'-(3-dimethylaminopropyl)

	carbodiimide
NHS	N-Hydroxysuccinimide
ED	Ethylenediamine
PES	Polyethersulfone
PSf	Polysulfone
LBL	Layer-by-layer
PDMS	Polydimethylsiloxane
EPS	extracellular polymeric substances
PDA	Polydopamine
TGA	Thermal Gravimetric Analysis
FE-SEM	Field Emission scanning Electron Microscopy
AFM	Atomic Force Microscopy
HR-TEM	High Resolution Transmission Electron Microscopy
EKA	Electrokinetic Analyzer
XRD	X-ray Diffraction
XPS	X-ray Photoelectron Spectroscopy
ATR-FTIR	Attenuated total reflection-Fourier transform infrared spectroscopy
BSE	Back-scattering Electron
ICP-MS	Inductively Coupled Plasma Mass Spectroscopy

BSA

Bovine Serum Albumine

DI water

Di-ionized water

# 1 INTRODUCTION

## 1.1 Motivation

Global demand for clean water is growing in parallel with population growth; in coming years, water will present itself as a pivotal environmental issue. Worldwide attention is focusing on the complimentary technologies of water supply, reuse, and purification. Membrane processes, among other energy-efficient technologies, enjoy excellent reputations due to their modular design, ease of preparation, and high efficacy. Unfortunately, usage of these technologies entail some inherent shortcomings, mostly attributed to membrane fouling and biofouling. Through this study, we propose novel methods to overcome the problems as mentioned above.

### *1.1.1 Water Scarcity throughout the World*

Water is the core of sustainable development. Water resources, and the wide range of services they are involved in support poverty reduction, economic growth, and environmental sustainability. Water plays a significant role in the social well-being and economic livelihoods of billions<sup>1</sup> notably in terms of areas ranging from food and energy security to human and environmental health. According to the joint monitory report of the World Health Organization (WHO) and the United Nations Children's Fund (UNICEF), although 1.6 billion people are using a higher quality of pipelines and safe water, 748 million do not use an improved water source, and 2.5 billion do not use improved sanitation facilities<sup>2, 3</sup>. Nowadays, one-third of the world's population is living in water-stressed countries, and by 2025 this number is predicted to increase to nearly two-thirds<sup>4</sup>. Several measures have been implemented to alleviate stresses on water supplies, such as water preservation, infrastructure repair and improvement of water distribution and irrigation systems.

While these measures are necessary and crucial, they only preserve existing water resources and do nothing to expand them. The only available methods for increasing our water supply are water desalination and water reuse processes<sup>5</sup>. Of these, water desalination shows much promise as it offers high quality and stable, fresh water, and can be scaled for different regions of the world with varying capacities. Water desalination technologies are categorized into two important spheres: thermal processes and membrane-based processes. Early-stage implementation of large-scale thermal water desalination plants has occurred in the arid Persian

Gulf nations. These processes involve heating and evaporating seawater; the steam is then condensed to produce distilled fresh water. While technically capable of producing water, these facilities consume substantial amounts of energy and emit huge volumes of greenhouse gasses.

Membrane based processes offer some of the most energy-efficient technologies for seawater desalination. Reverse osmosis (RO) is one such process, where seawater is pressurized against semi-permeable membranes to separate water molecules (which can pass) from salts (which are rejected). RO is the most efficient membrane based desalination method, and is the current benchmark for comparison with any new desalination technologies.

## **1.2 Osmosis-Based Membrane Processes for Water Desalination and Reuse**

There are four established pressure-driven industrial membrane processes: microfiltration (MF), ultrafiltration (UF), reverse osmosis (RO), and electrodialysis (ED)<sup>6</sup>. The membranes for each of these processes require different structures and pore sizes. While MF and UF membranes consist of mostly asymmetric porous layers, RO membranes are composed of multi-layers: a dense, active polyamide top layer, an asymmetric, porous polysulfone middle layer and a polyester non-woven bottom layer. Based on pore size and structure, membranes are capable of separating different substances and contaminants from water. The membrane structure and applications are depicted in Figure. 1.

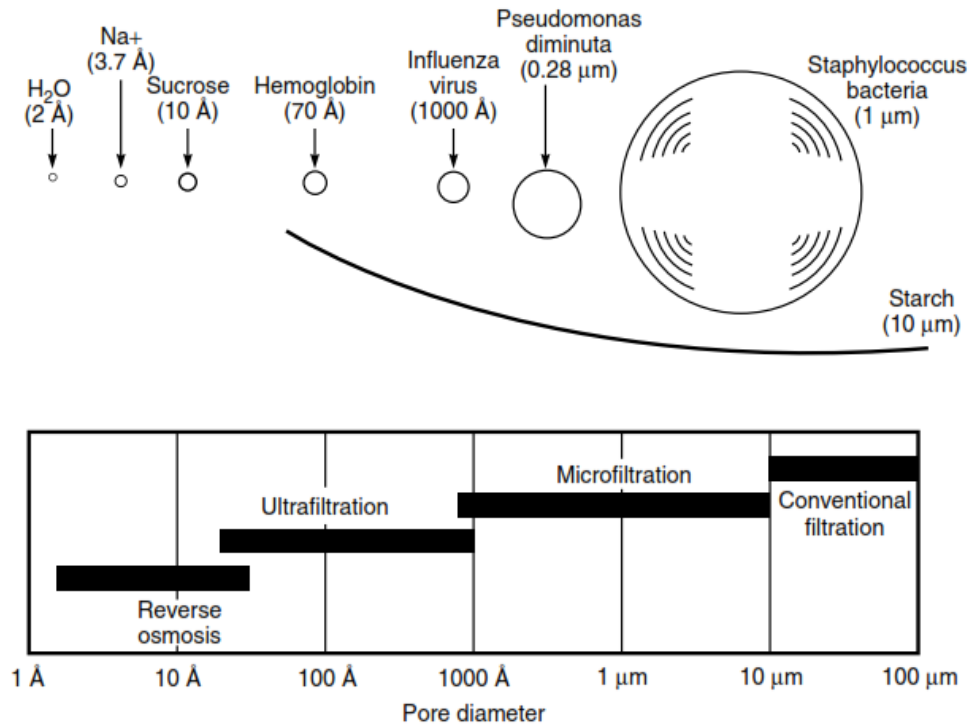


Figure 1: A schematic comparison of pore size range for different pressure-driven membranes and the different types of contaminants that can be separated by each membrane process<sup>6</sup>.

RO is used mainly in water desalination and currently occupies 50% of the desalination market. Desalination aims to increase the overall supply of fresh water via desalination of seawater and saline aquifers that comprise 97.5% of all water on the Earth. Therefore, filtration of a tiny portion could have a significant impact on water supplies and mitigate future shortages. Although desalination technologies in all forms are often considered to be capital- and energy-intensive processes, RO consumes less energy and is impacted less from corrosion and scaling than thermal desalination processes<sup>7,8</sup>.

Reverse osmosis uses membranes that are permeable to water but essentially impermeable to salt. Pressurized salt-containing water contacts the feed side of the membrane and purified water is withdrawn as a low-pressure permeate. The separation mechanism occurring in RO systems is solution-diffusion; where water molecules are dissolved in the polyamide active layer of the membrane, and then diffuse through the porous middle layer. The water flux  $J_i$  is a function of the applied pressure and concentration gradients across the membrane:

$$J_i = A(\Delta p - \Delta \pi) \quad (1-1)$$

where  $\Delta p$  is the pressure difference across the membrane,  $\Delta \pi$  is the osmotic pressure difference across the membrane, and  $A$  is constant.

The salt flux  $J_j$  across the RO membrane is described as:

$$J_j = B(C_{j0} - C_{jl}) \quad (1-2)$$

where  $B$  is the salt permeability constant and  $C_{j0}$  and  $C_{jl}$ , respectively, are the salt concentration on the feed and permeate sides of the membrane. Selectivity can be calculated in different ways, but conventionally it is measured as the salt rejection coefficient  $R$  as:

$$R = \left[1 - \frac{C_{jl}}{C_{j0}}\right] \times 100\% \quad (1-3)$$

Although RO systems (Figure 2) have a relatively low rate of energy consumption, they do require the use of high-cost electrical energy and still are impacted by fouling and biofouling problems. A portion of the electrical energy usage is inevitable due to the reversible thermodynamic process, which is independent of the system and mechanisms. However, through the implementation of novel, robust, high flux, low fouling membranes, energy usage can be significantly reduced.

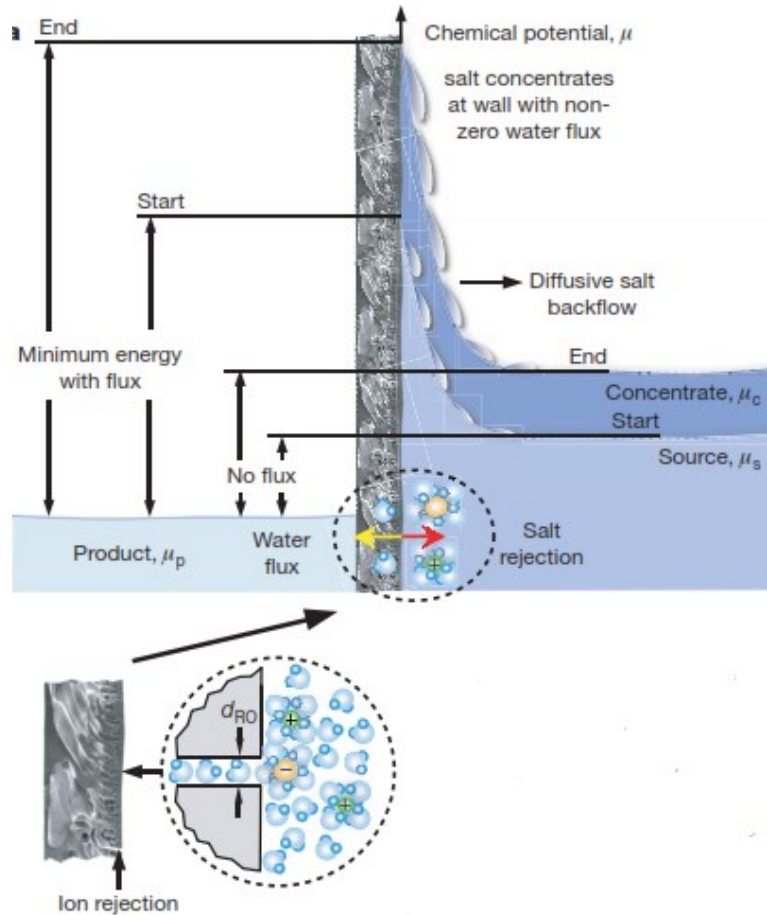


Figure 2: Schematic picture of the reverse osmosis process used for seawater desalination<sup>5</sup>.

Other emerging osmosis-based desalination/separation processes include forward osmosis (FO) and pressure-retarded osmosis (PRO) where a semi-permeable membrane is placed between two solutions of different concentrations: a highly concentrated saline draw solution and a more dilute feed solution. The osmotic pressure difference between the two solutions drives water flow from feed to draw side. FO can address several drawbacks of RO and other pressure-driven membrane processes.

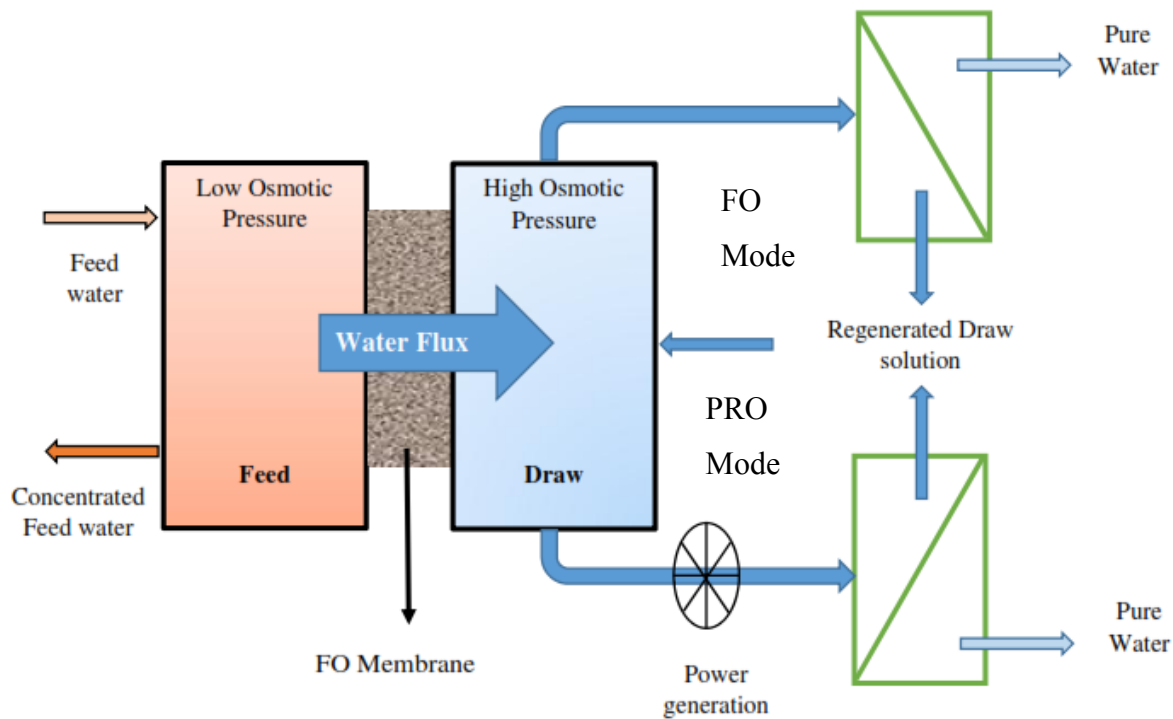


Figure 3: Schematic picture of FO and PRO systems for water treatment

Despite recent developments in FO, there are still challenges that need to be overcome before it can be successfully implemented. There is still some confusion about the energy consumed during the FO process<sup>9</sup>. The ideal draw solution has remained elusive and is considered to be the “Holy Grail” in FO. To be considered optimal, the draw solution needs to be inexpensive, stable, non-toxic, highly soluble and mobile, have a molecular size large enough to limit reverse salt flux through the FO membrane’s active layer, and be able to mitigate internal concentration polarization (ICP)<sup>10, 11</sup>. Fouling and biofouling of FO membranes are also a major challenge. Fouling is the deposition and adsorption of feed water constituents to the membrane surface. Such constituents include organic and inorganic compounds, colloidal particles, and microorganisms. Fouling deteriorates the membrane performance and decreases the membrane lifespan, which in turn increases operating costs for desalination. Although FO membranes are considered to have lower fouling propensities than RO membranes because of their loosely packed layers, the membrane surface is intrinsically prone to fouling and biofouling, and therefore requires some modifications to counteract this problem.

### 1.3 Fouling and Biofouling Mitigation through Surface Modification

Fouling propensity in FO is governed by hydrodynamic operating conditions and the affinity of foulants to the membrane surface. Therefore, fouling resistant membranes are characterized by biocidal, hydrophilic, inert surfaces, and smooth topographies that prevent foulant attachment. There are two different categories of membranes used in FO systems: asymmetric cellulose triacetate (CTA) and polyamide thin-film composite (PA TFC) membranes. The majority of studies on fouling in FO processes are related to CTA membranes due to CTA being the primary type of membranes available in the commercial market until recently<sup>12-17</sup>. However, state-of-the-art TFC membranes have been shown to have higher water permeability and salt rejection. They are increasingly being studied because they are inherently prone to fouling due to their rough surfaces and the presence of different types of functional groups on the surface such as carboxylic groups<sup>4</sup>.

Various methods of surface property modifications<sup>18</sup> have been employed for fouling and biofouling mitigation; the addition of different types of functional groups<sup>12</sup>, polymer brushes<sup>19</sup>, modified nanoparticles,<sup>20</sup> and other biocidal materials<sup>21</sup>. Surface modifications aim to increase the membrane's hydrophilicity, smoothness, and biocidal properties. The use of nanomaterials in surface modifications has recently attracted great attention because of the special properties nanomaterials can provide to a large surface area and biocidal properties they can add. Due to their significant biocidal and hydrophilic properties, silver nanoparticles (Ag NPs) and graphene oxide nanosheets (GO) have gained focal attention.

### 1.4 Biocidal Nanomaterials

#### 1.4.1 Silver Nanoparticles

Metallic nanoparticles are of particular interest due to their unique properties and a myriad of promising applications in areas such as environmental science and engineering<sup>22</sup>. Due to its broad spectrum of antimicrobial properties, silver is widely used in biomedical applications, water and air purification, cosmetics, clothing, and other household products. With the advent of nanotechnology, the applications of silver have been expanded, and it is now the engineering nanomaterial most commonly used in consumer products<sup>23</sup>. Ag NPs are nanoscale clusters of metallic silver atoms, Ag<sup>0</sup>, engineered for a specific practical purpose: typically antimicrobial and sterile applications.

The intrinsic properties of metal nanostructures can be designed and tailored by controlling their size, shape, composition, crystallinity, and structure (e.g. solid versus hollow)<sup>24, 25</sup>. The most common method of producing of Ag NPs is through the chemical reduction of a silver salt (the precursor to silver) by dissolving it in water with a reducing agent such as sodium borohydride ( $\text{NaBH}_4$ ), citrate, glucose, hydrazine, or ascorbate<sup>26</sup>. Strong reductants such as  $\text{NaBH}_4$  lead to small monodisperse particles, which are easier to control than larger particles. Weaker reductants generate large polydisperse particles through slower reactions. To produce Ag NPs with controlled size, a two-step method is utilized. In the first step, smaller nuclei particles are prepared by employing a strong reducing agent. In the second step, they are enlarged by a weak reducing agent<sup>27</sup>. Another effective method for controlling the size and shape of Ag NPs is using polymeric capping agents such as poly vinylpyrrolidone (PVP). Ag NP size, shape and stability can be simply controlled by tuning the ratio between the capping agent (PVP) and precursor salt ( $\text{AgNO}_3$ )<sup>28</sup>. This ratio can also be used to optimize the thickness of the PVP layer and the location of PVP chains on the surface of seed particles. Finally, this optimization can alter the resistance of each crystal face to growth (addition of silver atoms) and can also lead to the formation of silver nanostructures with distinct shapes and sizes.

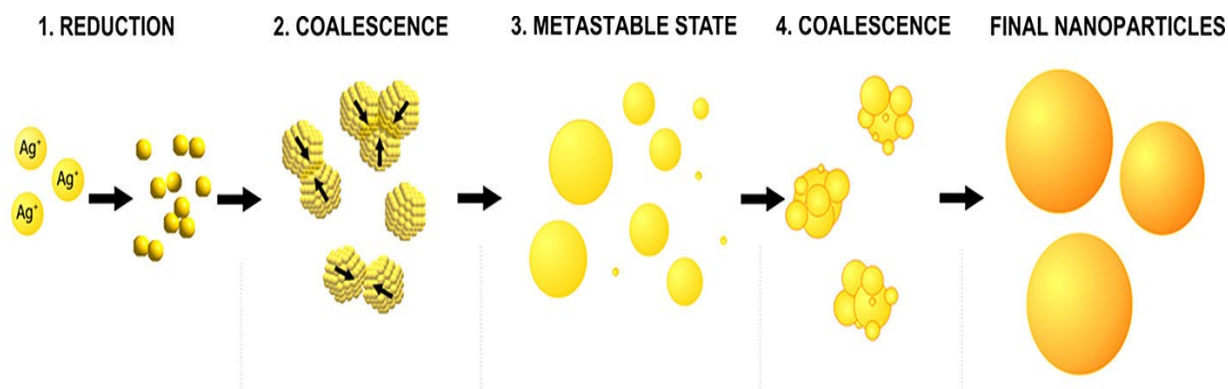
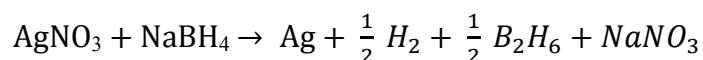


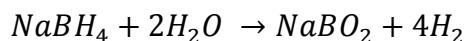
Figure 4: Schematic illustration of the 4-step silver formation mechanism<sup>29</sup>.

As depicted in Figure 4, silver nitrate is first reduced by  $\text{NaBH}_4$  (1) followed by rapid growth due to coalescence (2). After these initial steps, the mean radius of silver is approximately 1 nm. After reaching the metastable phase (3), the electrostatic stability of the particles decreases due to the hydrolysis of borohydride, which leads to a second coalescence step (4) and stable particle formation (5). At the fifth step, the size of Ag NPs increases to about 7 nm<sup>29, 30</sup>.

The reduction of silver nitrate by sodium borohydride is governed by the following equation:



Sodium borohydride also reacts with water relatively slowly<sup>31</sup>:



Although the mechanism of bacterial inactivation by Ag NPs is not fully elucidated, the three most common mechanisms of toxicity proposed are (1) release silver ions and generate ROS; (2) interact with membrane proteins affecting their correct function; (3) accumulate in the cell membrane affecting membrane permeability; and (4) enter into the cell where it can generate ROS, release silver ions, and affect DNA. Some of the observed and hypothesized interactions between Ag NPs and bacterial cells are illustrated in Figure 5.

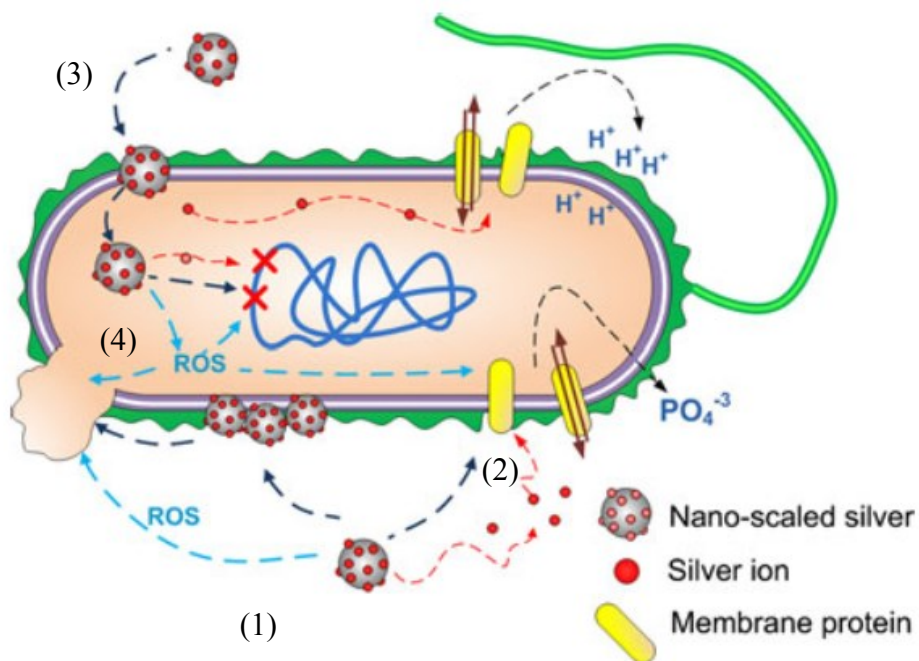


Figure 5: Diagram summarizing nanoscaled silver interaction with bacterial cells. Nanoscaled silver may (1) release silver ions and generate ROS; (2) interact with membrane proteins affecting their correct function; (3) accumulate in the cell membrane affecting membrane permeability; and (4) enter into the cell where it can generate ROS, release silver ions, and affect DNA. Generated ROS may also affect DNA, cell membrane, and membrane proteins, and silver ion release will likely affect DNA and membrane proteins<sup>23</sup>.

Ag NP toxicity is influenced by several factors such as particle size, shape, crystallinity, surface chemistry, and capping agents, as well as other environmental factors such as pH, ionic strength, and the presence of ligands, divalent cations, and macromolecules. As particle size decreases, the specific surface area increases thus exposing a higher number of atoms on the surface to redox and biochemical reactions. Furthermore, one of the key mechanisms of bacterial inactivation is the release of silver ions. In general, the rate of release is proportional to the particle surface area; smaller particles release more rapidly than larger particles and macroscopic materials<sup>32,33</sup>. Atom densities at [1 1 1] facet also increase the toxicity of Ag NPs. Therefore, Ag NP shape has an important effect on its toxicity<sup>34</sup>. Truncated triangular NPs exert stronger antibacterial activity than spherical and rod-shaped Ag NPs because they have more [1 1 1] facets and can be more reactive<sup>35</sup>. The stability of Ag NPs also influences biocidal activity since aggregation of NPs cause a decrease of biocidal activity<sup>36</sup>. Different types of surfactants and polymers (e.g. sodium dodecyl sulfate and PVP) are used to make NPs stable and enhance biocidal activity. However, some ligand-capped Ag NPs are less bioactive because the capping agent hinders the release of silver<sup>37</sup>.

Environmental conditions such as pH, ionic strength, the presence of complexing agents and natural organic matter, as well as NPs properties affect the toxicity of Ag NPs. They affect the aggregation of Ag NPs by either screening electrical double layer repulsion<sup>38</sup> or ion-release that is governed by aquatic media pH, redox potential, ionic composition, and exposure to light<sup>34</sup>.

The applications of Ag NPs in membrane science have been widely studied. Used in both surface modification and bulk incorporation, Ag NPs increase the biocidal activity of membranes for mitigation of biofouling. Zodrow et al<sup>39</sup> incorporated Ag NPs in polysulfone (PSf) membranes to study antimicrobial properties and bacterial attachment to the membrane surface. They concluded that the modified membranes, specifically the Ag<sup>+</sup> ions, were effective against two strains of bacteria. An adverse issue observed in the use of this method was a rapid depletion of silver due to dissolution. The researchers proposed encapsulating silver for a controlled release and then regenerating the silver after depletion. Mauter et al<sup>40</sup> encapsulated antimicrobial Ag NPs in positively charged polyethyleneimine (PEI) and covalently bonded it to plasma-modified PSf ultrafiltration membranes in the presence, and absence of 1-ethyl-3-(3-dimethylaminopropyl) carbodiimide hydrochloride (EDC). They concluded that this new method

of antimicrobial Ag NP surface modification increased the durability and biocidal properties of the final reactive nanocomposite membranes. The results showed that the concentration of released silver decreased by more than ten times after only two days. They concluded that using EDC to fix the Ag NPs in place aided the biocidal properties of the membranes significantly. They also proposed Ag NP regeneration for increased long-term effectiveness of nanocomposite membranes.

A problem with surface modification of PSf membranes lies in the difficult and non-permanent functionalization of the surface through plasma treatment. Sawada et al<sup>41</sup> developed hydrophilic polyethersulfone (PES) hollow fiber membranes through photo-polymerization of an acrylamide layer and formation of Ag NPs by chemical reduction. Both organic and biofouling were investigated, and they concluded that the acrylamide grafting layer was effective for improving the membrane hydrophilicity. They improved organic antifouling properties with a bovine serum albumin (BSA) solution. Finally, antimicrobial properties of Ag NP membranes were confirmed through the halo zone test and the shake flask method. Although both organic antifouling and antimicrobial properties were achieved, the modification process was difficult and complicated.

Kim et al<sup>42</sup> developed nanosilver and multi-walled carbon nanotube (MWNTs) thin-film nanocomposite (TFN) membranes. The TFN membrane was synthesized by the interfacial polymerization of a support layer containing acid-modified MWNTs and a thin-film layer of Ag NPs. They concluded that incorporation of MWNTs and Ag NPs increased both the water permeability of the membranes and their hydrophilicity. Salt rejection remained unchanged, and the modified membranes showed enhanced anti-biofouling properties. However, the study was limited by the fast release of silver ions and the lack of a regeneration process. Furthermore, Ag NPs were distributed within the polyamide layer, and their efficacy in preventing cell-attachment was controversial. The antimicrobial properties of the membranes were examined through the disk diffusion method that is more of a qualitative as opposed to a quantitative test.

Liu et al<sup>43</sup> synthesized novel antibacterial silver nanocomposite nanofiltration (NF) and forward osmosis membranes using layer-by-layer assembly. They prepared a polyacrylonitrile porous layer and incorporated Ag NPs through dispersion in a polyelectrolyte solution (Polycation poly (allylamine hydrochloride) and polyanion poly (sodium 4-styrene-sulfonate)).

They concluded that their method is highly flexible in silver loading, and the resulting membranes showed high performance and excellent antibacterial properties. The most significant problem with this research was the distribution of Ag NPs on the membrane surface of the membranes. Scanning electron microscopy (SEM) and energy-dispersive X-ray spectroscopy (EDS) images showed large aggregation of Ag NPs on the membrane surface. Other drawbacks of this method included poor regeneration of the Ag NPs and the lack of direct contact between the silver and the bacteria.

Poornima et al<sup>44</sup> prepared silver-enhanced block copolymer membranes with biocidal activity. Silver NPs were deposited on the surface and pore walls of the block copolymer membranes, with highly ordered pore structures. To study the distribution of the Ag NPs, they changed the pH and silver ion concentration and observed pH 9 as the best condition for the distribution and highest efficacy. Based on SEM images, the Ag NPs were highly aggregated on the surface of the membranes. Also, the silver content on the membranes decreased drastically after 10 hrs, with the concentration of Ag in the permeate reaching 600 µg/L after two days, a level higher than the standard for Ag concentration in drinking water<sup>45</sup>.

Rahaman et al<sup>19</sup> employed the combination of anti-fouling polymer brushes and biocidal Ag NPs via polyelectrolyte layer-by-layer (LBL) self-assembly for the surface modification of TFC RO membranes. They capped Ag NPs with PEI and used poly (acrylic acid) (PAA) and PEI LBL. They also used two different polymer brushes: poly (sulfobetaine) for increasing surface hydrophilicity and poly (dimethylsiloxane) (PDMS) for reducing surface energy of membranes, both for mitigation of the biofouling problem. Although the combination of polymer brushes, LBL self-assembly, and Ag NPs provided hydrophilic, anti-attachment, and antibacterial surfaces, silver content decreased to almost zero after two days. Furthermore, the modification process was difficult and time-consuming, and the efficacy of Ag NPs in bacterial inactivation was controversial because of the capping of silver by PEI.

Yin et al<sup>46</sup> attached Ag NPs onto TFC membranes through covalent bonding using cysteamine. In this study, no capping agent was used, and Ag NPs were covalently bonded onto the membranes. Covalent bonding improved the Ag NP distribution and stability on the surface and increased their biocidal properties. However, bacterial testing was only qualitative, the Ag loading in this method was limited, and its regeneration after depletion was still an unsolved

problem. Ben-Sasson et al<sup>47</sup> formed Ag NPs in situ on the surface of TFC RO membranes and studied the effects of silver nitrate and sodium borohydride concentrations on silver loading, membrane performance, and the antibacterial properties of the membranes. The in situ formation process provided an easy formation procedure, potential high loading content of silver, and effective biocidal inactivation of about 75%. They also studied biofilm formation, and results showed that Ag NPs significantly suppressed formation, with a 41% reduction in total biovolume and a significant reduction in extracellular polymeric substances (EPS), dead, and live bacteria on the functionalized membrane. Although their work was significant in simplifying the surface modification process and increasing loading content, again, the method suffered from a lack of regeneration, a high release of silver in water, and incomplete bacterial inactivation.

Tang et al<sup>48, 49</sup> functionalized ultrafiltration PSf membranes using silver nanoparticles through in situ formation and LBL methods. They first functionalized membranes with a bioinspired polydopamine (PDA) film, followed by in situ formation of Ag NPs to mitigate membrane biofouling. The modification method, in terms of silver formation, was easy; simply exposing the membranes to a silver nitrate solution caused the Ag<sup>+</sup> ions to be reduced by the catechol groups in PDA. Results showed increased silver loading with exposure time. Without the use of reductants such as sodium borohydride, silver loading was limited; silver loading became sufficiently comparable to other methods only after long exposure times (24 hr) and regeneration remained unsolved.

#### 1.4.2 Graphene Oxide Nanosheets

It has been only 10 years since the isolation of graphene<sup>50</sup> and just over 5 since the 2010 Nobel Prize in Physics was awarded jointly to Andre Geim and Konstantin Novoselov for “groundbreaking experiments regarding the two-dimensional material graphene”<sup>51</sup>. Graphene is the thinnest, strongest material known, is highly transparent, and has high electrical and thermal conductivity<sup>52</sup>. Graphene sheets comprise a 2D layer of sp<sup>2</sup>-hybridized carbon atoms arranged in hexagonal lattice<sup>53</sup>.

Graphene possesses several properties that make it appealing for different types of applications. The most studied aspect of graphene is its electrical properties. Electrons in graphene have high mobility, reaching 10000 cm<sup>2</sup> V<sup>-1</sup>S<sup>-1</sup> to 50000 cm<sup>2</sup> V<sup>-1</sup>S<sup>-1</sup> at room temperature. It can sustain current densities up to six orders of magnitude higher than copper.<sup>54</sup>

Despite having the thickness of a single atom, graphene is also the strongest possible material with a Young's modulus of  $E = 1.0 \text{ TPa}$  and an intrinsic strength of  $130 \text{ GPa}$  in a perfect atomic form.<sup>55</sup> Graphene is the extreme case of a high-surface-area material (with a theoretical value for specific surface area:  $2630 \text{ m}^2\text{g}^{-1}$ ) since every atom of a single-layer graphene sheet is exposed on both sides of its environment. It can be more efficient than CNTs when preparing polymeric nanocomposites. Also, graphene represents an excellent support to anchor chemical functionalities or nanomaterials, and thus, can be employed to synthesize graphene-based nanocomposites as novel materials.<sup>56</sup> One of the most popular approaches to graphene-based materials is using graphene oxide (GO) due its lower production costs. GO is an oxidized form of graphene, offering high densities of oxygen-containing functional groups (carboxyl, hydroxyl, carbonyl, and epoxy) in the 2D carbon lattice (Fig. 6). The most popular preparation method for GO is the chemical oxidation of graphite to form graphite oxide and subsequent exfoliation by ultrasonication (Hummers method<sup>57</sup>). Due to the abundance of functional groups on the surface, the hydrophilic nature, and the higher interlayer distance, GO can be easily dispersed in water and form stable suspensions in aqueous media. This hydrophilic nature, combined with both high specific surface area and functional group density make GO nanosheets a suitable material for chemical functionalization.

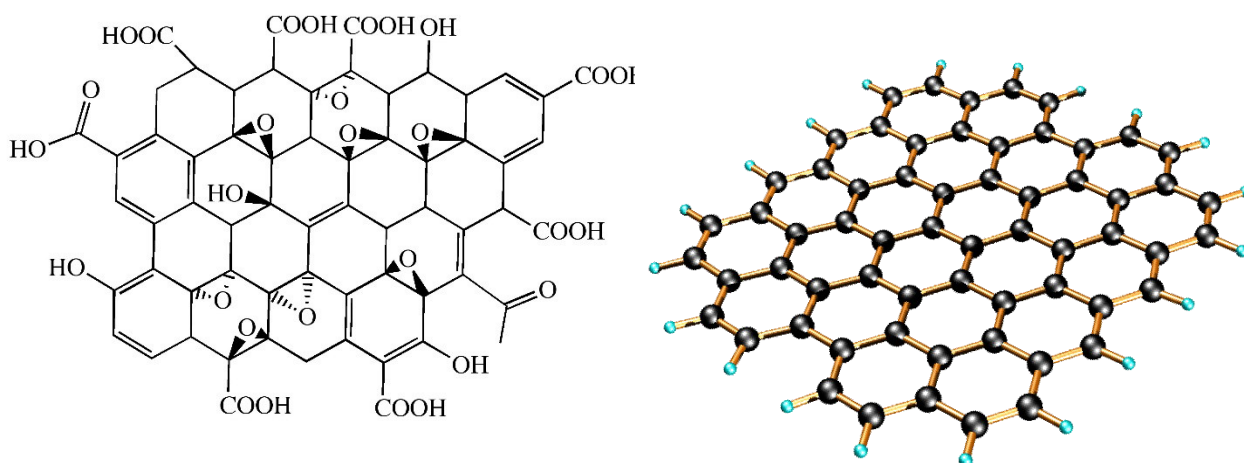


Figure 6: Chemical and 3D structures of GO nanosheets.

Graphene-based materials show promise in the design of antimicrobial surfaces that could be effective in contact-mediated action. The advantage of graphene-based antibacterial materials is that they do not deplete over time, or release biocides into the environment. Although the exact bacterial inactivation mechanism of graphene-based materials is still controversial, some evidence suggests possible pathways of antimicrobial activity.<sup>58-60</sup> Graphene-bacteria interactions range from sheet adsorption on the cell membrane surface, membrane puncturing and penetration through the lipid bilayer, lipid extraction by the graphene sheet, as well as oxidative stress.

In the past few decades, efforts have been made to develop inorganic nanostructures with controlled shape, size, crystallinity, and performance for a variety of applications such as electronics, optics, medicine, environmental science, and engineering. To enhance their properties, and better control their shape, size, and distribution, a great number of inorganic nanomaterials have been combined with graphene and its derivatives. The most popular inorganic nanostructures are metals like Au<sup>61, 62</sup>, Ag<sup>63-66</sup>, Pd<sup>67</sup>, Pt<sup>68</sup>, Cu<sup>67</sup>, TiO<sub>2</sub><sup>69</sup>, ZnO<sup>70</sup>, etc. There two general methods for the fabrication of nanocomposites: *ex situ* hybridization and *in situ* crystallization. *Ex situ* hybridization involves the mixture of graphene-based nanosheets and pre-synthesized, or commercially available, nanocrystals in a solution. Surface modification using one or both graphene nanosheets and nanocrystals is often carried out to improve the

attachment and bonding between the nanosheets and nanostructures. Although *ex situ* hybridization can fabricate nanocomposites with desired functionalities, final nanocomposites sometimes suffer from low density and non-uniform distribution of nanostructures. In contrast, *in situ* crystallization can produce a higher nanostructure density and result in better distribution via surface functionalization. The chemical reduction method is the most popular procedure for forming metal nanostructures. Precursors of noble metals such as  $\text{HAuCl}_4$ ,  $\text{AgNO}_3$ ,  $\text{K}_2\text{PtCl}_4$ , and  $\text{H}_2\text{PdCl}_6$  are simply reduced in situ by reducing agents such as amines,  $\text{NaBH}_4$ , and ascorbic acid<sup>56</sup>.

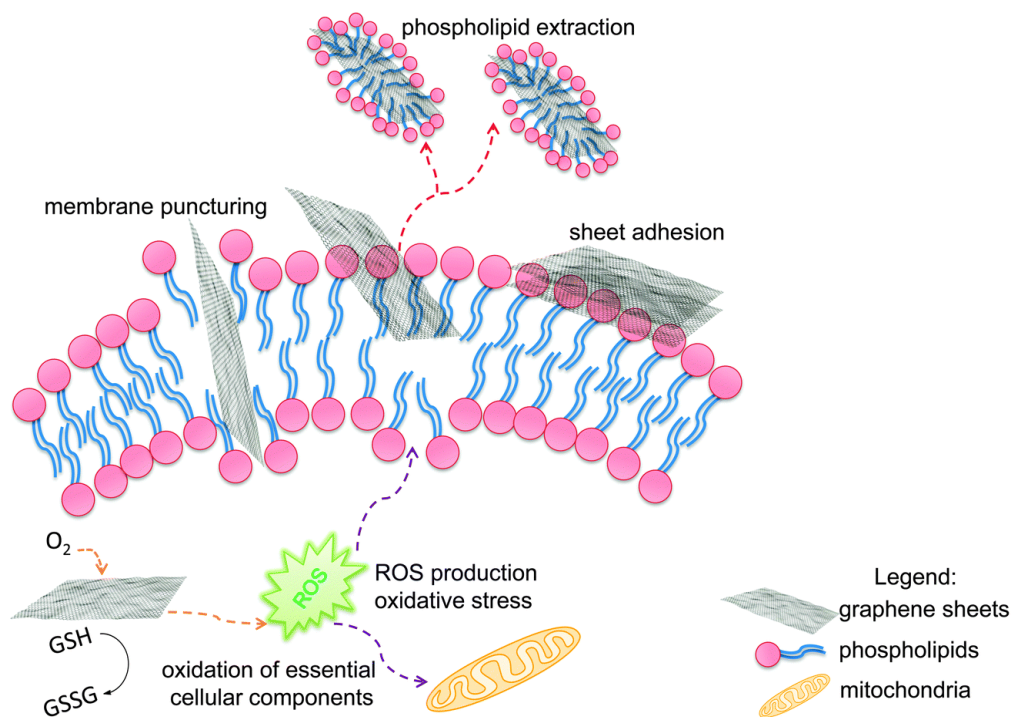


Figure 7: Mechanisms of cellular inactivation of graphene nanomaterials with bacteria: puncturing the cell membrane, generating reactive oxygen species (ROS), extracting phospholipids from the lipid bilayer and adhering on the cell surface<sup>71</sup>.

Graphene, and its derivatives, are used in membrane and desalination technologies in two different ways: (1) as a barrier layer for water purification, and (2) as an antimicrobial agent for

membrane modification, incorporated in bulk or deposited on the surface. Although graphene is one atom thick, it is an impermeable material in its pristine form, which allows it to be used as a barrier for gas and liquid permeation<sup>72, 73</sup>. Hu et al. used GO nanosheets as water separation membranes<sup>74</sup>. The GO membrane was made via layer-by-layer deposition of GO nanosheets, which were cross-linked with EDC on a polydopamine-coated PSf support. Cross-linking provides layer stability and enables the stacking of GO nanosheets. Although novel membranes show very high flux (roughly 4-10 times greater than that of most commercial NF membranes), their rejection is poor, ranging from 6-46% rejection of monovalent and divalent salts<sup>74</sup>.

Until the technical and economic limitations of graphene-based membranes can be overcome, polymeric membranes will remain the dominant, state-of-the-art materials for membrane processes. Graphene-based nanomaterials can be integrated into the design of polymeric membranes by increasing their mechanical strength or reducing their organic and biofouling propensity. The loose mechanical properties of membranes and their compaction during high-pressure processes can be solved by adding a small amount of GO, even 1 wt% directly into the polymeric solution<sup>75, 76</sup>.

The surface modification of membranes using graphene-based nanomaterials can also increase membrane life span and performance by preventing organic and biological fouling. For this purpose, GO nanosheets can be deposited directly on the native functional groups of the membrane surface or by using an intermediate compound to provide more reactive sites (Fig. 8). The deposition of GO nanosheets can also be achieved using the layer-by-layer technique for a more controlled covering of the membrane surface<sup>77</sup>. Graphene-based nanomaterials can also mitigate biofouling because of their antibacterial properties. Graphene nanosheets can inactivate bacteria upon direct contact by causing physical and oxidative damage to the cell membranes. The advantage of using graphene-based nanomaterials over other biocidal nanoparticles is that they will not be depleted from the surface by dissolution in water; also, if strong covalent bonds are made between the graphene nanosheets and the membrane surface, they would be almost permanently present and effective<sup>78</sup>. However, graphene-based nanomaterials by themselves are not enough for the complete inactivation of bacteria. The best way to modify the surface of membranes may be through the use of a composite of graphene-based nanomaterials and biocidal nanoparticles.

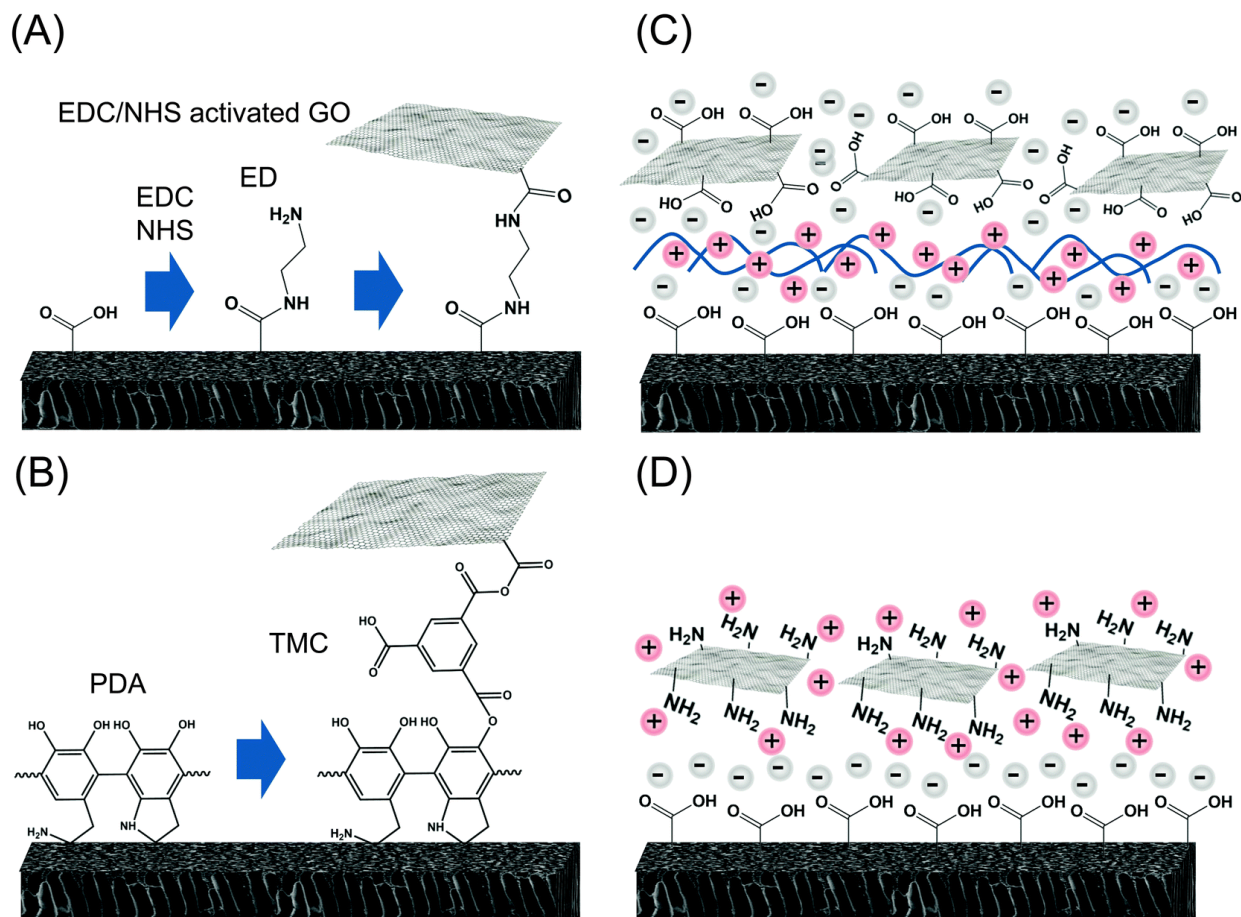


Figure 8: Surface functionalization of membranes with graphene nanomaterials. (A) Covalent binding of GO to the native functional groups of the membrane<sup>78</sup>. 1-Ethyl-3-(3-dimethylaminopropyl) carbodiimide (EDC) and N-hydroxysuccinimide (NHS) are used to activate carboxyl groups and attach ethylenediamine (ED) to the membrane by amide coupling. Then, EDC/NHS-activated GO sheets are covalently attached to the remaining amine group of ED. (B) Polydopamine (PDA) mediated binding of GO<sup>74</sup>. The membrane is first coated with PDA, which provides reactive sites for 1,3,5-benzenetricarbonyl trichloride (TMC) cross-linking between PDA and GO. (C) Polymer-mediated adsorption of GO via electrostatic interactions<sup>79, 80</sup>. Positively-charged polymers are applied on a negatively-charged membrane. Then, GO sheets, which are negatively charged, are deposited on the positive polymer layer. (D) Membrane coating using functionalized GO material<sup>81</sup>. GO sheets are aminated to provide positive charges, which can then be used to coat negatively charged membranes via electrostatic interaction. Adapted from ref.71.

## **1.5 Objective**

The objectives of this study is the development of antimicrobial thin-film composite forward osmosis membranes through surface modification by different types of biocidal nanomaterials. Silver nanoparticles (AgNPs), graphene oxide nanosheets (GO), and differing values of their combination were used, and the following items were investigated:

1. Physical and chemical properties of synthesized biocidal nanomaterials.
2. Surface properties of the membranes modified with synthesized nanomaterials.
3. Antimicrobial properties of pristine and modified membranes examined through static colony forming unit (CFU) measurements after contacting membrane surfaces with some model pathogenic and non-pathogenic, and gram positive and gram negative bacteria, all which are commonly found in brackish and seawater.
4. Performance evaluation of pristine and modified membranes in both reverse osmosis (RO) and forward osmosis (FO) modes of operation in cross-flow cells.
5. Nanomaterial regeneration after depletion in water through a method identical to the modification method and investigation of its successes.

## **1.6 Organization of Dissertation**

This dissertation comprises four sections ordered in a chronological sequence and based on my two publications:

Section 1: A short introduction about biocidal nanomaterials and antimicrobial surfaces.

Section 2: Surface Modification of Thin-Film Composite Forward Osmosis Membrane by Silver-Decorated Graphene-Oxide Nanosheets.

Section 3: In Situ Silver Decoration on Graphene Oxide-Treated Thin-Film Composite Forward Osmosis Membranes: Biocidal Properties and Regeneration Possibility.

Section 4: Conclusion and recommendations for future studies.

## 2 SURFACE MODIFICATION OF THIN FILM COMPOSITE FORWARD OSMOSIS MEMBRANE BY SILVER-DECORATED GRAPHENE-OXIDE NANOSHEETS

### 2.1 Introduction

Forward osmosis (FO) has recently been considered to be a promising technological approach for seawater desalination and water reuse because of the energy efficiency of the overall process of water separation<sup>4, 82</sup>. Although the FO process is less prone to fouling than reverse osmosis (RO), membrane fouling (notably biofouling) remains one of the important limitations to widespread application<sup>83</sup>. Thin film composite polyamide (PA) FO membranes are highly susceptible to biofouling because of their intrinsic physicochemical surface properties<sup>14</sup>. Although using oxidizing agents is a common method for controlling biofouling<sup>84, 85</sup>, other alternative methods must be considered because PA layers are sensitive to chemical oxidation and degrade in the presence of common disinfectants.

Membrane surface modification is one of the well investigated methods for preventing biofilm formation<sup>86</sup>. Different methods of surface modification have been reported<sup>83, 87</sup> including grafting macromolecules<sup>12, 88-90</sup>, preparing antifouling surfaces by functionalization<sup>20</sup> with photocatalytic nanoparticles (NPs) such as TiO<sub>2</sub><sup>91, 92</sup> and carbon-based nanomaterials,<sup>21, 93</sup> and using biocidal NPs such as silver (Ag) NPs either incorporated into the support layer<sup>39, 41</sup> or attached to the surface of the TFC membranes<sup>46</sup>. Problems associated with using biocidal NPs are their tendency toward agglomeration and detachment from the surface, releasing into the water. One of the best approaches to overcoming such problems is to use carbon-based nanocomposites (instead of using a single type of NPs)<sup>94</sup>.

Graphene oxide (GO), as a single-atomic-thick sheet consisting of hydrophilic oxygenated functional groups in the form of carboxyl, hydroxyl, ether, and epoxy, has attracted interest in different scientific areas<sup>53, 95</sup>. Several intrinsic characteristics of GO nanosheets, such as their smoothness, atomic-level thickness, high water slip length, and low cost of bulk production through the chemical oxidation of graphite, establish potential new applications in water purification<sup>96-98</sup>. Furthermore, specific efforts have investigated using GO to improve membrane durability by preventing the attachment of hydrophobic foulants or by forming a protective layer against chlorine attack<sup>77</sup>. Because of its highly functionalized basal planes and edges, GO presents special features when used as a support for noble metal nanoparticles such as

gold (Au) and silver (Ag). Au and Ag are widely used as sensors or catalysts<sup>56</sup> in electrical and environmental applications. Ag-decorated GO nanocomposites have been established as a new type of effective, easily synthesized, and cost effective biocidal materials in health and environmental applications<sup>66, 99, 100</sup>. GO nanosheets, employed to stabilize Ag nanoparticles and enhance the contact between Ag and bacteria, result in a synergetic effect for these new nanocomposites<sup>101</sup>. Although there are some studies suggesting special core-shell<sup>102</sup> or nanoscrolls structure<sup>66</sup>, based on different silver salt and chemical reductant or post-synthesizing procedure, majority of GO/Ag nanocomposite morphologies provide a very well-distributed silver decoration.

AgNPs are well studied for their enhancement of antifouling properties; for instance, Rahaman *et al.* used the combination of AgNPs with polymer brushes to prepare antifouling TFC RO membranes<sup>19</sup>. Yin *et al.* covalently bonded AgNPs onto the surface of TFC RO membranes to reduce membrane biofouling<sup>46</sup>, and Mauter *et al.* grafted AgNPs irreversibly onto the ultrafiltration (UF) membrane surface with a high silver release capacity<sup>40</sup>. The two major problems in using AgNPs for the surface modification of membranes are the high tendency of these NPs to agglomerate, leading to insufficient contact with bacteria, and the instability of the NPs on the membrane surface<sup>44, 63, 65</sup>. However, only a handful of studies investigated incorporating GO nanosheets on the membrane surface, either by electrostatic attraction or covalent bonds between GO and TFC RO membranes. Choi *et al.* used a layer-by-layer assembly of GO nanosheets on TFC RO membranes to protect these membranes against chemical degradation resulting from chlorine attack. Perreault *et al.* covalently bonded GO to the surface of TFC RO membranes and reported an increase in the hydrophilicity and antibacterial properties (~65% inactivation of bacteria) of the membranes<sup>78</sup>. However, neither AgNP nor GO alone can exploit their full potential in controlling membrane biofouling. Therefore, novel composite materials of individual nanomaterials are required to fully develop their potential for biofouling mitigation. In this manuscript, we use composite GO nanosheets and AgNPs as a new and promising class of biocidal materials for membrane surface modification.

In this study, silver-decorated GO nanosheets are used to functionalize PA TFC membranes. Silver-decorated GO nanocomposites were prepared through wet chemical reduction and covalently bonded to the surface of TFC FO membranes. TFC membranes were first

chemically treated by cysteamine through a click chemistry reaction. Unreacted acyl chloride groups from the interfacially polymerized PA layer and amine groups of the cysteamine formed amide bonds. The thiol groups of cysteamine then reacted with the as-prepared silver decorated GO nanosheets. The results of this study show the synergetic effect of the combination of GO nanosheets and AgNPs in the inactivation of bacteria without any adverse effects on membrane transport properties. This finding highlights a novel path for establishing a new class of biocidal materials.

## **2.2 Materials and Methods**

### *2.2.1 Materials*

The following chemicals were used as received: silver nitrate (99.9999% on a trace metal basis, Sigma-Aldrich), ethanol (Sigma-Aldrich), cysteamine (95%, Sigma-Aldrich), and sodium borohydride (99.99%, Sigma-Aldrich). De-ionized (DI)-water was prepared in a Millipore Milli-Q purification system. The TFC FO membranes were obtained from Hydration Technology Innovation, LLC and were soaked in a DI-water bath for 24 hours prior to modification.

### *2.2.2 Synthesis and Characterization of AgNPs and GO/Ag Nanocomposites*

Graphene oxide (GO) nanosheets were purchased from Cheap Tubes Inc. (Grafton, VT, USA); these nanosheets were synthesized by a modified Hummers method<sup>103</sup>. The single layer sheets were 0.7-1.2 nm thick and displayed a size distribution of 300-800 nm. The GO nanosheets were decorated with silver (Ag) through an in situ reduction of silver nitrate on the surface. The GO (50 mg) was dispersed in 100 mL of DI water through probe sonication (Branson 3510) for 1 h at 70% of the maximum power output. In total, 100 mL of silver nitrate solution (20 mM) was prepared and added to the GO suspension. The resulting mixture was mixed at room temperature for 30 min, and 10 mL of a sodium borohydride solution (5 mM) was added dropwise. Mixing continued for 5 h to complete the formation of AgNPs. Over time, the reaction mixture changed from a dark brown to a grayish color. The resulting GO/Ag nanocomposite mixture was centrifuged for 15 min at 12,500 rpm, rinsed with DI water three times and dried overnight in an oven at 80°C. The formation of GO/Ag nanocomposites was evaluated by UV-Vis absorption spectroscopy (UV-Vis LAMDA650, Perkin Elmer), X-ray diffraction (XRD Philips PW1710), thermal gravimetric analysis (TGA Q5000 V3.15 Build 263), and high-resolution transmission electron microscopy (HRTEM Tecnai G2 F20). Further

characterization of the nanocomposite was accomplished using Raman and attenuated total reflectance-Fourier transform infrared (ATR-FTIR) spectroscopy techniques.

### 2.2.3 Surface Modification and Characterization of TFC FO Membranes

TFC FO membranes were purchased from Hydration Technology Innovation (HTI) and were functionalized with GO/Ag nanocomposites using a cysteamine solution (Figure 9). Unreacted acyl halide groups on the surface of TFC polyamide membranes reacted with the amine functional group of cysteamine through a click chemistry reaction and formed strong amide bonds, providing the membrane surface with thiol functionality for subsequent covalent bonding of GO/Ag nanocomposites onto the membrane surface. TFC membranes were cut and placed on a glass plate and covered with a frame; only the active side was exposed to the cysteamine solution. Frames were clamped with clips to prevent any leakage. The entire assembly was then placed on an orbital shaker, rotating at 70 rpm at room temperature. Membranes were immersed in a cysteamine ethanol solution (20 mM) for 30 min and were then removed, rinsed with DI water three times, and immersed in the as-prepared GO/Ag nanocomposite suspension for 12 h. The resulting functionalized membranes were then washed with DI water three times and were refrigerated (4°C) until use.

The intrinsic membrane transport properties (e.g., water permeability and salt permeability) were evaluated in RO cross-flow cell based on standard methodology for evaluating membrane performance in osmotically driven membrane processes<sup>104</sup>. The permeation cell was designed to provide an effective surface area of 42.75 cm<sup>2</sup>. The membrane was compacted overnight with DI water at 70 psi until a steady water permeate flux was reached. In the RO mode in the experiment, the water flux (J) and water permeability (A) of the membranes were evaluated using the following equations:

$$J = \frac{\Delta V}{A_m \Delta t} \quad (2-1)$$

$$A = \frac{J}{\Delta P} \quad (2-2)$$

where  $A_m$  is the effective membrane surface area,  $\Delta V$  is the collected permeate volume during  $\Delta t$  and  $\Delta P$  is the applied pressure difference.

The salt rejection was determined by measuring the rejection of a 50 mM NaCl solution using a calibrated conductivity meter (Oakton Instruments, Vernon Hills, IL, USA). The salt rejection of the membranes was calculated using the following equation:

$$R = \left(1 - \frac{C_p}{C_f}\right) \times 100\% \quad (2-3)$$

where  $C_p$  and  $C_f$  are the salt concentrations in the permeate and feed solutions. The salt concentrations were determined by measuring the conductivity of the solution using a calibrated conductivity meter. The salt permeability coefficient (B) was calculated as follows:

$$\frac{1-R}{R} = \frac{B}{A(\Delta P - \Delta \pi)} \quad (2-4)$$

where A is the water permeability,  $\Delta P$  is the transmembrane pressure,  $\Delta \pi$  is the osmotic pressure of the feed solution and R is the salt rejection.

The membrane performance in the FO mode was also evaluated using a lab scale cross-flow cell with the same dimensions as the RO cell. Both the feed (DI water) and draw solution (1 M NaCl) were circulated at the same flow rate (0.2 L/min) and applied pressure. The temperature of the feed and draw solution was maintained constant at 25°C. To precisely measure the water flux, a digital analytical balance was employed to measure the weight change of the draw solution. The salt reverse flux of the membranes was calculated by measuring the conductivity of the draw solution before and after the FO process using a calibrated conductivity meter (Oakton Instruments, Vernon Hills, IL). The FO water flux ( $J_V$ ) and reverse salt flux ( $J_S$ ) were calculated as follows:

$$J_V = \frac{\Delta V}{A_m \Delta t} = \frac{\Delta m / \rho}{A_m \Delta t} \quad (2-5)$$

$$J_S = \frac{\Delta(C_t V_t)}{A_m \Delta t} \quad (2-6)$$

Where  $\Delta m$  is the weight change of the draw solution,  $A_m$  is the effective surface area, and  $C_t$  and  $V_t$  are the salt concentration and volume of the feed solution after the process, respectively.

The elemental composition of the virgin and functionalized membranes was determined by X-ray photoelectron spectroscopy (XPS, SK-Alpha). Samples were irradiated with a beam of

monochromatic Al K $\alpha$  X-rays with an energy of 1.350 keV. Changes in the functional groups of the samples during the chemical reaction were studied using attenuated total reflectance-infrared spectroscopy (Nicolet 6700 / Smart iTR), which was conducted using a germanium crystal on desiccator-dried samples. The surface morphology of the membrane was observed by field-emission scanning electron microscopy (FE-SEM; JEOL, JSM-7600 TFE) to verify the presence of GO/Ag nanocomposite. Prior to imaging, the surface of the membranes was coated with a thin layer (15 nm) of carbon; the carbon was sputtered onto the layers by carbon evaporation (EDWARDS AUTO306). Roughness parameters of the membranes were determined using atomic force microscopy (AFM, Dimension 3100) in the tapping mode.

The surface hydrophilicity and surface energy of the membranes were evaluated through contact angle measurements of DI water using the sessile drop method (VCA, video contact angle system, AST Products, Inc., Billerica, MA, USA). The right and left angles of the water drop were measured using the system software (VCA optima XE). At least three desiccator-dried samples and approximately five points for each sample were selected for contact angle measurements. The data were averaged between the samples. The relative wettability of the membranes was evaluated by calculating the membrane-liquid interfacial free energy<sup>105, 106</sup> as

$$-\Delta G_{ML} = \gamma_L (1 + (\cos \theta)/r) \quad (2-7)$$

where  $\theta$  is the average contact angle,  $\gamma_L$  is the pure water surface tension (72.8 mJ/m<sup>2</sup> at 25° C) and  $r$  is the roughness area ratio (ratio of the actual surface to the planar surface area for rough materials,  $r = 1 + SAD$ ; SAD is the surface area difference parameter obtained from AFM measurements).

The streaming potential of the virgin and functionalized membranes, as an indicator of membrane surface charge, was measured using an electrokinetic analyzer (EKA Anton Paar) at various pH values with a 1 mM KCl electrolyte solution. The procedure and calculations followed the method described by Walker *et al.*<sup>107</sup>.

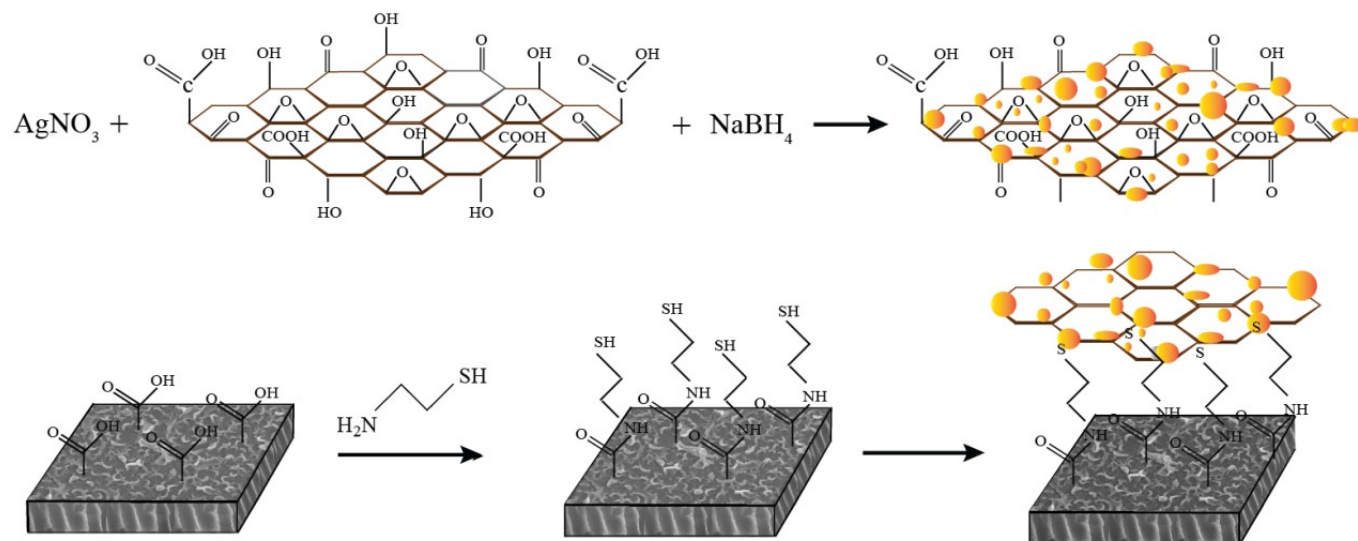


Figure 9 covalently bonded AgNP-decorated GO nanosheets through click chemistry on TFC FO membranes: (A) in situ AgNPs synthesized onto the GO nanosheets, (B) amide forming reaction and thiol functionalization of the TFC FO membrane, and (C) covalent binding of the GO/Ag nanocomposite to the TFC FO membrane surface.

#### 2.2.4 Antimicrobial Activity of GO/Ag Functionalized Membranes

Bacterial inactivation was evaluated by determining and comparing the number of viable bacteria present on surfaces of virgin and functionalized membranes through a simple plate counting method. Briefly, *Escherichia coli* (PGEN-GFP (LVA) ampR) was grown overnight at 37° C in Luria-Bertani (LB) broth medium. The bacterial solution was diluted and cultured for 2 h to reach the log phase and was verified by an optical density measurement at 600 nm. The resulting bacterial solution was centrifuged and washed three times with 0.9% saline solution before being diluted to  $10^7$  CFU mL<sup>-1</sup> in 0.9% saline solution. For the exposure phase, 1.5 cm<sup>-2</sup> membranes were punched and placed in a plastic holder with the active layer facing the bacterial solution. The holders were maintained at room temperature for 1 h. After 1 h of incubation, the excess solution was discarded, and the membranes were washed with a sterile saline solution. To

remove attached bacteria from the membrane surface, the membrane coupons were bath-sonicated for 7 min in a 10 mL isotonic solution. Finally, 100  $\mu$ L serial dilutions (representing over 6 orders of magnitude) of the bacterial solution were spread on LB agar plates with ampicillin and incubated overnight at 37°C. The number of colonies was then counted.

### 2.2.5 Silver Release Experiments

The reservoir method was used to measure the silver ion loading and releasing from GO/Ag functionalized membranes<sup>40</sup>. For ion releasing measurements, both the functionalized and virgin membrane samples were cut into 1 inch coupons and incubated in 20 mL of DI water for 24 h; the samples were then acidified with 1% HNO<sub>3</sub>. The silver loading was conducted with a similar procedure, but the solution was acidified prior to incubation. Silver ion concentrations in the samples were then measured by inductively coupled plasma mass spectroscopy (ICP-MS Perkin Elmer NexION 300X). The ion release experiments for both the control and functionalized membrane were conducted for 6 days.

## 2.3 Results and Discussion

### 2.3.1 Successful Graphene Oxide/ Silver Nanocomposite Synthesis Confirmed by UV-Vis, TEM, TGA and XRD Analyses

The GO/Ag nanocomposite was synthesized through the in situ reduction of silver nitrate onto GO nanosheets and was characterized by UV-Vis, XRD, TGA and TEM (Figure 1). The UV-Vis spectra of GO, Ag nanoparticles, and GO/Ag suspension indicates the formation of a nanocomposite (Figure 10 A). GO exhibits two different characteristic bands at 230 nm, corresponding to the electronic  $\pi$ - $\pi^*$  transition of the C=C aromatic bond and a shadow shoulder at 305 nm assigned to the  $n$ - $\pi^*$  of C=O bonds. Additionally, AgNPs exhibit a band at 400 nm in the absorption spectrum, which is attributed to a surface plasmon. The UV-Vis spectrum of GO/Ag shows both characteristic GO and Ag bands and verifies the formation of GO/Ag nanocomposites. The presence of AgNPs in the GO/Ag nanocomposite was also confirmed through XRD measurements. GO/Ag XRD patterns (Figure 10 B) represent the prominent Bragg peaks at  $2\theta$  values of 38.1°, 44.3°, 64.5°, and 77.5°, assigned to the (1 1 1), (2 0 0), (2 2 0) and (3 1 1) crystallographic planes of face-centered cubic (fcc) AgNPs, respectively. The peak at  $2\theta = 10.1^\circ$  of GO nanosheets (attributed to the stacking of the GO layer) was completely removed because the anchoring of AgNPs on the surface of the GO sheets prevented the restacking of the

layered structure of GO<sup>100</sup>. The formation of GO/Ag nanocomposite was also reflected in the TGA (Figure 10 C). Graphene oxide exhibits a two-step decomposition. The first drop appears at 220°C and is attributed to the decomposition of labile oxygen containing functional groups, and the second drop occurs at 550°C and is attributed to the pyrolysis of the carbon skeleton of GO. However, AgNPs do not show a decomposition step in the TGA. For the GO/Ag nanocomposite, the combination of the two different behaviors is observed, and the mass ratio of GO and Ag can be estimated in the final composite.

The morphological features of the GO/Ag nanocomposite were investigated by HRTEM. TEM images revealed a well-dispersed layer of spherical AgNPs decorating the surface of the GO nanosheets (Figure 10 D). The results indicate that GO plays a decisive role in the nucleation and growth of Ag nanoparticles, and the presence of GO and its functional groups act as a morphological driver/controller for silver NPs, preparing for the formation of the spherical NPs. The oxygen containing functionalities on the GO surface provides reactive sites for the nucleation and growth of AgNPs. However, the AgNPs synthesized without GO and without using any capping agent displayed an aggregated morphology (additional TEM images of GO, Ag NPs and GO/Ag nanocomposites are provided in the Supporting Information in Figure 16).

### *2.3.2 Graphene Oxide/ Silver Nanocomposites were Covalently Bonded to the Surface of the TFC Polyamide Membrane*

The enhanced stability of the functionalized GO/Ag nanocomposite on the membrane surface was obtained using a cysteamine linker with amine and thiol functional groups at each end. The amine group reacts with the un-reacted acyl chloride functional groups on the surface of the TFC membrane from interfacial polymerization. The presence of acyl chloride groups was verified by an elemental analysis using an XPS method on the surface of a pristine membrane. Cl2p has a peak of approximately 198 eV (Figure 19, supporting information), and the area below that peak is estimated to be approximately 1% Cl element by weight. XPS results for the cysteamine treated membrane also indicated that all acyl chlorides were consumed during the reaction, the Cl content of the surface became zero, and the new surface showed the presence of sulfur, which displays a peak at 162 eV (Figure 19, supporting information). The thiol groups on the membrane surface would react with and anchor AgNPs<sup>108</sup>. AFM images (Figures 11 C and D) reveal that after GO/Ag nanocomposites bonded onto the TFC membrane surface, both the

surface roughness and surface morphology of the membrane significantly changed. The graphene oxide nanosheets flattened the surface of the membrane; therefore, the overall roughness decreased (Supporting information, Table 1). The SEM images further confirm the change in the morphology of the GO/Ag functionalized membrane surface when compared to pristine membranes (Figures 11 A and B). As shown in Figure 11 B, the spherical AgNPs are distributed predominantly on the surface of the GO nanosheets and less on the edge or within the valley-like region of the TFC membrane surface. Higher contrast images of AgNPs and membrane surfaces were obtained using backscattered electron microscopy (BCE); the images are provided in the supporting information (Figure 15). The BCE images verified the presence and uniform distribution of AgNPs on the surface of GO and TFC membranes. The size and shape of the AgNPs observed also agreed with the TEM observations (Figure 10).

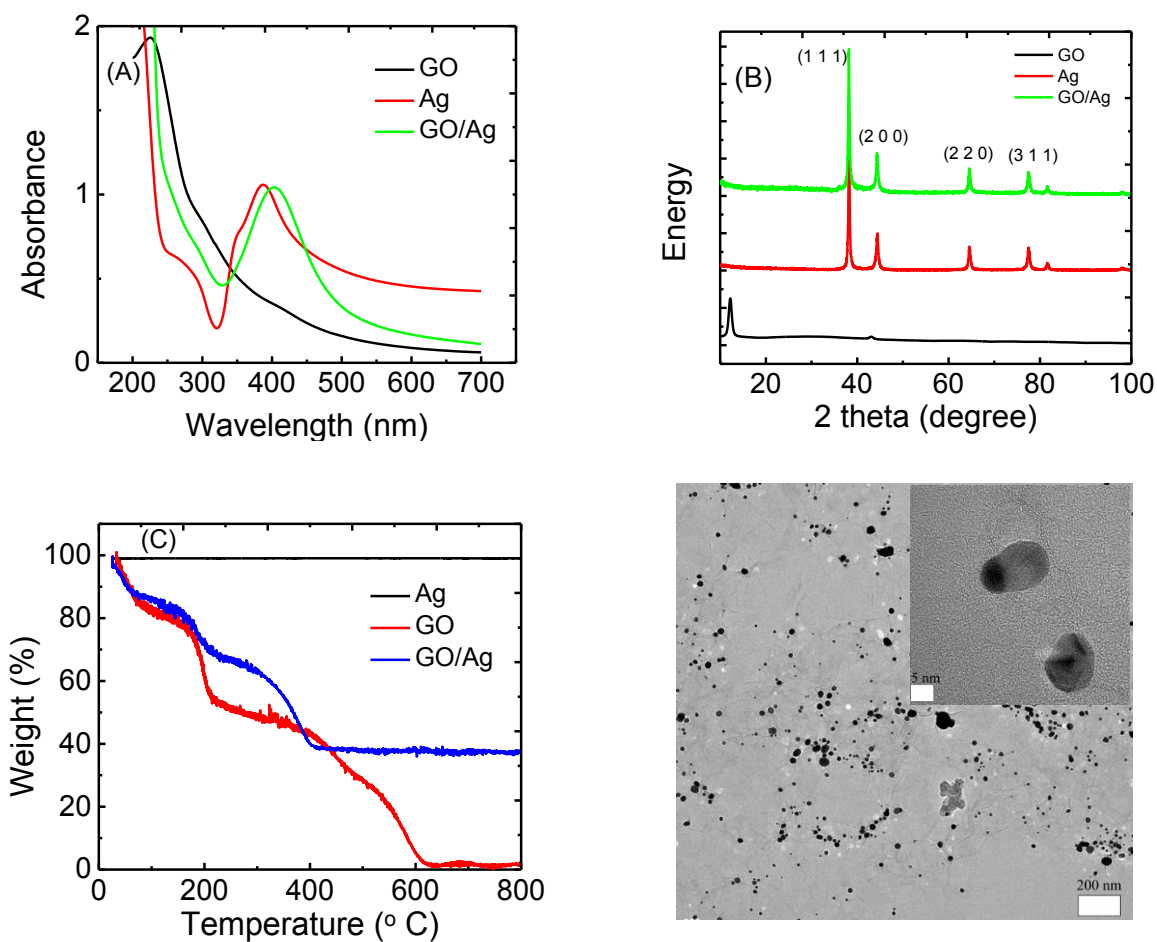


Figure 10 Characterization of the GO/Ag nanocomposite. (A) UV-Vis spectra, (B) XRD patterns, (C) thermogravimetric curves for Ag NPs, GO nanosheets, and GO/Ag nanocomposites, and (D) HR-TEM images of the GO/Ag nanocomposite.

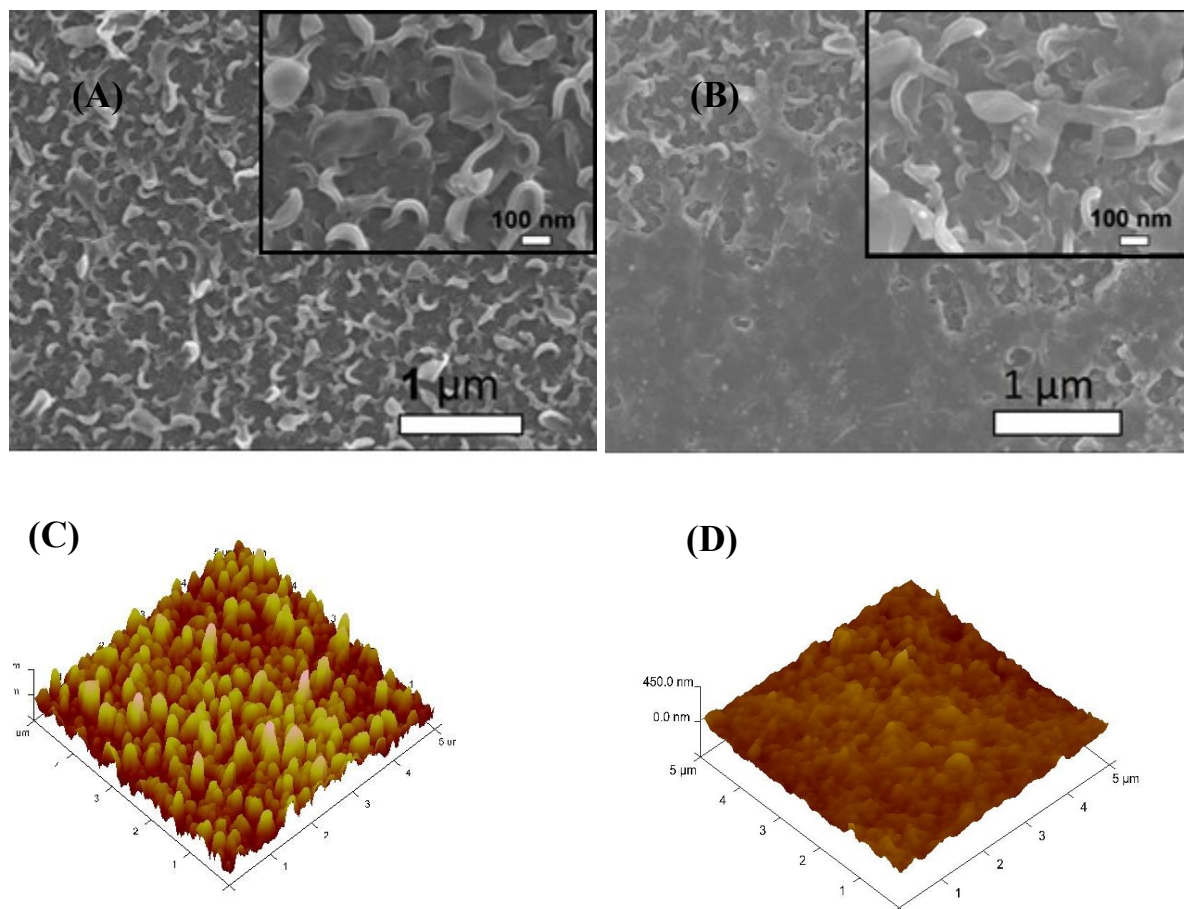


Figure 11 FESEM images of (A) the polyamide active layer of the TFC membrane and (B) the GO/Ag functionalized polyamide active layer of the TFC membrane. AFM images of (C) the TFC membrane and (D) the GO/Ag functionalized TFC membrane.

The progress of the reaction was also studied using the ATR-FTIR method. The ATR-FTIR spectra in Figure 13C (details in the supporting information Figure 17) show that after treating the TFC membranes with cysteamine, the intensity of the peak at  $850\text{ cm}^{-1}$  (C-Cl bond in the stretching mode) decreased, indicating the consumption of the acyl chloride group, and a new peak at  $1020\text{ cm}^{-1}$  appeared, which can be attributed to the formation of a new aliphatic amine C-N bond in the stretching mode. Additionally, the TFC membranes have two small peaks located at  $1147\text{ cm}^{-1}$  and  $1585\text{ cm}^{-1}$  that are assigned to the C-O-C stretching and the phenyl ring vibration of the polysulfone support layer, respectively. These results verify the binding of the

GO/Ag nanocomposite onto the surface of the TFC membranes. A Raman spectroscopy analysis was conducted to characterize disordered carbonaceous materials such as GO nanosheets. In comparison with the virgin TFC FO membrane, which displays no characteristic peak in the Raman spectra, the GO/Ag is represented by two strong characteristic peaks at  $1320\text{ cm}^{-1}$  (D band) and  $1570\text{ cm}^{-1}$  (G band) with 532 nm laser excitation. The Raman spectroscopy results indicate the presence of the GO/Ag nanocomposites on the surface of the TFC FO membranes.

The physical stability of the GO/Ag nanocomposite bonded to the TFC membranes was evaluated through an XPS analysis. To investigate the role of GO in stabilizing the silver NPs on the membrane surface, the membranes functionalized with AgNPs (synthesis procedure is provided in supporting information) and GO/Ag nanocomposites were sonicated for 7 min, and the silver content of each membrane (after sonication) was estimated in an XPS analysis. Metallic Ag  $3d$  peaks are centered at 373.9 and 367.9 eV, consistent with the reported values<sup>109</sup>. Although more Ag was loaded on the membranes decorated with Ag NPs than on GO/Ag functionalized membranes, the Ag loss by physical stress was enhanced by using GO as a support for Ag NPs. In total, 50 percent of the Ag NPs were lost during sonication, whereas only 6 percent were lost from GO/Ag functionalized membranes (Figure 20, supporting information).

### *2.3.3 Membrane Transport Properties were not Significantly Affected by GO/Ag Functionalization*

The FO process is operated without applying any high transmembrane pressure. Therefore, any surface modification may influence the membrane permselectivity properties, unlike other pressure-driven membrane processes. The intrinsic transport properties of the membrane, *i.e.*, pure water permeability (A) and salt permeability (B), were evaluated in a RO mode experiment. The water flux and reverse salt flux of a 1 M NaCl solution in the FO mode were also evaluated to determine the effect of GO/Ag nanocomposite functionalization on the performance of the TFC FO membrane. Both the pure water permeability (A) and salt permeability coefficient (B) of the functionalized TFC membrane did not significantly change from those of the control TFC membranes. The pure water permeability decreased by approximately 6%, and the salt permeability coefficient increased by 13% (Figure 13 A). Because the cysteamine treatment has no adverse effect on the membrane performance<sup>46</sup>, the change in pure water permeability and salt permeability coefficient can be attributed to the

formation of a barrier layer of GO/Ag, which can hinder water flux. The water flux of TFC membranes in the FO mode slightly decreased after modification (2% decrease), and the value of the reverse salt flux increased by approximately 20% (Figure 4B). These changes may be attributed to the formation of an additional layer on the surface of the membrane, which may act as a barrier and decrease the water flux. Moreover, the

GO nanosheets possess frictionless surfaces which can affect the formation of an internal boundary layer, changing shear stresses and thus affecting membrane transport properties (since there is no external pressure applied in FO process). Also the presence of silver nanoparticles on the membrane surface, which can release positively charged Ag ions, can change the charge distribution and charge interactions between feed solution and membrane surfaces interface. These two factors can affect the membrane transport properties in FO mode.

According to the contact angle measurements, Figures 13 C and 13 D show the water contact angle of the membrane decreasing from 55° for the virgin TFC FO membrane to 24° for the functionalized membrane, indicating that the GO/Ag functionalization provides a highly hydrophilic surface. This change in hydrophilicity of the membrane with GO/Ag functionalization is attributed to the presence of hydrophilic oxygen-containing functional groups on the GO nanosheets. Additionally, the hydrophilicity is a critical factor for controlling the fouling of the FO membranes. The surface zeta potential, the type of charge, and the density of the exposed charge are the other crucial parameters that determine the fouling properties of the membrane. The observed zeta potential (Figure 18 in the supporting information) for a pristine TFC PA membrane agreed with the protonation behavior of polyamide functional groups. At a low pH, the unreacted amine groups remaining after the interfacial polymerization (characterized by a broad peak at 3500 cm<sup>-1</sup> in the ATR-FTIR spectra in Figure 12 C) were protonated, whereas the carboxylic groups remained unchanged. As the pH increased to a value above the pK<sub>a</sub> of the carboxylic group, these groups were deprotonated, and the surface charge of the membrane became negative and remained constant<sup>110</sup>. By functionalizing the surface with GO/Ag nanocomposites, the protonation of the unreacted amine groups occurred in a similar manner when the pristine TFC membrane was immersed in a low pH solution. At higher pH values, however, numerous carboxylic groups were present on the surface of the GO nanosheets, and

thus, deprotonation occurred to a higher extent than for pristine membranes. As a result, functionalized membranes impart more negative charges.

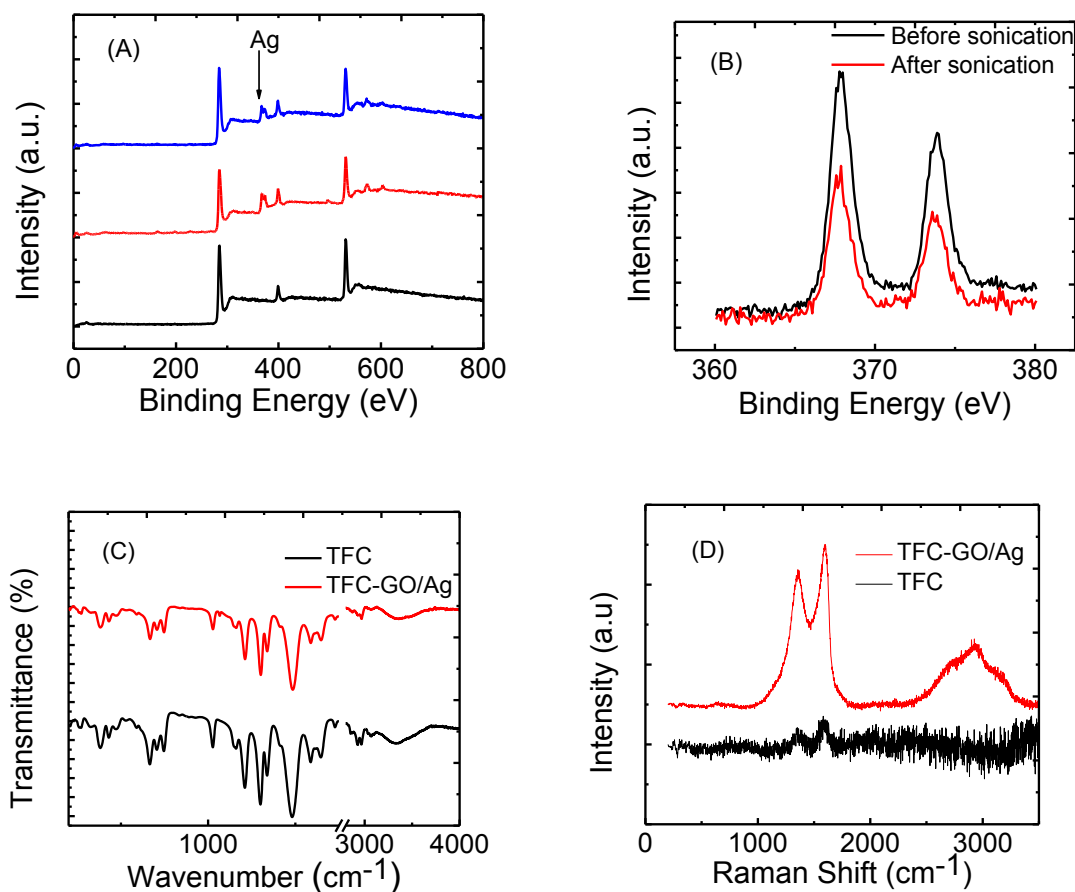


Figure 12 Surface characterization of virgin and functionalized TFC FO membranes: (A) XPS analysis of the TFC (black), GO/Ag nanocomposite functionalized membranes before (red) and after (blue) sonication, (B) XPS analysis at a higher magnification, (C) ATR-FTIR spectra of the virgin and functionalized TFC membranes, and (D) Raman spectra of the control and functionalized TFC membranes.

#### 2.3.4 The Functionalized Membrane Exhibited Strong Antimicrobial Activity

As reported elsewhere,<sup>111</sup> microbial inactivation occurs through a three-step mechanism. The primary step is cell deposition onto the carbon-based nanomaterials. Similar to single-wall

carbon nanotubes, graphene oxide inactivates bacteria by direct cell contact and membrane damage<sup>112</sup> and through charge transfer and formation of reactive oxygen species<sup>113</sup>. Silver nanoparticles also exhibit significant antimicrobial properties through different proposed mechanisms such as the following: *i*) releasing Ag<sup>+</sup> ions, which strongly bind to thiol groups in enzymes and proteins on the cellular surface and cause destabilization of the membrane and cellular walls; *ii*) attaching to the surface of the bacteria and producing holes in the membrane and cellular wall, allowing the AgNPs to penetrate into the bacteria; or *iii*) producing reactive oxygen species under oxidizing conditions that are capable of irreversibly damaging cellular DNA replication<sup>113</sup>. In the case of the GO/Ag nanocomposite, a synergetic phenomenon in bacterial inactivation is observed, which is called the capture-killing mechanism<sup>111</sup>. Graphene oxide plays an important role as a support for the AgNPs and prevents the AgNPs from agglomerating. The GO also dictates a spherical morphology to the AgNPs and thus provides a larger active surface area, a shape that results in higher antimicrobial activity. In addition, the graphene oxide displays the ability to capture bacteria on its surface<sup>111, 114</sup>, which, for the GO/Ag nanocomposite, results in a higher chance of bacterial inactivation by AgNPs. Additionally, graphene oxide can rupture the membrane wall because of its sharp edges<sup>112, 115</sup>.

Using *E. coli* (GFP level 1) as a model organism, the antimicrobial activity of control and functionalized TFC membranes was investigated in static bacterial inactivation tests. The results show that even over a short period of contact (*i.e.*, 1 h), the GO/Ag nanocomposite functionalized membranes significantly reduced the number of viable *E. coli* cells by 96%, which is higher than that of either independent graphene oxide or AgNP functionalized membranes (Figure 14). To better understand the synergetic effects of the GO nanosheets and AgNPs in GO/Ag nanocomposites, TFC functionalized membranes with AgNPs and GO were prepared and examined in an antibacterial analysis. The results show significant differences in bacterial inactivation of the three modified membranes. Silver NP modified membranes displayed a 60% inactivation, whereas GO nanosheet functionalized membranes displayed an approximately 40% bacterial inactivation. Silver decorated graphene oxide showed a remarkably high inactivation (approximately 96%). These results can be attributed to a synergetic effect of the combination of silver NPs and graphene oxide, which have different approaches to bacterial inactivation. GO/Ag nanocomposites can inactivate bacteria not only through silver ions being released and penetrating into the cells<sup>113</sup> but also through the sharp edges of GO nanosheets

rupturing the membrane wall<sup>112</sup>. The biocidal effect of cysteamine was also studied as a control sample. In comparison with the TFC membrane, a negligible biocidal effect was observed resulting from the cysteamine.

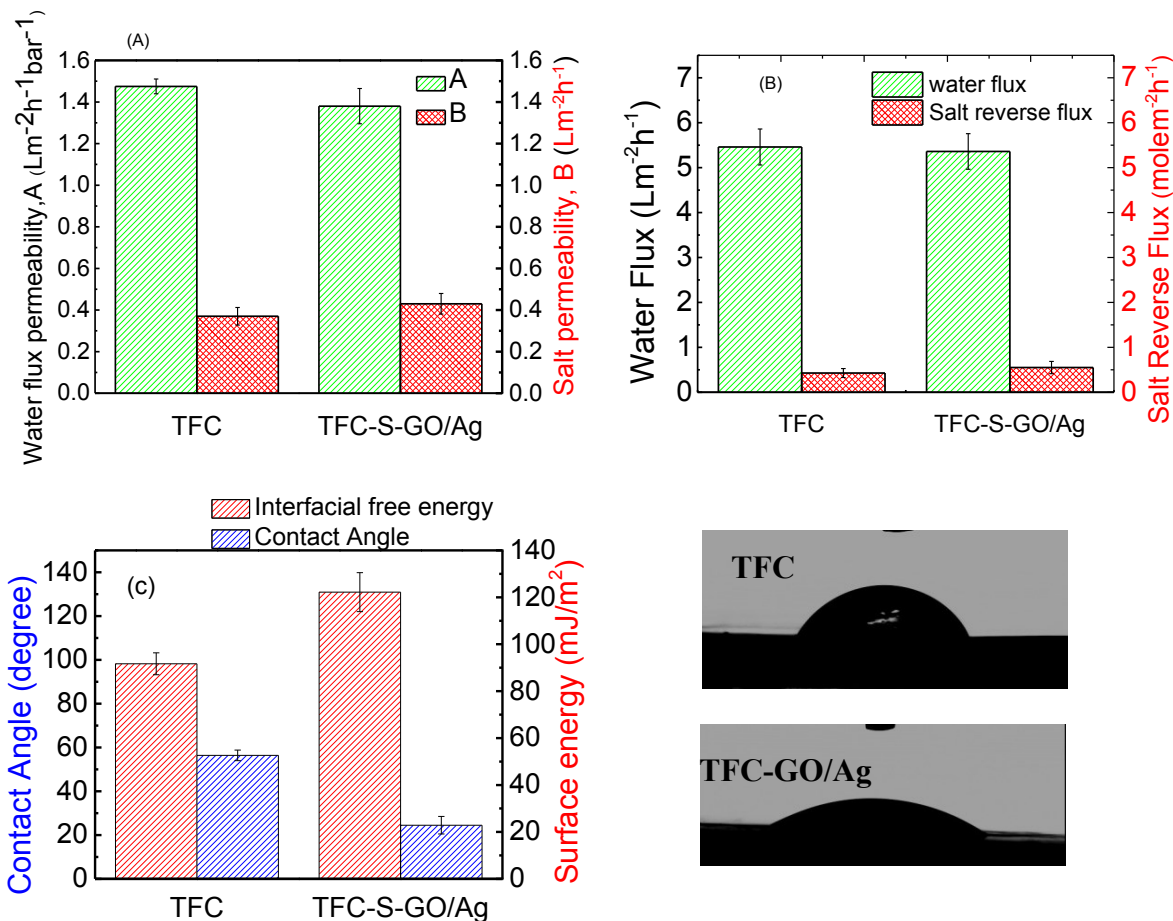


Figure 13 Membrane properties before and after modification. (A) The water permeability and salt permeability of the TFC and GO/Ag functionalized TFC membranes (in the RO mode). (B) The water flux and salt reverse flux (in the FO mode) of the TFC and GO/Ag functionalized TFC membranes. (C) The water contact angle of the TFC and GO/Ag functionalized TFC membranes. (D) Water droplets on the TFC and GO/Ag functionalized TFC membrane surfaces.

### *2.3.5 Silver Ion Release Behavior was Different for Composite and only AgNP Modified Membranes*

The silver ion loading and release behavior were analyzed by ICP-MS. To investigate the effect of the GO support on the release of AgNPs, AgNP decorated TFC membranes were compared with a GO/Ag functionalized membrane. The reactant concentration of AgNPs during synthesis was constant to allow for rational comparisons. The results show that the silver content for the AgNP decorated membranes (13.38  $\mu\text{g/L}$ ) was approximately three times greater than that for the GO/Ag decorated membrane (5  $\mu\text{g/L}$ ), agreeing with the XPS elemental composition. However, the release behavior of these two functionalized membranes was different. Whereas silver ions are released moderately over time for the AgNP decorated membrane, the release of silver ions from the GO/Ag decorated membrane occurred immediately in the first day and remained constant with time (Figure 14 B). However, the bacterial inactivation results indicate that the GO/Ag decorated membranes were more effective compared with GO and AgNP functionalized membranes. These results indicate that the Ag decorated membranes can inactivate bacteria by releasing ions; however, the GO/Ag functionalized membranes can release ions and rupture cells because of the sharp edges of the GO nanosheets, enhancing the bacterial inactivation. The synergetic performances for the GO/Ag functionalized membrane can be attributed to the combined mechanisms of bacterial inactivation that have been engendered by the GO nanosheets and silver NPs. Although the results of this paper are comparable to other publications<sup>19, 40</sup> with regards to the silver loading and releasing rate, the earlier defined regeneration process should be incorporated for practical long-term real-world applications. Because the membrane is functionalized with GO, the regeneration process can be accomplished easily through the in situ synthesis of AgNPs (information regarding the membrane preparation is provided in the supporting information).

## **2.4 Conclusions**

GO/Ag nanocomposite functionalization of TFC FO membranes provides an effective antimicrobial surface that has better characteristics than either GO or AgNPs independently. This enhanced effectiveness likely results from the synergistic effect of the capture-killing mechanism displayed by this system. In addition, the higher hydrophilicity of the resulting membranes, the low material cost, and the ease of preparation (dip coating method) result in a more efficient and effective approach than other modification methods. Finally, using graphene oxide as a support

for biocidal metal nanoparticles provides an opportunity for the regeneration of biocidals after release. However, additional studies must be conducted to examine the in-situ regeneration of the GO/Ag nanocomposite to fully exploit this potential.

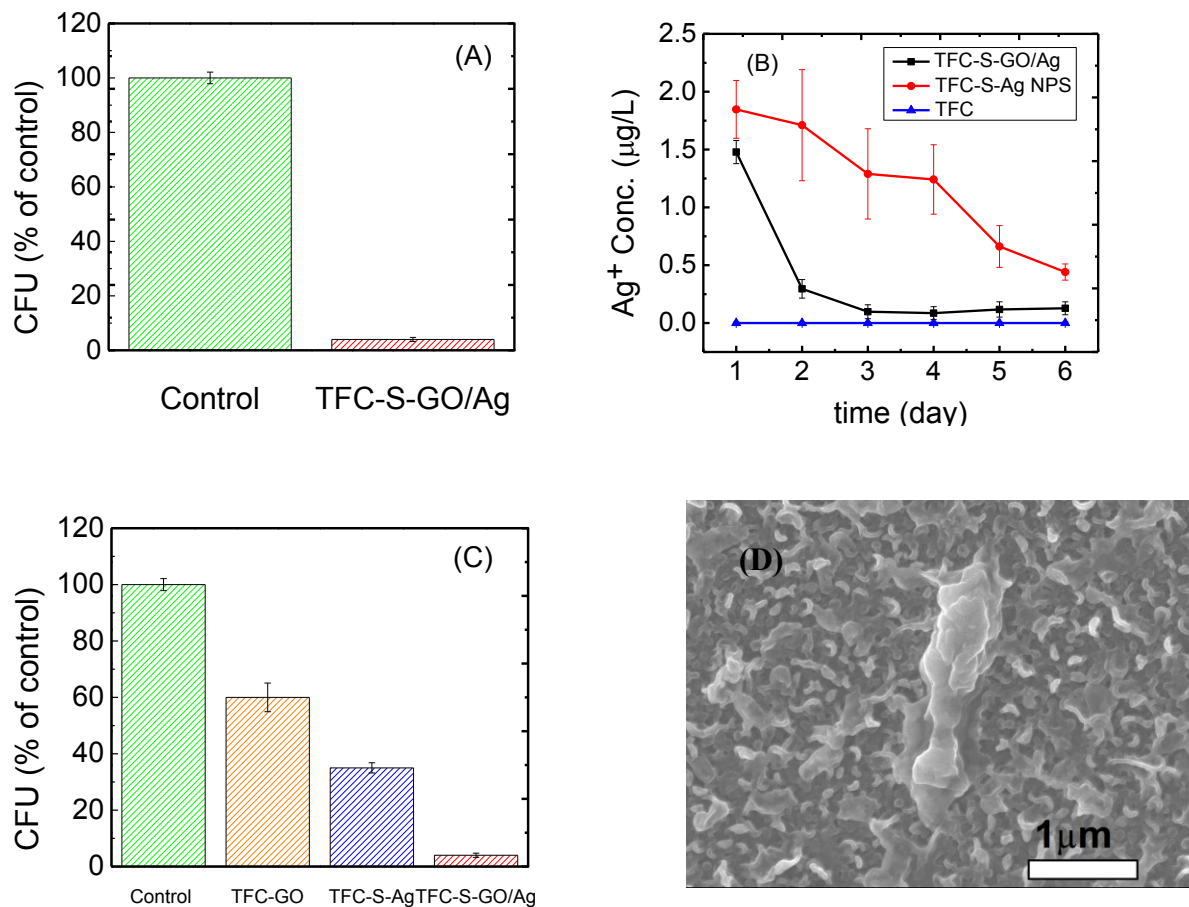


Figure 14 Colony-forming units (CFU) after *E. coli* cells had been in contact with the control and GO/Ag functionalized membranes for 1 h at room temperature: (A) CFU for the virgin and GO/Ag functionalized membranes, (B) the silver ion release rate from the GO/Ag functionalized membranes, (C) CFU for the virgin, GO, AgNPs, and GO/Ag functionalized TFC membranes, and (D) an SEM image of the inactivated bacteria on the GO/Ag functionalized TFC membrane.

## 2.5 Supporting Information

### 2.5.1 *Materials and Methods*

Two series of functionalized membranes were prepared to investigate the synergetic effects of combining GO nanosheets with Ag NPs. Ag NPs were synthesized by chemically reducing silver nitrate with sodium borohydride. In this study, 10 mL of 5 mM sodium borohydride was added dropwise to 100 mL of 5 mM silver nitrate solution. During this process, the reaction medium was placed in an ice bath and stirred vigorously. The combined effect of low medium temperature and dropwise addition helped the formation of fine nanoparticles. The Ag NPs suspension was kept in a dialysis bag for two days. Next, the suspension was centrifuged for 30 min, washed three times, dried overnight in an oven, and then re-suspended in DI water. Similar to the conditions explained in the manuscript, the TFC membranes were also treated with cysteamine. This step was followed by dip-coating them in the Ag NPs suspension for 12 hr in a shaker at a speed of 100 rpm. The membranes were then washed three times by DI water. The GO functionalized TFC membranes were prepared by the dip-coating method, where 50 mg of GO nanosheets were added to 100 mL of DI water, followed by sonication for 30 min at 70% maximum power output.

To ensure durable covalent bonding of GO onto the TFC membrane, a previously published protocol was adapted from Perreault et al.<sup>78</sup>. Briefly, carboxylic groups of the polyamide were first converted to amine-reactive esters by direct contact of the membrane surface with 1-ethyl-3-[3-(dimethylamino) propyl]carbodiimide hydrochloride (EDC) and N-hydroxysuccinimide (NHS). An amide formation reaction with a reactive ester was used to bond ethylenediamine to the active membrane layer surface. The GO nanosheets were functionalized with EDC-NHS to free the amine groups of ED from the membrane surface. The steps are as follows: First, 4 mM EDC, 10 mM NHS and 0.5 M NaCl were dissolved in 10 mM MES buffer. The solution was adjusted to pH 5 with HCl and NaOH. The solution was then put in contact with the membrane surface for 1 h. Next, the membranes were washed and rinsed with DI water three times and then submerged in a solution of 10 mM ED, 0.15 mM NaCl in 10 mM HEPES buffer at pH 7.5. Finally, the membrane surface was washed with DI water to remove any unlinked ED.

Next, 100 mg of the GO nanosheets were exfoliated by dispersing them in 100 mL of 10 mM MES buffer at pH 6 and probe sonicating them for 15 min. This process also helped to prepare a stable suspension. Just before contacting the GO suspension (pH 7.5) with the ED functionalized TFC FO membranes, 2 mM EDC and 5 mM NHS were added to the suspension. The GO functionalized membranes were washed, rinsed three times, and stored in DI water at 4°C until use.

### 2.5.2 Nanoparticles and Nanocomposites Characterization

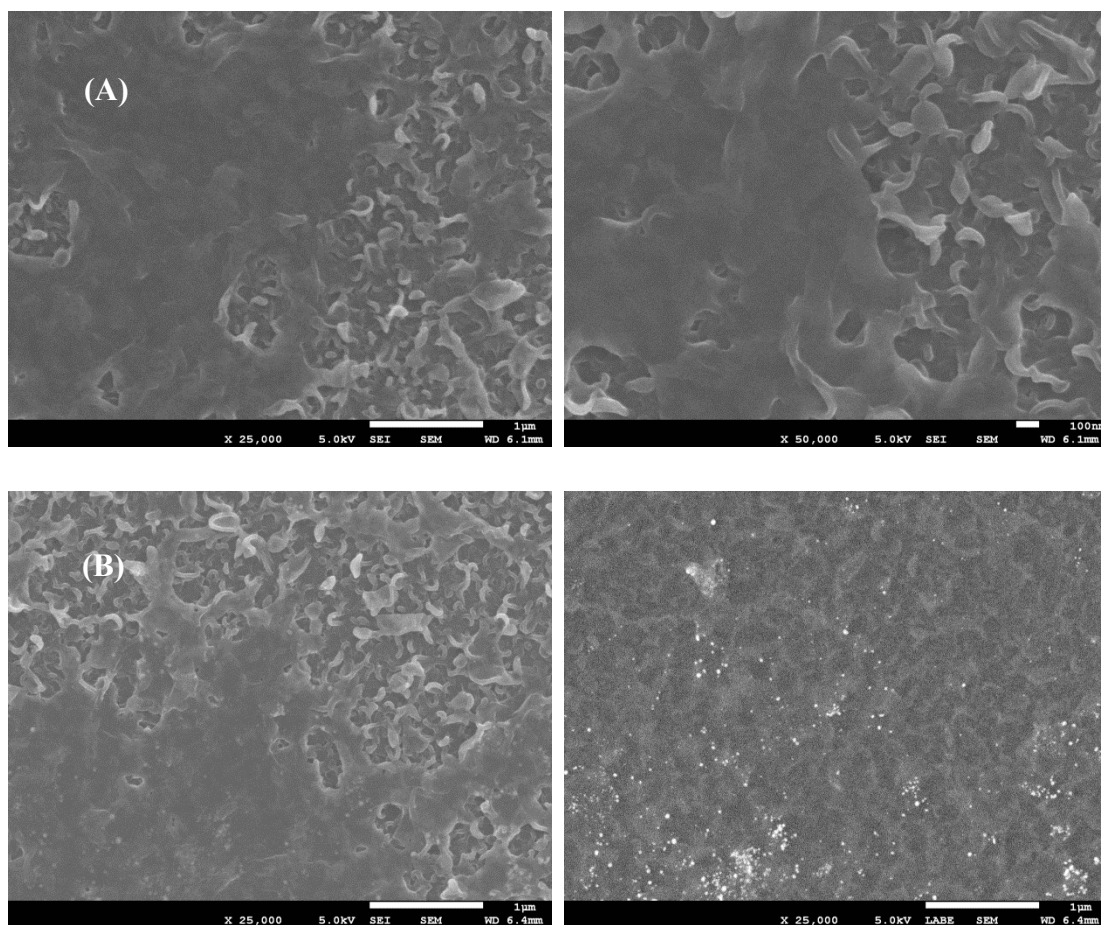
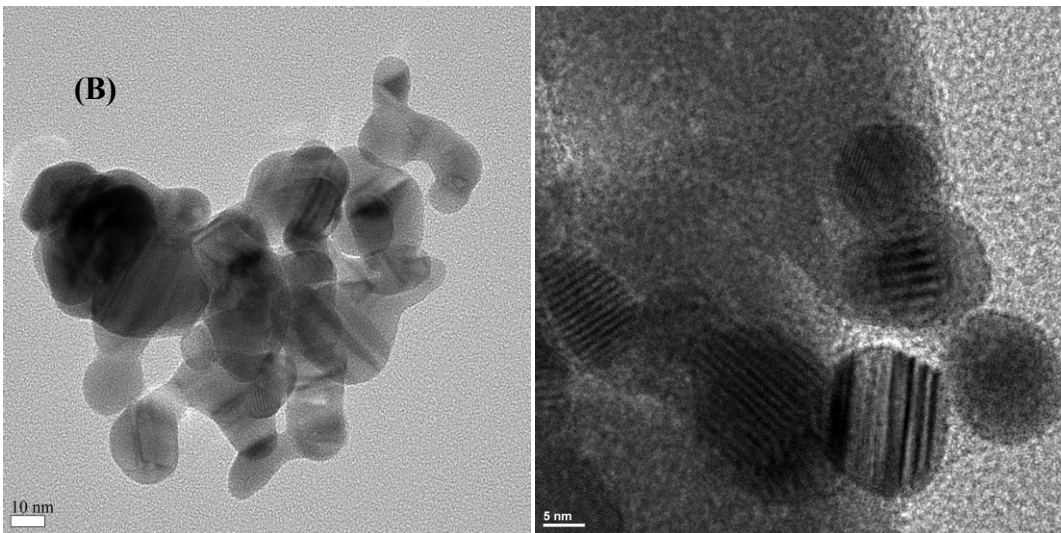
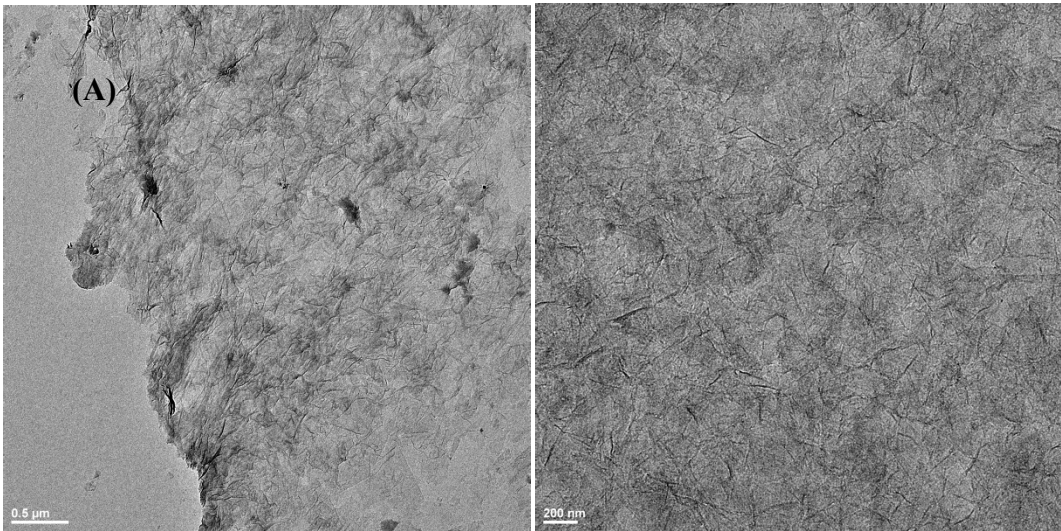


Figure 15 FE-SEM images and backscatter electron imaging for (A) GO functionalized TFC, and (B) GO/Ag nanocomposite functionalized TFC. Elements with higher atomic numbers backscatter electrons more strongly than elements with lower atomic numbers and, therefore, appear brighter on the image.



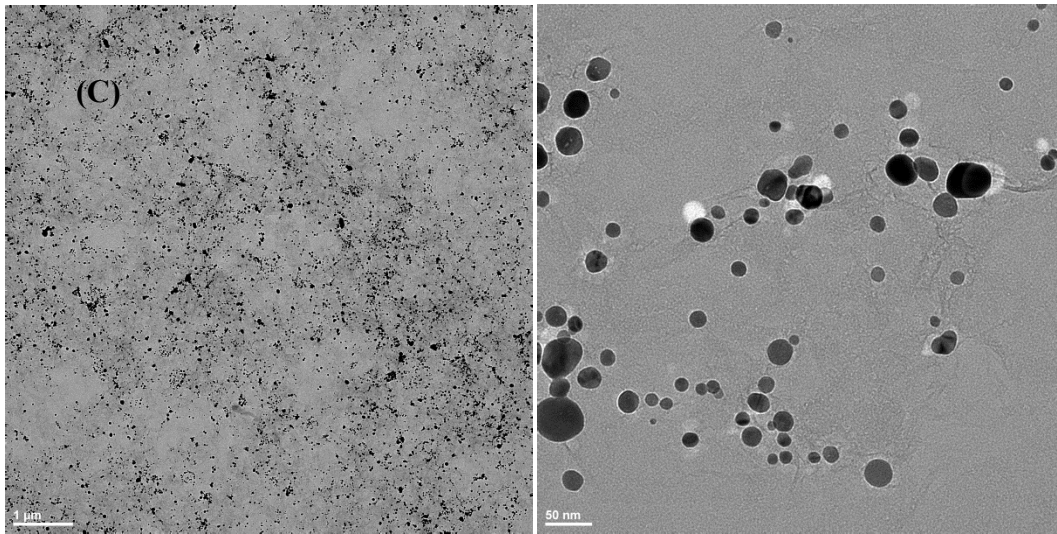


Figure 16 TEM images of (A) GO, (B) Ag NPs, (C) GO/Ag nanocomposite

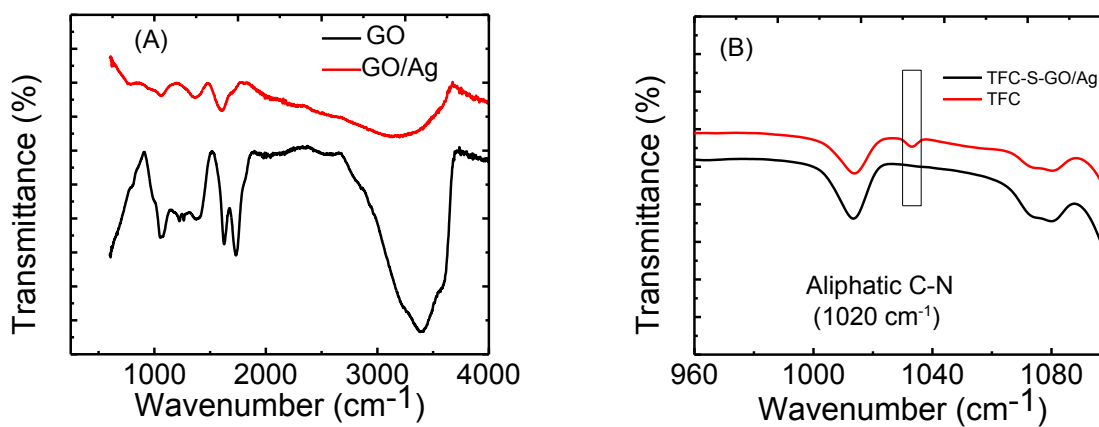


Figure 17 ATR-FTIR spectra of (A) GO nanosheets and GO/Ag nanocomposite, and (B) Control TFC and GO/Ag nanocomposite functionalized TFC membranes.

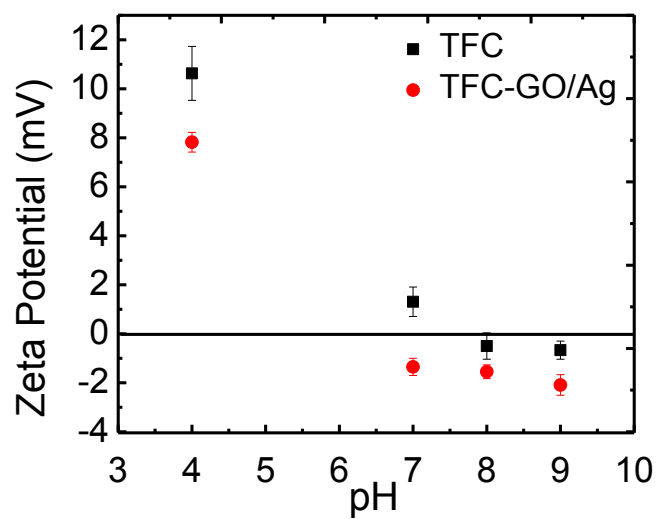


Figure 18 Zeta potential of the surface of the pristine and functionalized membranes as a function of solution pH. Measurements were taken at room temperature (23°C) in a solution of 1 mM KCl, by adjusting the pH with dropwise addition of HCl and NaOH.

Table 1 Surface roughness properties of the pristine and the GO/Ag functionalized TFC FO membranes

Sample	$R_{\max}$ (nm)	$R_a$ (nm)	$R_q$ (nm)	SAD (%)
TFC FO	$486 \pm 22$	$52.2 \pm 0.5$	$65.5 \pm 1.5$	$67.4 \pm 2.1$
TFC-GO/Ag	$310 \pm 33$	$25.2 \pm 2.8$	$35.2 \pm 4.24$	$13.2 \pm 1.2$

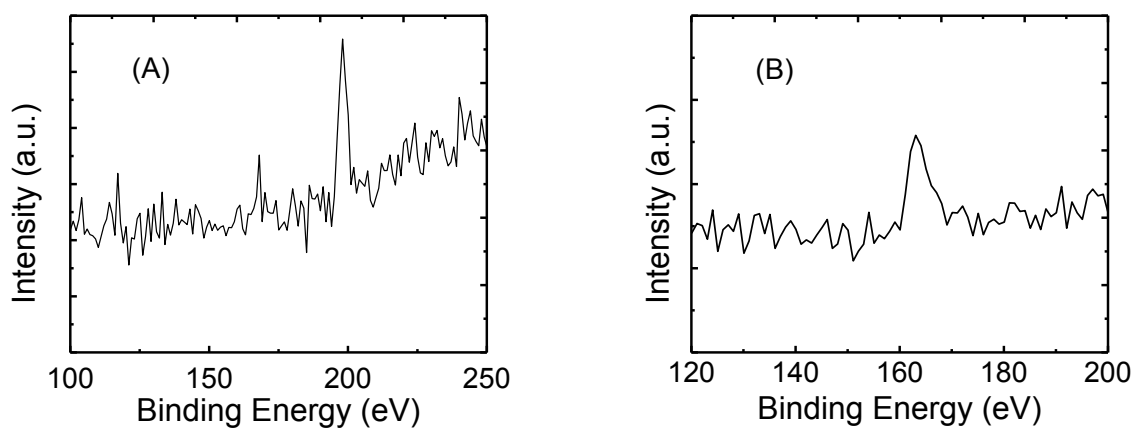


Figure 19 XPS results for (A) pristine membrane, and (B) cysteamine treated TFC FO membranes. The peaks at 198 eV for Cl2P and at 162 for Sulfor S2P are shown in (A) and (B), respectively.

Table 2 Elemental composition by XPS analysis of the membrane surface of pristine and functionalized membranes, before and after sonication.

Sample	C (%)		O (%)		N (%)		S (%)		Ag (%)		Cl (%)	S (%)
	Before	After	Before	After	Before	After	Before	After	Before	After		
TFC	71.95±0.44	-	21.19±1.59	-	6.86±1.34	-	-	-	-	-	1.5 ± 0.1	0
TFC-GO/Ag	71.8±1.07	69.8±2.25	18.56±0.81	20.28±.8	8.06±0.29	8.98±0.87	1.07±0.07	0.74±0.3	0.5±0.1	0.47±0.19	0	1.12 ± .03

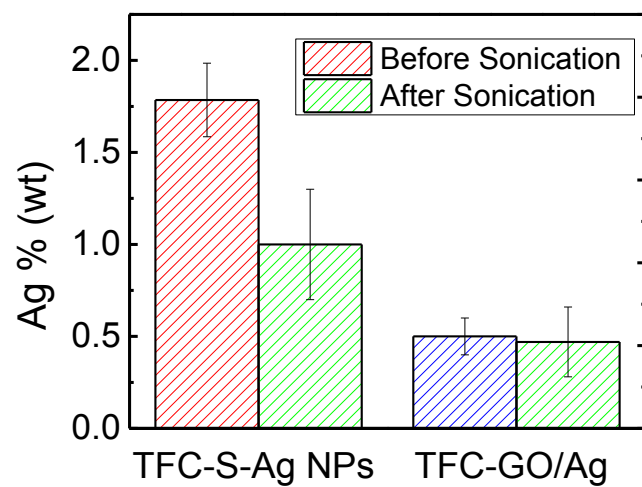


Figure 20 XPS results showing physical stability of silver NPs for Ag NPs decorated and GO/Ag functionalized membranes. 7 min bath sonication was applied to the membranes and silver % present on the surface was measured.

### **3 IN SITU SILVER DECORATION ON GRAPHENE OXIDE-TREATED THIN FILM COMPOSITE FORWARD OSMOSIS MEMBRANES: BIOCIDAL PROPERTIES AND REGENERATION POTENTIAL**

#### **3.1 Introduction**

With increasing application of membrane-based water treatment and desalination processes,<sup>4, 9, 116</sup> attention to fouling and biofouling as major limitations is increasing accordingly. Surface modification is receiving great recognition, among the different methods of fouling and biofouling mitigation, as an effective and flexible approach by providing variable modifiers and procedures.<sup>18, 83, 87</sup> Instead of using modified<sup>20</sup> and biocidal nanoparticles,<sup>21, 91, 117, 118</sup> membrane hydrophilicity can be increased by introducing polymer brushes<sup>19</sup> or hydrophilic polymers<sup>12, 119</sup> for fouling and biofouling control.

Silver nanoparticles (Ag NPs) are one of the most effective biocidal NPs and have been widely investigated in terms of their formation mechanisms,<sup>25, 28, 120, 121</sup> biocidal properties,<sup>23, 33, 113</sup> and their applicability in either membrane surface modification<sup>40, 44, 46-49</sup> or membrane bulk incorporation.<sup>39, 41, 43</sup> Although Ag NPs provide significant and effective biocidal properties, their intrinsic tendency to aggregate, and their fast release in aquatic media have raised concerns as to their long-term efficacy and the possibility of regeneration.<sup>122</sup> The combination of Ag NPs and carbon-based nanomaterials introduces a new class of emerging nanomaterials which offer physical durability and more effective biocidal properties.<sup>56, 123</sup>

Among a variety of carbon-based materials, graphene oxide (GO) nanosheets have attracted great attention because of their special physical and chemical properties.<sup>53</sup> Oxygen-containing functional groups of GO<sup>124</sup> can serve as anchors for the Ag NP nuclei and govern their shape, size, and distribution. GO nanosheets also show extensive biocidal properties and toxicity toward microorganisms<sup>125-127</sup> thus increasing the efficacy of the biocidal properties of

GO-Ag nanohybrids.<sup>71</sup> GO-Ag nanocomposites, among other types of nanohybrids, have attracted attention for antimicrobial applications,<sup>66, 100, 128</sup> and more recently, for the functionalization of nanofiber mats<sup>129</sup> and thin film composite (TFC) forward osmosis (FO) membranes.<sup>130</sup> Although GO-Ag nanocomposites present strong biocidal properties, their application still suffers from drawbacks such as the difficulty of synthesis, limited Ag loading, and lack of regeneration potential.

In continuation of last chapter on the use of GO-Ag nanocomposites for surface modification of FO membranes,<sup>130</sup> this study focuses on using GO nanosheets as a sublayer modifier for *in situ* Ag NP formation on TFC FO membranes to overcome the aforementioned limitations. The effects of the presence of GO on the loading and release of silver, membrane surface hydrophilicity, biocidal properties, and membrane performance were investigated. Finally, the possibility of Ag NP regeneration after depletion in water for seven days was studied.

## 3.2 EXPERIMENTAL

### 3.2.1 Materials

The following chemicals were used as received from Sigma-Aldrich: Silver nitrate (99.9999% trace metal basis), N-(3-Dimethylaminopropyl)-N'-ethylcarbodiimide hydrochloride (EDC), N-Hydroxysuccinimide (NHS), Ethylenediamine (ED), MES and HEPES buffer, and sodium borohydride (99.99%). The sample of graphene oxide was purchased from Cheap Tubes Company (Brattleboro, USA). Deionized (DI) water was prepared in a Millipore Milli-Q purification system. The TFC FO membranes were obtained from HTI and were soaked in DI water for 24 hr before modification.

### 3.2.2 Surface modification with GO nanosheets

GO nanosheets (1mg/ml) were dispersed in a 10 mM MES buffer solution by probe sonication (Branson 3510) for 15 min to exfoliate the nanosheets and prepare a stable suspension. 2 mM of EDC and 5 mM NHS were added to the GO suspension (pH 7.5) just before a four-hour contacting with the pre-treated - EDC/NHS solution, followed by an ED solution - membrane surface. Treating membranes surface through dip-coating method by the combination of EDC/NHS and ED treatment will give membrane surface amine functionality ready to react with modified GO nanosheets. The treated membranes were then rinsed with DI

water three times to remove loosely attached and excess GO from the surface. The detailed procedure of membrane functionalization is presented as supporting information

### 3.2.3 *In situ Ag NP formation on GO modified membranes*

Ag NPs were formed in situ on the surface of GO-modified membranes through wet chemical reduction of  $\text{AgNO}_3$  by  $\text{NaBH}_4$ . The active surface of each membrane was covered with a silver nitrate solution (5mM) for 10 min followed by rinsing with DI water. The treated surface was then covered with a sodium borohydride solution (5mM) for 5 min, followed by rinsing with DI water. All steps were assisted by shaking at a speed of 50 rpm. Finally, the silver decorated membranes were rinsed with DI water three times to detach loose silver NPs from the surface (Figure 21).

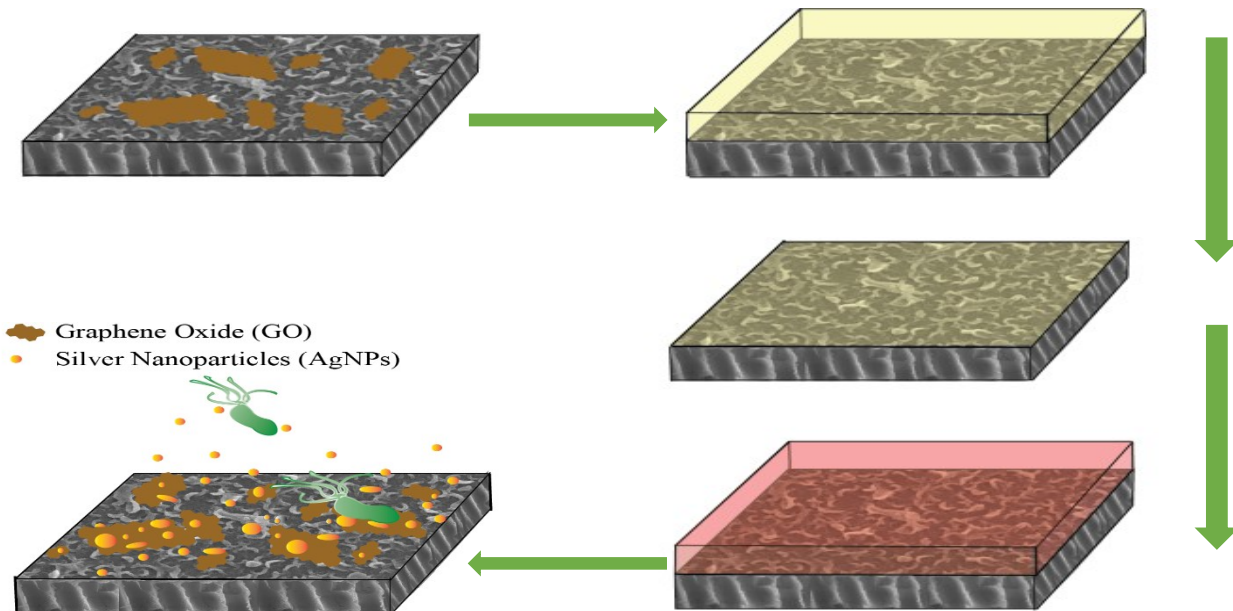


Figure 21 In situ Ag NP formation on the surface of GO-modified membranes: Modified membrane (A) is covered by  $\text{AgNO}_3$  (B) followed by discarding solution and rinsing with DI water (C) and covered by  $\text{NaBH}_4$  (D) to form silver decorated membranes (E)

### 3.2.4 *Membrane characterization*

The distribution of the Ag NPs and the morphology of the pristine and functionalized membranes were observed by field-emission scanning electron microscopy (FE-SEM JEOL, JSM-7600 TFE). The roughness parameters of the membranes were determined using atomic force microscopy (AFM, Dimension 3100) in tapping mode. The elemental composition of the

virgin and functionalized membranes were determined by X-ray photoelectron spectroscopy (XPS, SK-Alpha). Samples were irradiated with a beam of monochromatic Al K $\alpha$  X-rays with 1.350 keV of energy. Raman spectroscopy of pristine and modified membranes was conducted (Invia Reflex-Renishaw) in 532 nm laser excitation to confirm the presence of GO nanosheets on the membrane surface. Surface hydrophilicity and surface energy were evaluated by contact angle measurements of DI-water, diiodomethane, and glycerol using the sessile drop method. Membrane performance tests were conducted by using a cross-flow in RO and FO mode.<sup>104</sup> Details of the performance tests are depicted in the supporting information.

### 3.2.5 *Anti-microbial properties of modified membranes*

The biocidal properties of the pristine and modified membranes were examined using the colony forming unit (CFU) counting method. Briefly, the membranes were submerged in a bacterial suspension from 0.5 to 6 h. Three strains of bacteria; namely, *E. coli* D21 (Gram negative and non-pathogenic), *E. coli* O157:H7 (Gram negative pathogen) and *E. faecalis* (Gram positive pathogen) were used. The membranes were removed from the suspension and sonicated in bacteria-free electrolyte (0.9% NaCl) for 7min. After serial dilutions, the detached bacteria were then cultured on agar plates and the number of CFU were counted after overnight incubation at 37 C.

### 3.2.6 *Loading, stability and release of Ag NPs*

The reservoir method was used to measure the silver ion loading, stability under physical stress (7 minutes bath sonication), and ions released from functionalized membranes. Functionalized and virgin membrane samples were cut into 1-inch coupons and were incubated in 40 mL of DI water for 24 h, followed by acidification with 1% HNO<sub>3</sub>. Silver ion concentrations in the samples were then measured by inductively coupled plasma mass spectroscopy (ICP-MS Perkin Elmer NexION 300X).

### 3.2.7 *Regeneration of Ag NPs on the membrane surfaces*

To study the regeneration of Ag NPs, silver decorated GO-functionalized membranes were immersed in DI water for seven days. Fresh DI water was replaced every 24 hours and the ion-release process was assisted by a shaker set to 50 rpm. Ag NPs were regenerated on the

surface of the membranes in the same manner as described in section 2.3. The success of the regeneration process was then confirmed by antimicrobial examination, contact angle measurements, loading measurements, and XPS analysis.

### 3.3 Results and Discussion

#### 3.3.1 *Ag NPs were formed successfully and their loading increased in the presence of GO nanosheets*

The surface morphology of pristine and modified membranes was observed by SEM. Backscattered electron (BSE) SEM images in Figure 22 indicate the presence of bright spots with strong Ag signals on the surface of the modified membranes, elucidated through EDX analysis (results not shown). Furthermore, the Ag NP size and distribution are different for samples with and without GO nanosheets. In the presence of GO nanosheets, well-distributed and finer Ag NPs were formed in comparison with Ag NPs formed directly on the surface of pristine membranes. GO nanosheets, with their abundance of oxygen-containing functional groups, play a decisive role in governing the size and distribution of the in situ-formed Ag NPs by providing more active sites for the nucleation of Ag NPs. By increasing the number of nuclei, their room for growth would be limited, thus resulting in smaller-sized Ag NPs. The surface topography and roughness parameters of pristine and modified membranes were studied through AFM analysis as depicted in Figure 22 and the supporting information (table 3), respectively. Although in situ silver formation on the surface of the TFC membranes slightly decreases roughness, GO nanosheets flatten the surface and decrease surface roughness drastically. Decreasing surface roughness hinders the attachment of foulants and microorganisms on the surface during operation, resulting in more mitigation of fouling and biofouling.

The presence and content of metallic silver were also confirmed by studying the elemental composition of the membrane surfaces through XPS analysis. Strong signals of Ag (3d) in both the Ag and GO-Ag-functionalized membranes was clearly observed in XPS spectra (Figure 23 (A) and (B)) thus confirming the successful formation of Ag NPs. The intensity of Ag (3d) signals for GO-Ag-functionalized membranes were stronger than the signals for Ag-functionalized membranes, indicating that silver content increases in the presence of GO nanosheets.

Silver loading and releasing behavior were investigated more precisely by ICP-MS analysis. The results (Figure 23 (C) and (D)) show that silver loading on GO-functionalized membranes is almost four times more than the loading on pristine ones. Although silver loading on GO-Ag-functionalized membranes was greater, silver releasing was also higher and lasted longer in comparison with Ag-functionalized membranes. The stability of Ag NPs under physical stress was also investigated and results (Figure 29, supporting information) clearly demonstrate that GO significantly increased Ag stability after seven minutes of sonication. Finally, the Ag concentration in both the feed and permeate solution was measured after 24-hour performance tests of Ag-modified and GO-Ag-modified membranes in RO mode. Results for both modified membranes showed the presence of approximately 2 ppb of silver on feed side and 0.2 ppb silver on permeate side, which is negligible in comparison with the maximum contamination limit of Ag in drinking water (i.e., 100  $\mu\text{g/L}$ ) established by the World Health Organization.<sup>45, 48</sup>

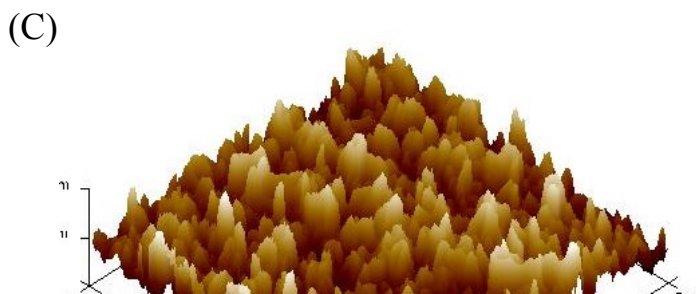
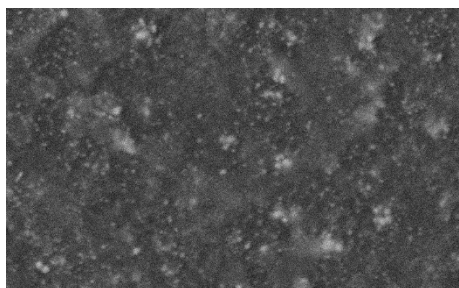
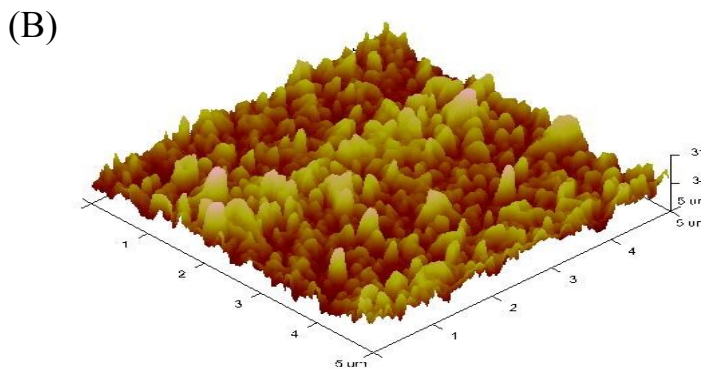
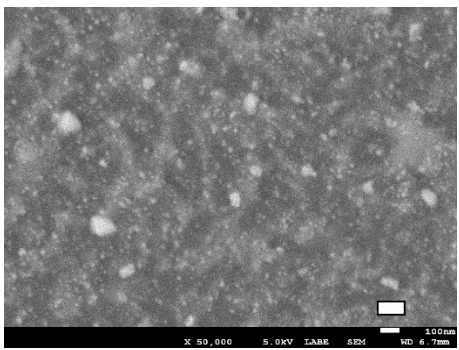
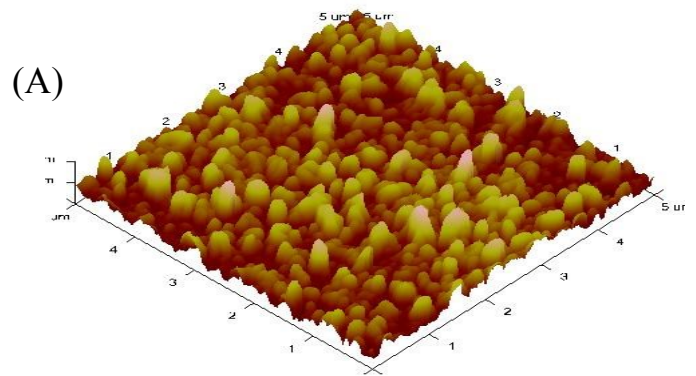
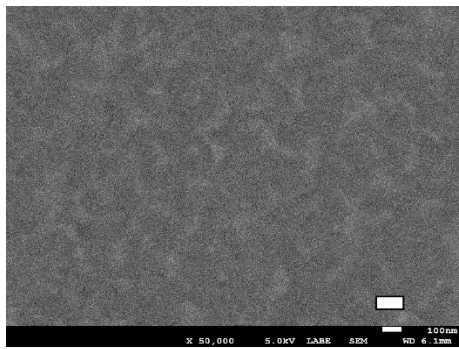


Figure 22 BSE-SEM and AFM images of pristine (A), TFC-Ag in situ (B), and TFC-GO-Ag (C) functionalized membranes. The white scale bar represents 100 nm.

### *3.3.2 Membrane surface hydrophilicity changed after modification while performance remained unchanged*

Membrane hydrophilicity and surface energy have substantial effects on membrane fouling and biofouling.<sup>131</sup> The Van-Oss theory, which is used, in particular, for surfaces coated with organometallic materials and ions,<sup>106, 132, 133</sup> was employed to measure surface energy. Figures 24 (A) and 24 (B) represent water contact angle and interfacial free energy of cohesion (hydrophilicity) of pristine and modified membranes. The results indicate that the incorporation of Ag NPs onto both pristine and GO-modified membranes decreased their contact angle and increased their hydrophilicity. For GO-modified membranes, increased hydrophilicity can be attributed to the presence of oxygen-containing functional groups. For Ag-modified membranes decreased contact angle may be a result of the presence of Ag NPs which can convert to ions and alter the surface charge distribution. This effect is similar to the presence of cations in water which leads to hydrophilicity.<sup>106</sup> For GO-Ag-modified membranes, both surface functional groups (attributed to GO) and Ag NPs (presence of cations) play a role in increasing hydrophilicity. Increasing hydrophilicity can also lead to an increase in water flux for both FO and RO modes of operation which are shown in Figure 24 (C) and (D), respectively. Membranes modified with both GO and GO-Ag have a higher flux than pristine membranes while Ag-modified membranes have the same flux as pristine membranes. Although salt rejection in RO mode and reverse salt flux in FO mode rise, this incremental change is not substantial.

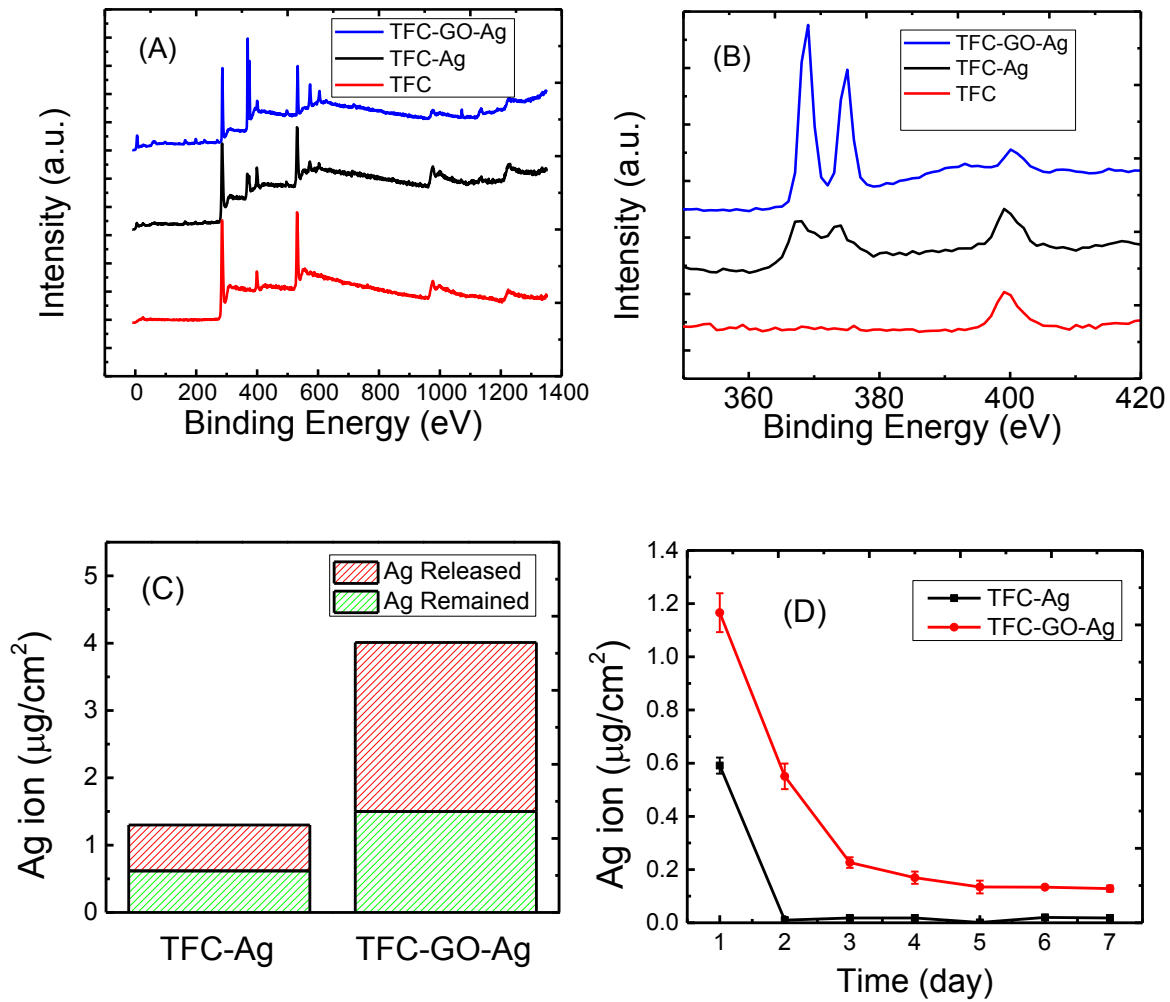


Figure 23 XPS spectra of pristine (A) and modified membranes (B). ICP-MS results of loading and stability (C) as well as releasing behavior (D) of functionalized membranes.

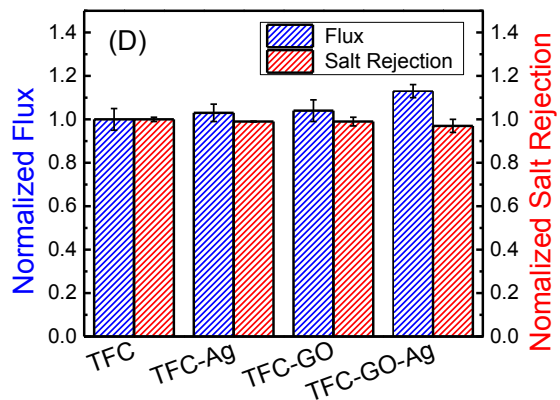
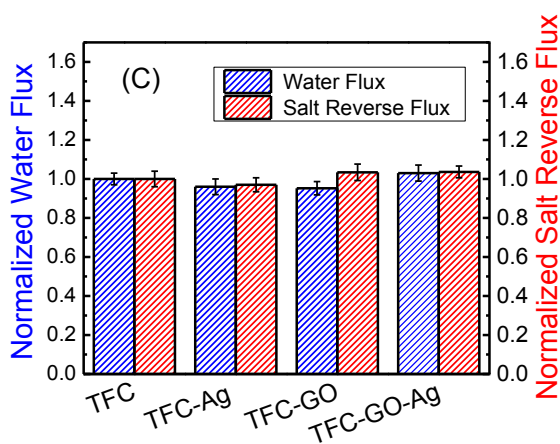
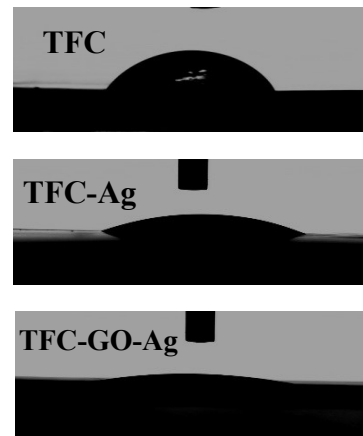
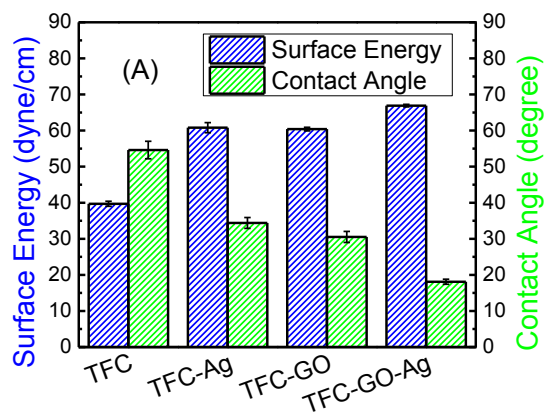


Figure 24 Water contact angle and surface energy (A) and drop shape (B) of pristine and modified membranes. Performance of pristine and modified membranes in FO mode (Results are normalized to 5.46 (LMH) flux and 0.43 (moleMH) reverse salt flux for pristine membrane) (C) and RO mode (Results are normalized to 21.5 (LMH) flux and 97 (%) salt rejection for pristine membrane) (D).

### 3.3.3 Bacterial growth inhibition increased in the presence of GO nanosheets

The antimicrobial behavior of different membrane surfaces: pristine, GO-modified, *in situ* Ag-modified, and GO-Ag-modified membranes; was examined using a non-pathogenic *E. coli* model to represent anti-biofouling potential. In comparison with the polyamide pristine membrane, membranes modified with GO nanosheets and *in situ* formed Ag NPs exhibited 50% and 80% inactivation, respectively (Figure 25 (A)). The inactivation of GO-Ag-modified membranes was even higher; almost 100%. This synergetic effect is due to the antibacterial properties and inactivation mechanism of both GO nanosheets and Ag NPs. GO nanosheets are contact-based biocidal materials and are believed to potentially rupture the cell membranes with their sharp edges<sup>78, 112, 115</sup> or mediate lipid peroxidation induced by the oxidative nature of GO. GO nanosheets can also stop bacterial growth through cell entrapment when they are used in suspension.<sup>134</sup> Releasing reactive oxygen species (ROS) or direct oxidation of cellular component also plays a role in bacterial inactivation.<sup>125-127, 134</sup> The mechanism of inactivation of Ag NPs<sup>113</sup> is being researched further, yet still remains controversial. There are reports on the inactivation properties of Ag NPs claiming the nanoparticles enter the cell and selectively attack the respiratory chain, causing cell division which eventually leads to cell death<sup>113</sup> but other contradicting reports relegate elemental Ag antimicrobial properties as these effects may be the result of the silver ion ( $\text{Ag}^+$ ) reacting with the cysteine from the membrane cell to damage it.<sup>33,</sup><sup>135</sup> These reports suggest that Ag NPs may serve as a more effective  $\text{Ag}^+$  delivery vehicle, so Ag NPs of smaller size may influence a larger specific surface area and result in a faster  $\text{Ag}^+$  release rate as compared to larger Ag NPs. Loading and releasing results (Figure 23 (C) and (D)) indicate that GO-Ag-modified membranes have more silver on the surface and also release more silver ions ( $\text{Ag}^+$ ) as a function of time. Considering each mechanism of inactivation, the bacterial inactivation capability of GO-Ag would then come from higher loading, smaller Ag NP size, and more  $\text{Ag}^+$  ions released.

To further evaluate the antimicrobial behavior of the modified membranes, time-dependent static (no pressure, no flow) bacterial inactivation tests were performed using three different strains of bacteria; namely *E. coli* D21f2 (Gram-negative and non-pathogenic), *E. coli*

O157:H7 (Gram-negative and pathogenic) and *E. faecalis* (Gram-positive and pathogenic). The results show that the modified membranes exhibited strong anti-bacterial effects to all tested bacteria, whereas for the pristine membrane, bacteria remained viable with an increasing number of CFU observed over time (Figure 25(B), (C) and (D)).

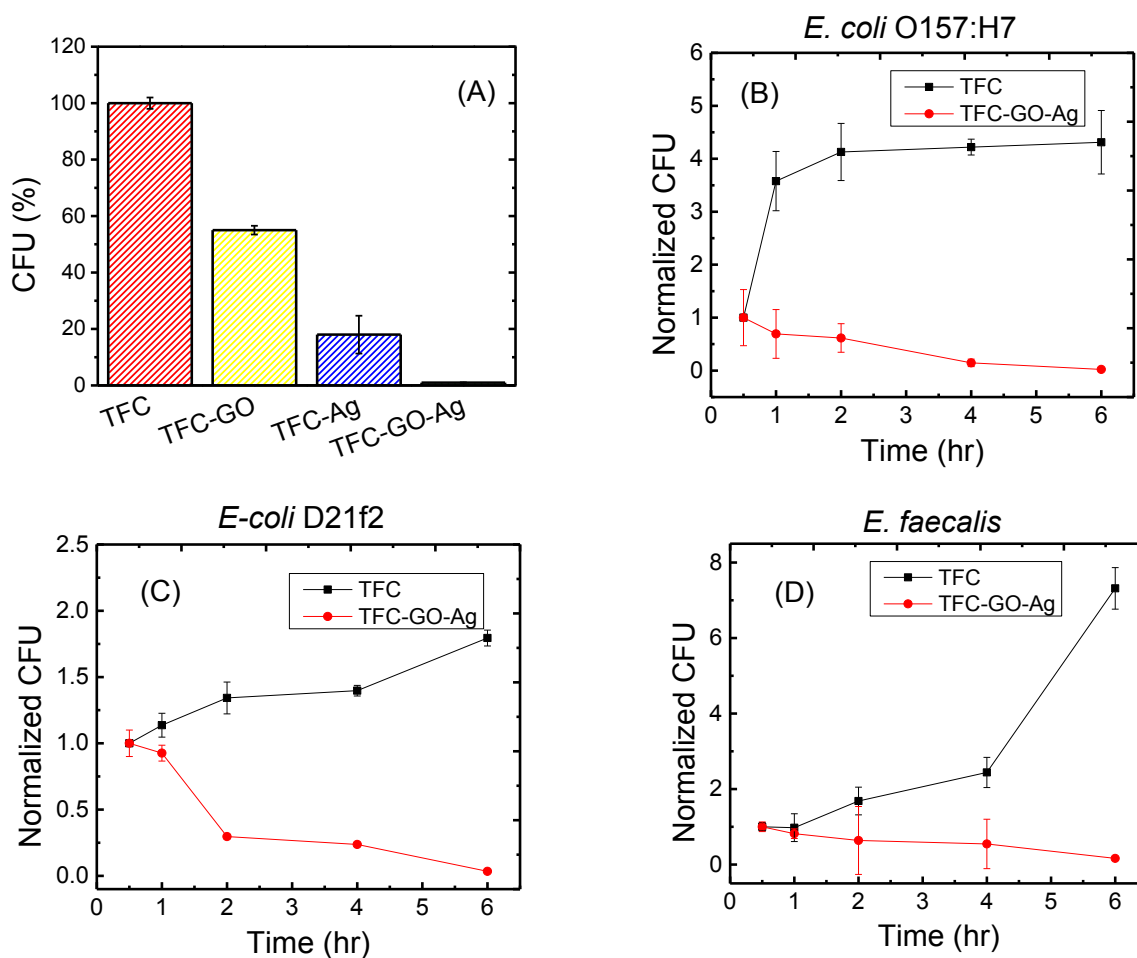


Figure 25. The number of live cells (CFU) on the pristine, Ag, GO and GO-Ag-modified surfaces over 1 hr contact with *E. coli* D21f2 bacterial suspension (A). The number of CFU on the pristine, GO, and GO-Ag modified membranes over 0.5-6 hours contact with *E. coli* O157:H7 (B), *E. coli* D21f2 (C) and *E. faecalis* (ATCC 29212) (D) bacterial suspensions. For each series of membranes, CFU values were normalized by the CFU value for 0.5 h contact.

### 3.3.4 *Ag NP regenerated successfully on the surface of GO-Ag-modified membranes*

The regeneration of NPs after their release has always been a drawback of using biocidal metal NPs such as silver or copper. In this study, after 7 days of storage in water to allow ion release, Ag NPs were regenerated on the surface of GO-Ag-modified. The surface contact angle and antimicrobial properties of the membranes after 7 days of ion-release and after regeneration are shown in Figure 26. Results clearly indicate that membrane properties changed after a week in water. Surface contact angle increased and surface energy decreased which means the membranes lost their hydrophilicity, yet did not deplete to the point of pristine filters. This can be attributed to presence of the GO nanosheets which were covalently bonded to the surface. After the 7 day release process, the membranes were tested using XPS peak analysis of C1S (Figure 30 supporting information). The patterns and sub-peaks for these membranes resembled those of the GO-modified membrane and were completely different from the results for the pristine membrane, confirming that GO remained on the surface even after being in water for one week. Presence of GO nanosheets was also confirmed by Raman spectroscopy (Figure 26 D), where both characteristic D band ( $1350\text{ cm}^{-1}$ ) and G band ( $1590\text{ cm}^{-1}$ ) were present in all modified membranes, even for those kept in water for 7 days. Bacterial inactivation, much like the membrane hydrophilicity, also decreased from 98% to 80% after the depletion treatment.

After the regeneration process, membranes regained their hydrophilicity and antimicrobial properties, with contact angle decreasing to 30 degrees and bacterial inactivation reaching 95%. The change in silver loading (metallic silver) was also examined by XPS. Signals of Ag3d decreased after releasing but increased again after regeneration in total agreement with ICP-MS results (Figure 26 (C)). Results indicate that a simple regeneration process (10 minute immersion of membranes in  $\text{AgNO}_3$  followed by immersion in  $\text{NaBH}_4$  solution for 5 minutes) significantly improved membrane properties after they were lost in the releasing process.

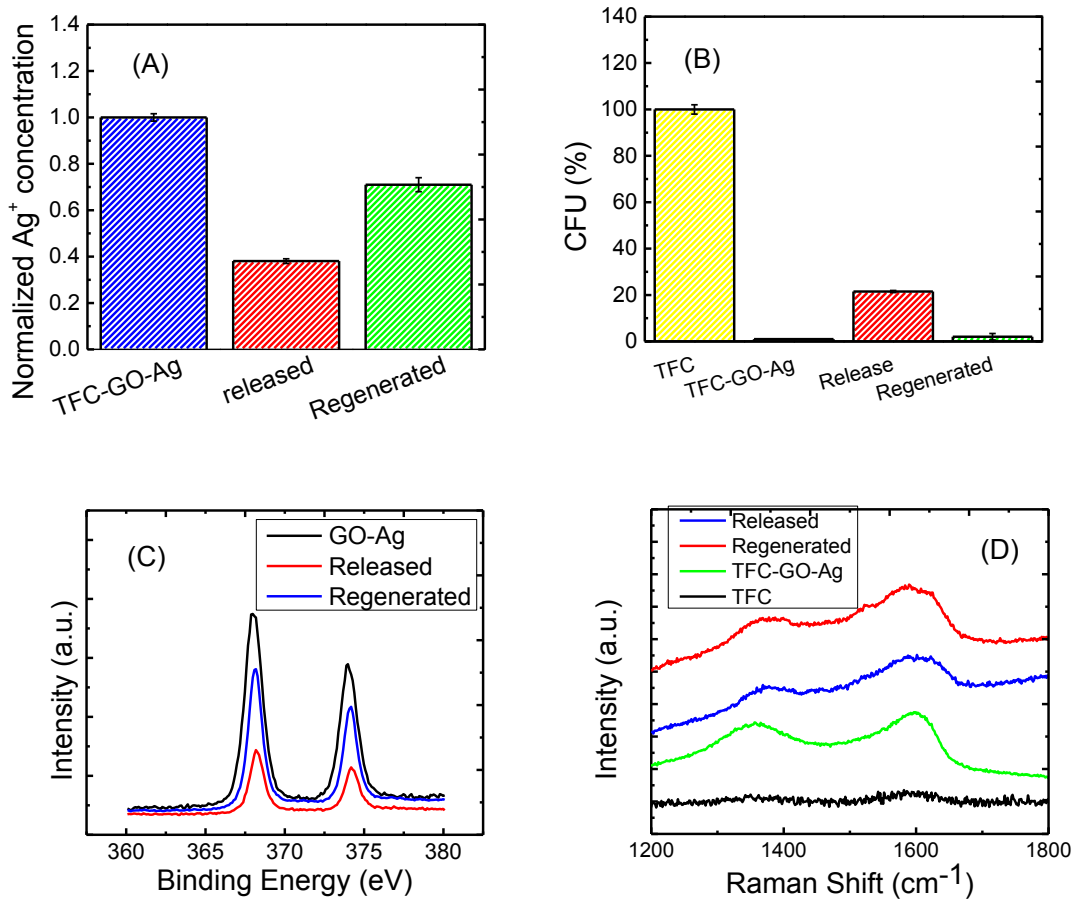


Figure 26 Normalized silver content on the surface of membranes (A), antimicrobial properties of pristine and modified membranes (B), and XPS spectra for Ag (3d) (C), Raman shift of pristine and modified membranes (D) before and after regeneration.

### 3.4 Conclusion

In summary, Ag NPs formed *in situ* on the surface of both pristine and covalently-bonded GO-modified membranes. Results show that *in situ* formation of Ag NPs on the GO-modified membrane surface produces higher silver loading, higher and longer lasting ion-release, and more effective antimicrobial properties as compared to the formation of Ag NPs on pristine TFC FO membranes. GO-Ag-modified membranes showed high hydrophilicity which resulted in increased water flux in both RO and FO modes of operation without significant adverse effects on salt rejection. The regeneration of GO-Ag-modified membranes was also examined. Ag NPs were successfully formed using an identical *in situ* procedure on the surface of the modified membranes that had been kept in DI water for seven days. Results show that membrane hydrophilicity and antimicrobial ability decrease during the releasing process, however, the regeneration process allows the membrane to regain its properties until it is fairly consistent with the freshly modified counterpart. The simple regeneration method which has been developed in this study will allow on site modification and regeneration of different types of industrial membrane modules (hollow fiber, spiral wound). In comparison with the other methods of surface modification this technique is cost effective and less time consuming (facile coating process that requires low concentration of chemicals) and could easily be applied to modify other surfaces contacted with contaminated water.

### 3.5 Supporting Information

#### 3.5.1 TFC membrane modification

TFC FO membranes were coated with EDC/NHS followed by ED to modify functional groups on the surface. Carboxylic groups of polyamide membranes converted to amine-reactive esters by direct contact between the membranes and the EDC/NHS solution. An amide formation reaction with a reactive ester was used to bond ethylenediamine to the active layer of the membrane surface. The steps are as follows: first, TFC membranes were cut and placed on a glass plate and covered with a frame; only the active side was exposed to the treating solution. Frames were clamped with clips to prevent any leakage. The entire assembly was then placed on a shaker, rotating at 50 rpm at room temperature. Second, 4 mM EDC, 10 mM NHS and 0.5 M NaCl were dissolved in 10 mM MES buffer. The solution was adjusted to pH 5 with HCl and

NaOH. The solution was then put in contact with the membrane surface for 1 h. Next, the membranes were washed and rinsed with DI water three times and then covered with a solution of 10 mM ED, 0.15 mM NaCl in 10 mM HEPES buffer at pH 7.5. Finally, the membrane surface was washed with DI water to remove any unlinked ED.

Next, 100 mg of GO nanosheets were dispersed in 100 mL of 10 mM MES buffer at pH 6 and probe sonicated for 15 min to exfoliate them. This process also helped prepare a stable suspension. Just before contacting the GO suspension (pH 7.5) with the ED functionalized TFC FO membranes, 2 mM EDC and 5 mM NHS were added to the suspension. The GO functionalized membranes were washed, rinsed three times, and stored in DI water at 4°C until in situ Ag formation.

### 3.5.2 Scanning Electron Microscopy

Membrane samples were desiccated overnight then coated with 5 nm carbon. The carbon was sputtered onto the samples by carbon evaporation (EDWARDS AUTO306) and were examined in field-emission scanning electron microscopy (FE-SEM; JEOL, JSM-7600 TFE). Backscattered electron (BSE) images were also collected with BSE collector JEOL 7600. BSE intensities are a function of the atomic number of elements and can be useful for clarifying the presence of Ag NPs and their distribution on the surface of membranes.

### 3.5.3 Contact Angle Measurements

The surface hydrophilicity of pristine and modified membranes was examined at room temperature using the sessile drop method. The average of the left and right contact angles of at least four 20  $\mu$ L droplets were taken as the contact angle values. The Van-Oss theory was employed for measuring surface energy<sup>132, 133</sup>. Three different liquids: DI water, diiodomethene, and glycerol were used for contact angle measurements and surface energy calculation. The different contact angles were used for measuring Lifshitz-van der Waals ( $\gamma^{LW}$ ), the electron donor ( $\gamma^-$ ), and the electron acceptor ( $\gamma^+$ ) of the membrane surface energy as:

$$(1 + \cos \theta_l) \gamma_l^T = 2(\sqrt{\gamma_m^{LW} \gamma_l^{LW}} + \sqrt{\gamma_m^+ \gamma_l^-} + \sqrt{\gamma_m^- \gamma_l^+}) \quad (3-1)$$

Where the subscript  $l$  relates to liquid and  $m$  to the membrane. The surface energy of the membranes was calculated by:

$$\gamma_m^T = \gamma_m^{LW} + 2\sqrt{\gamma_m^+ \gamma_m^-} \quad (3-2)$$

### 3.5.4 Membrane Performance Evaluation

The permeation cell was designed to provide an effective surface area of 42.75 cm<sup>2</sup>. The membrane was compacted overnight with DI water at 400 psi until a steady water permeate flux was reached. In the RO mode, the water flux (J) of the membranes was evaluated using the following equation:

$$J = \frac{\Delta V}{A_m \Delta t} \quad (3-3)$$

The salt rejection was determined by measuring the rejection of a 50 mM NaCl solution using a calibrated conductivity meter (Oakton Instruments, Vernon Hills, IL, USA). The salt rejection of the membranes was calculated using the following equation:

$$R = \left(1 - \frac{C_p}{C_f}\right) \times 100\% \quad (3-4)$$

Where C<sub>p</sub> and C<sub>f</sub> are the salt concentrations in the permeate and feed solutions, respectively.

The membrane performance in the FO mode was also evaluated using a lab scale cross-flow cell with the same dimensions as the RO cell. Both the feed (DI water) and draw solution (1 M NaCl) were circulated at the same flow rate (0.2 L/min) and without applied pressure. The temperature of the feed and draw solutions was maintained constant at 25°C. To precisely measure the water flux, a digital analytical balance was used to measure the weight change of the draw solution. The reverse salt flux of the membranes was calculated by measuring the conductivity of the draw solution before and after the FO process using a calibrated conductivity meter (Oakton Instruments, Vernon Hills, IL). The FO water flux (J<sub>v</sub>) and reverse salt flux (J<sub>s</sub>) were calculated as follows:

$$J_V = \frac{\Delta V}{A_m \Delta t} = \frac{\Delta m / \rho}{A_m \Delta t} \quad (3-5)$$

$$J_S = \frac{\Delta(C_t V_t)}{A_m \Delta t} \quad (3-6)$$

Where  $\Delta_m$  is the weight change of the draw solution,  $A_m$  is the effective surface area, and  $C_t$  and  $V_t$  are the salt concentration and volume of the feed solution after the process, respectively.

### 3.5.5 Antimicrobial Evaluation of Membranes

Bacterial inactivation was evaluated by determining and comparing the number of viable bacteria present on surfaces of virgin and functionalized membranes through a simple plate counting method. Briefly, *E. coli* D21f2 (Gram negative and non-pathogenic) was grown overnight at 37° C in Luria-Bertani (LB) broth medium. The bacterial solution was diluted and cultured for 2 h to reach the log phase and was verified by an optical density measurement at 600 nm. The resulting bacterial solution was centrifuged and washed three times with 0.9% saline solution before being diluted to  $10^7$  CFU mL<sup>-1</sup> in 0.9% saline solution. For the exposure phase, 1.5 cm<sup>2</sup> membranes were punched and placed in a plastic holder with the active layer facing the bacterial solution. The holders were maintained at room temperature for 1 h. After 1 h of incubation, the excess solution was discarded, and the membranes were washed with a sterile saline solution. To remove attached bacteria from the membrane surface, the membrane coupons were bath sonicated for 7 min in a 10 mL isotonic solution. Finally, 100 μL serial dilutions (representing over 6 orders of magnitude) of the bacterial solution were spread on LB agar plates and incubated overnight at 37°C. The number of colonies was then counted.

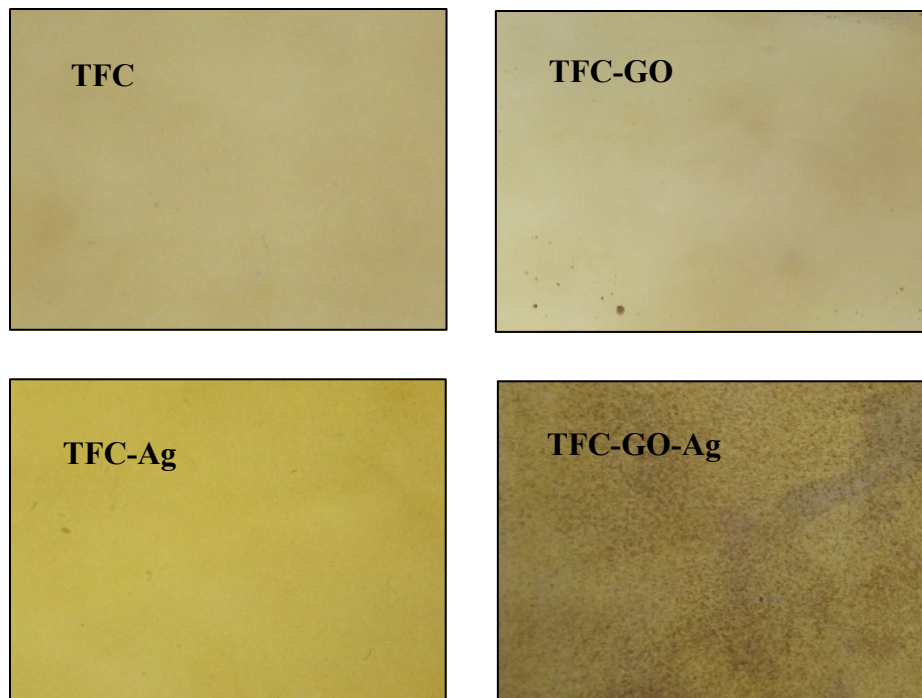


Figure 27 Images of pristine, TFC-GO, TFC-Ag and TFC-GO-Ag-modified membranes.

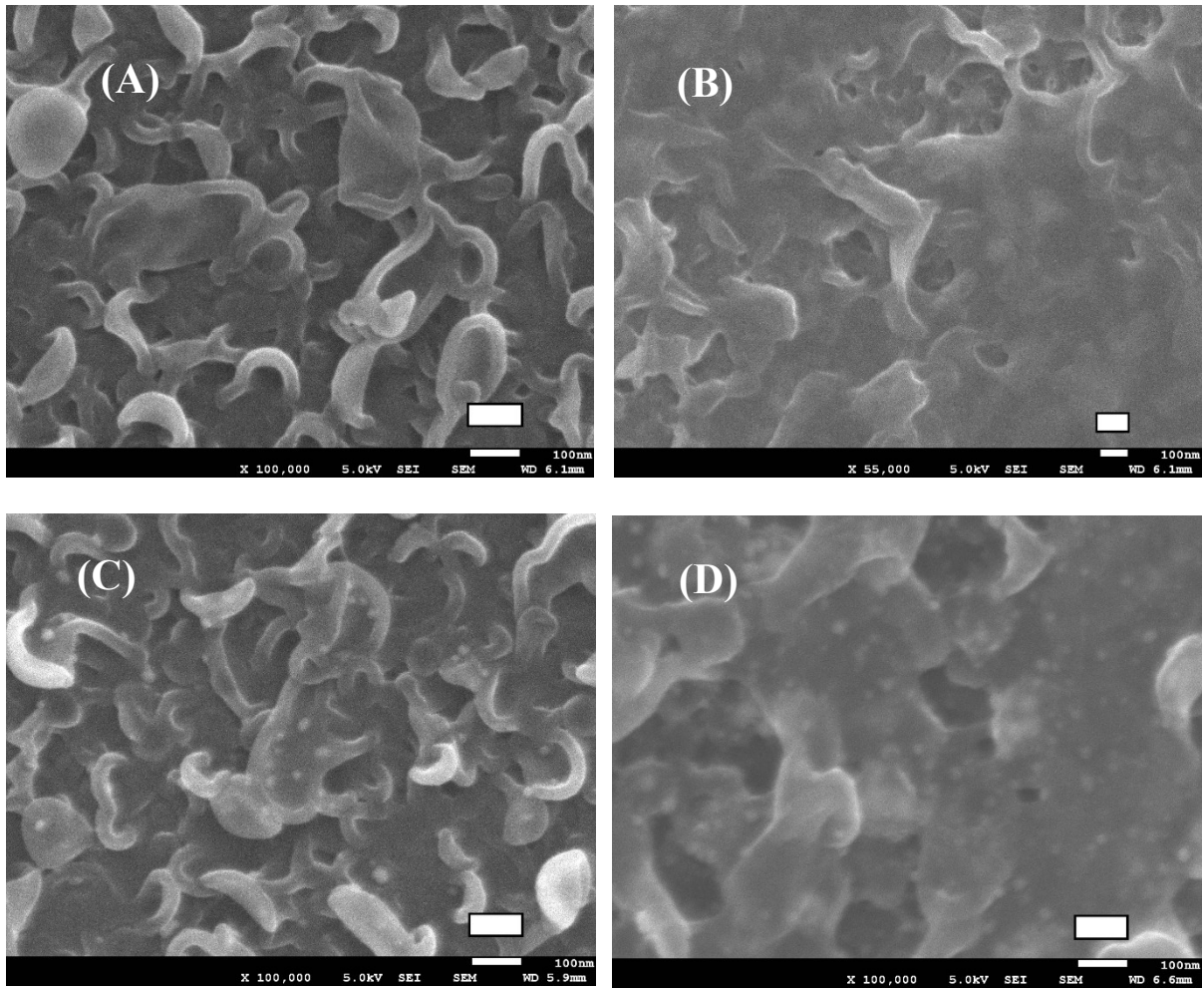


Figure 28 FE-SEM images of pristine (A), GO-modified (B), Ag-modified (C) and GO-Ag-modified membranes. White scale represents 100 nm.

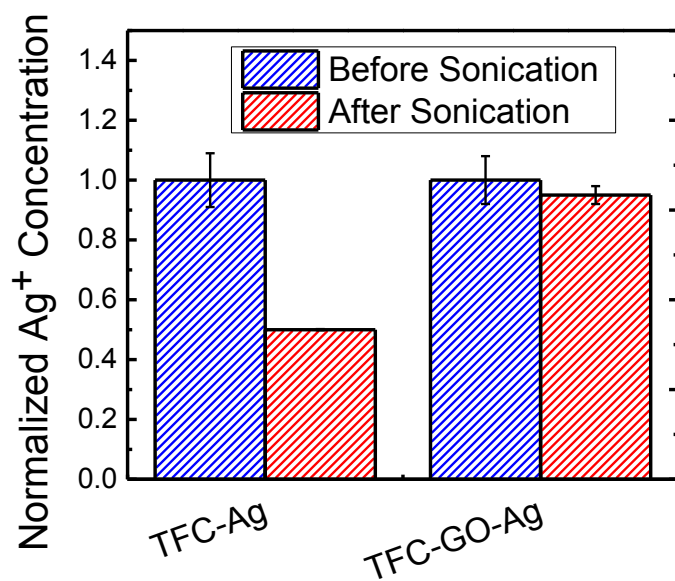


Figure 29 Physical stability of Ag NPs on the surface of modified membranes after 7 minutes of bath sonication. Ag loading was conducted by ICP-MS method for modified membranes before and after bath sonication.

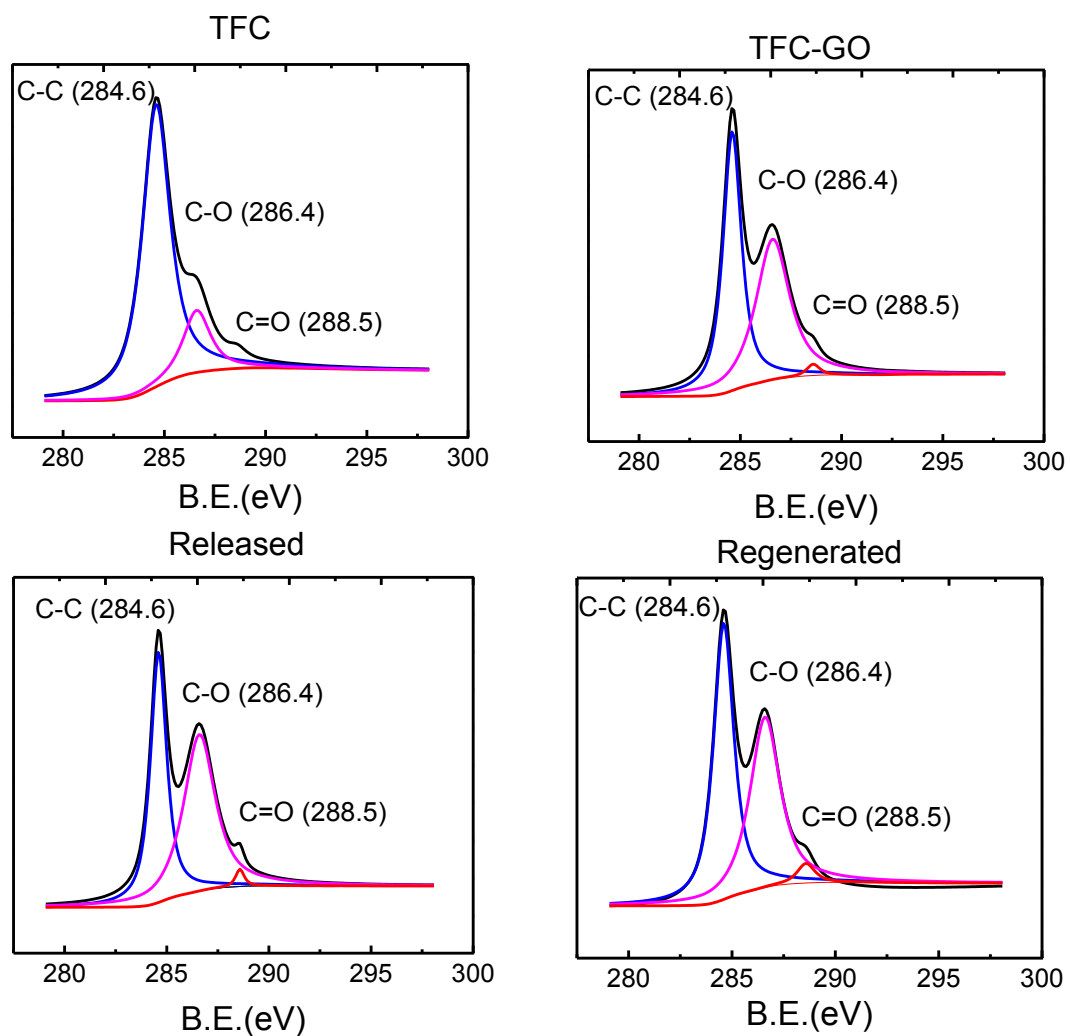


Figure 30 XPS peak analysis for TFC, TFC-GO, and TFC-GO-Ag before and after regeneration. Results show that after seven days of release, GO nanosheets are still present on the membrane surfaces.

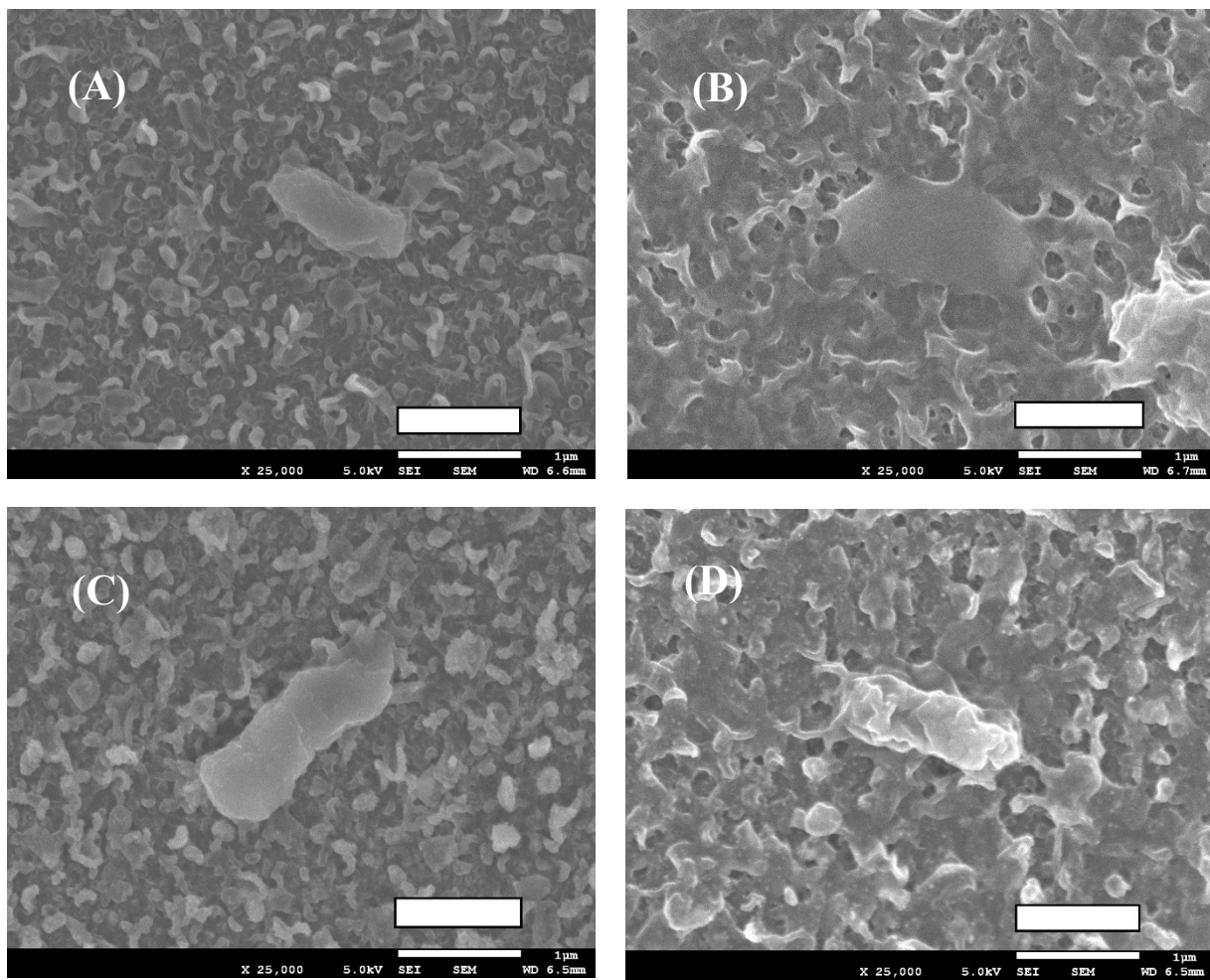


Figure 31 SEM images of cells (*E. coli* D21f2) after contacting with pristine (A), GO-modified (B), Ag-modified (C), and GO-Ag-modified (D) membranes for 1 h.

Table 3 Surface roughness properties of the pristine and functionalized TFC FO membranes.

Sample	$R_{\max}$ (nm)	$R_a$ (nm)	$R_q$ (nm)	SAD (%)
TFC FO	$486 \pm 22$	$52.2 \pm 0.5$	$65.5 \pm 1.5$	$67.4 \pm 2.1$
TFC- Ag	$483 \pm 13$	$47.2 \pm 2.8$	$59.1 \pm 4.24$	$79.9 \pm 2.2$
TFC-GO-Ag	$212 \pm 32$	$24.9 \pm 4.8$	$31.6 \pm 6$	$43.1 \pm 4.1$

#### 4 CONCLUSION and RECOMMENDATIONS

Biocidal Ag NPs and GO/Ag nanocomposite were synthesized and characterized. Biocidal nanomaterials then applied in two different ways of *ex situ* and *in situ* onto the surface of TFC FO membranes for preparing antimicrobial surfaces. Membrane characterization were done and their performance evaluation were conducted in RO and FO mode of operation. Results showed that making a composite of nanomaterials is more effective than each one per se. biocidal nanocomposite can provide capture-killing mechanism and also will inactivate bacteria in both media through releasing  $\text{Ag}^+$  ion and in contact through cell membrane rupturing by GO nanosheets. GO nanosheets also could govern shape, size, and distribution of Ag NPs and by decreasing the size and preventing aggregation will increase the efficacy of biocidal properties. Covalent bonding of nanomaterials to the surface will increase their stability. Although combination of nanomaterials has some advantages, it still suffering from limited loading and fast depletion of Ag NPs through ion-release process without the possibility of regeneration. To overcome those limitations, *in situ* formation of Ag NPs on the surface of GO-treated TFC FO membranes were conducted to still enjoy the advantages of combination of two different types of biocidal materials and increasing Ag loading content and providing the regeneration possibility. In this approach, GO nanosheets were covalently bonded onto the membrane surface and then Ag NPs formed *in situ* onto GO-modified surface through wet chemical reduction of  $\text{AgNO}_3$  by  $\text{NaBH}_4$ . Results showed new nanocomposite had the similar biocidal properties with the former one but silver loading was greater and its release was more controllable and longer lasted. Another advantage of new modification method was the regeneration possibility. GO-Ag modified membranes were kept in DI water for seven days for ion-release process then Ag NPs were regenerated *in situ*. Results showed after seven days GO nanosheets remained on the surface but silver content decreased significantly. After regeneration modified membranes regained their both hydrophilic and biocidal properties almost 80 percent. New facile and quick regeneration method can be applied easily in real-world membrane systems in different configurations such as hollow fiber and spiral wound modules.

Real biofouling tests for the future would be insightful for comprehensive understanding of antibiofouling performance of modified membranes. Also investigation of toxicity and bacterial inactivation mechanisms by the GO/Ag nanocomposite will provide more insights about the synergetic effects of the combination of two biocidal nanomaterials. Combination of

polymer brushes with GO nanosheets also can be considered as an alternative of using biocidal nanomaterials alone.

## 5 REFERENCES

1. *Water for Sustainable World*; United Nations Educational, Scientific and Cultural Organization: France, 2015.
2. Patrick Gerland, A. E. R., Thomas Spoorenberg, Nevena Lalic, Leontine Alkema, Guiomar Bay, Hana Ševčíková, Bailey K. Fosdick, Thomas Buettner, Nan Li, Danan Gu, Jennifer Chunn, Gerhard K. Heilig, John Wilmoth, World population stabilization unlikely this century. *Science* **2014**, *346*, 234-237.
3. C. J. Vör, A. Y. H., S. E. Bunn, D. Conway, J. Gupta Fresh Water Goes Global. *Science* **2015**, *349*, 478-479.
4. Elimelech, M.; Phillip, W. A., The future of seawater desalination: energy, technology, and the environment. *Science* **2011**, *333*, (6043), 712-7.
5. Shannon, M. A.; Bohn, P. W.; Elimelech, M.; Georgiadis, J. G.; Marinas, B. J.; Mayes, A. M., Science and technology for water purification in the coming decades. *Nature* **2008**, *452*, (7185), 301-10.
6. Baker, R. W., *Membrane Technology and Applications*. 2nd ed.; John Wiley & Sons, Ltd.: 2004.
7. Zhou, Y.; Tol, R. S. J., Evaluating the costs of desalination and water transport. *Water Resources Research* **2005**, *41*, (3), n/a-n/a.
8. Veerapaneni, S. V. L., Bruce; Freeman, Scott; Bond, Rick, Reducing Energy Consumption for Seawater Desalination. *J. Am. Water Works Assoc.* **2007**, *99*, (6), 95-106.
9. Shaffer, D. L.; Werber, J. R.; Jaramillo, H.; Lin, S.; Elimelech, M., Forward osmosis: Where are we now? *Desalination* **2015**, *356*, 271-284.
10. Achilli, A.; Cath, T. Y.; Childress, A. E., Selection of inorganic-based draw solutions for forward osmosis applications. *Journal of Membrane Science* **2010**, *364*, (1-2), 233-241.
11. Ge, Q.; Ling, M.; Chung, T.-S., Draw solutions for forward osmosis processes: Developments, challenges, and prospects for the future. *Journal of Membrane Science* **2013**, *442*, 225-237.
12. Romero-Vargas Castrillón, S.; Lu, X.; Shaffer, D. L.; Elimelech, M., Amine enrichment and poly(ethylene glycol) (PEG) surface modification of thin-film composite forward osmosis membranes for organic fouling control. *Journal of Membrane Science* **2014**, *450*, 331-339.
13. Mi, B.; Elimelech, M., Chemical and physical aspects of organic fouling of forward osmosis membranes. *Journal of Membrane Science* **2008**, *320*, (1-2), 292-302.
14. Mi, B.; Elimelech, M., Organic fouling of forward osmosis membranes: Fouling reversibility and cleaning without chemical reagents. *Journal of Membrane Science* **2010**, *348*, (1-2), 337-345.
15. Kim, Y.; Elimelech, M.; Shon, H. K.; Hong, S., Combined organic and colloidal fouling in forward osmosis: Fouling reversibility and the role of applied pressure. *Journal of Membrane Science* **2014**, *460*, 206-212.
16. Mi, B.; Elimelech, M., Silica scaling and scaling reversibility in forward osmosis. *Desalination* **2013**, *312*, 75-81.

17. Boo, C.; Elimelech, M.; Hong, S., Fouling control in a forward osmosis process integrating seawater desalination and wastewater reclamation. *Journal of Membrane Science* **2013**, *444*, 148-156.
18. D. Rana , T. M., Surface Modifications for Antifouling Membranes. *Chem. Rev.* **2010**, *110*, 2448–2471.
19. Rahaman, M. S.; Thérien-Aubin, H.; Ben-Sasson, M.; Ober, C. K.; Nielsen, M.; Elimelech, M., Control of biofouling on reverse osmosis polyamide membranes modified with biocidal nanoparticles and antifouling polymer brushes. *Journal of Materials Chemistry B* **2014**, *2*, (12), 1724.
20. Tiraferri, A.; Kang, Y.; Giannelis, E. P.; Elimelech, M., Highly hydrophilic thin-film composite forward osmosis membranes functionalized with surface-tailored nanoparticles. *ACS Appl Mater Interfaces* **2012**, *4*, (9), 5044-53.
21. Tiraferri, A.; Vecitis, C. D.; Elimelech, M., Covalent binding of single-walled carbon nanotubes to polyamide membranes for antimicrobial surface properties. *ACS Appl Mater Interfaces* **2011**, *3*, (8), 2869-77.
22. Mark R. Wiesner, J.-Y. B., *Environmental nanotechnology*. McGraw Hill: 2007.
23. Marambio-Jones, C.; Hoek, E. M. V., A review of the antibacterial effects of silver nanomaterials and potential implications for human health and the environment. *Journal of Nanoparticle Research* **2010**, *12*, (5), 1531-1551.
24. Halas, J. B. J. a. N. J., Silver Nanoshells: Variations in Morphologies and Optical Properties. *J. Phys. Chem. B* **2001**, *105*, 2743-2746.
25. Sun, Y.; Xia, Y., Shape-controlled synthesis of gold and silver nanoparticles. *Science* **2002**, *298*, (5601), 2176-9.
26. Martínez-Castañón, G. A.; Niño-Martínez, N.; Loyola-Rodríguez, J. P.; Patiño-Marín, N.; Martínez-Mendoza, J. R.; Ruiz, F., Synthesis of silver particles with different sizes and morphologies. *Materials Letters* **2009**, *63*, (15), 1266-1268.
27. Neil Shirtcliffe, U. N., 1 and Siegfried Schneider, Reproducible Preparation of Silver Sols with Small Particle Size Using Borohydride Reduction: For Use as Nuclei for Preparation of Larger Particles. *Journal of Colloid and Interface Science* **1999**, *211*, 122–129.
28. Wiley, B.; Sun, Y.; Mayers, B.; Xia, Y., Shape-controlled synthesis of metal nanostructures: the case of silver. *Chemistry* **2005**, *11*, (2), 454-63.
29. Joërg Polte, K. R., Xenia Tuae, Maria Wuthschick, Ralph Kraehnert, Anna Fischer, Andreas F. Thuenemann, and Franziska Emmerling, Formation Mechanism of Colloidal Silver Nanoparticles: Analogies and Differences to the Growth of Gold Nanoparticles. *ASC NANO* **2012**, *6*, (7), 5791–5802
30. Arnim Henglein, M. G., Formation of Colloidal Silver Nanoparticles: Capping Action of Citrate. *J. Phys. Chem. B* **1999**, *103*, 9533-9539.
31. Keating, M.; Chen, Y.; Larmour, I. A.; Faulds, K.; Graham, D., Growth and surface-enhanced Raman scattering of Ag nanoparticle assembly in agarose gel. *Measurement Science and Technology* **2012**, *23*, (8), 084006.
32. C. Carlson, S. M. H., A. M. Schrand, L. K. Braydich-Stolle, K. L. Hess, R. L. Jones, and J. J. Schlager, Unique Cellular Interaction of Silver Nanoparticles: Size-Dependent Generation of Reactive Oxygen Species. *J. Phys. Chem. B* *13608–13619* **2008**, *112*, 13608–13619.
33. Xiu, Z. M.; Zhang, Q. B.; Puppala, H. L.; Colvin, V. L.; Alvarez, P. J., Negligible particle-specific antibacterial activity of silver nanoparticles. *Nano Lett* **2012**, *12*, (8), 4271-5.

34. Morones, J. R.; Elechiguerra, J. L.; Camacho, A.; Holt, K.; Kouri, J. B.; Ramirez, J. T.; Yacaman, M. J., The bactericidal effect of silver nanoparticles. *Nanotechnology* **2005**, *16*, (10), 2346-53.
35. Pal, S.; Tak, Y. K.; Song, J. M., Does the antibacterial activity of silver nanoparticles depend on the shape of the nanoparticle? A study of the Gram-negative bacterium *Escherichia coli*. *Appl Environ Microbiol* **2007**, *73*, (6), 1712-20.
36. Libor Kvítek, A. P. c. e., Jana Soukupova', Milan Kola'ř, Renata Vec'er'ova', Robert Pucek, Mirka Holecova', and Radek Zbor'íl, Effect of Surfactants and Polymers on Stability and Antibacterial Activity of Silver Nanoparticles (NPs). *J. Phys. Chem. C* **2008**, *112*, 5825-5834.
37. Alexander B. Smetana, K. J. K., George R. Marchin, and Christopher M. Sorensen, Biocidal Activity of Nanocrystalline Silver Powders and Particles. *Langmuir* **2008**, *24*, 7457-7464.
38. Nel, A. E.; Madler, L.; Velegol, D.; Xia, T.; Hoek, E. M.; Somasundaran, P.; Klaessig, F.; Castranova, V.; Thompson, M., Understanding biophysicochemical interactions at the nano-bio interface. *Nat Mater* **2009**, *8*, (7), 543-57.
39. Zodrow, K.; Brunet, L.; Mahendra, S.; Li, D.; Zhang, A.; Li, Q.; Alvarez, P. J., Polysulfone ultrafiltration membranes impregnated with silver nanoparticles show improved biofouling resistance and virus removal. *Water Res* **2009**, *43*, (3), 715-23.
40. Mauter, M. S.; Wang, Y.; Okemgbo, K. C.; Osuji, C. O.; Giannelis, E. P.; Elimelech, M., Antifouling ultrafiltration membranes via post-fabrication grafting of biocidal nanomaterials. *ACS Appl Mater Interfaces* **2011**, *3*, (8), 2861-8.
41. Sawada, I.; Fachrul, R.; Ito, T.; Ohmukai, Y.; Maruyama, T.; Matsuyama, H., Development of a hydrophilic polymer membrane containing silver nanoparticles with both organic antifouling and antibacterial properties. *Journal of Membrane Science* **2012**, 387-388, 1-6.
42. Kim, E.-S.; Hwang, G.; Gamal El-Din, M.; Liu, Y., Development of nanosilver and multi-walled carbon nanotubes thin-film nanocomposite membrane for enhanced water treatment. *Journal of Membrane Science* **2012**, 394-395, 37-48.
43. Liu, X.; Qi, S.; Li, Y.; Yang, L.; Cao, B.; Tang, C. Y., Synthesis and characterization of novel antibacterial silver nanocomposite nanofiltration and forward osmosis membranes based on layer-by-layer assembly. *Water Res* **2013**, *47*, (9), 3081-92.
44. Madhavan, P.; Hong, P. Y.; Sougrat, R.; Nunes, S. P., Silver-enhanced block copolymer membranes with biocidal activity. *ACS Appl Mater Interfaces* **2014**, *6*, (21), 18497-501.
45. *Guidelines for drinking-water quality, 2nd ed. Vol. 2. Health criteria and other supporting information. World Health Organization*; World Health Organization: Geneva, 1996.
46. Yin, J.; Yang, Y.; Hu, Z.; Deng, B., Attachment of silver nanoparticles (AgNPs) onto thin-film composite (TFC) membranes through covalent bonding to reduce membrane biofouling. *Journal of Membrane Science* **2013**, *441*, 73-82.
47. Ben-Sasson, M.; Lu, X.; Bar-Zeev, E.; Zodrow, K. R.; Nejati, S.; Qi, G.; Giannelis, E. P.; Elimelech, M., In situ formation of silver nanoparticles on thin-film composite reverse osmosis membranes for biofouling mitigation. *Water Res* **2014**, *62*, 260-70.
48. Tang, L.; Livi, K. J. T.; Chen, K. L., Polysulfone Membranes Modified with Bioinspired Polydopamine and Silver Nanoparticles Formed in Situ To Mitigate Biofouling. *Environmental Science & Technology Letters* **2015**, *2*, (3), 59-65.

49. Tang, L.; Huynh, K. A.; Fleming, M. L.; Larronde-Larretche, M.; Chen, K. L., Imparting antimicrobial and anti-adhesive properties to polysulfone membranes through modification with silver nanoparticles and polyelectrolyte multilayers. *J Colloid Interface Sci* **2015**, *451*, 125-33.
50. K. S. Novoselov, A. K. G., S. V. Morozov, D. Jiang, Y. Zhang, S. V. Dubonos, I. V. Grigorieva, A. A. Firsov, Electric Field Effect in Atomically Thin Carbon Films. *Science* **2004**, *306 C*, 666-669.
51. Dresselhaus, M. S.; Araujo, P. T., Perspectives on the 2010 Nobel Prize in Physics for Graphene. *ACS Nano* **2010**, *4*, (11), 6297-6302.
52. Wee, A. T., Graphene: the game changer? *ACS Nano* **2012**, *6*, (7), 5739-41.
53. Compton, O. C.; Nguyen, S. T., Graphene oxide, highly reduced graphene oxide, and graphene: versatile building blocks for carbon-based materials. *Small* **2010**, *6*, (6), 711-23.
54. Sreepasad, T. S.; Berry, V., How do the electrical properties of graphene change with its functionalization? *Small* **2013**, *9*, (3), 341-50.
55. Changgu Lee, X. W., Jeffrey W. Kysar, James Hone, Measurement of the Elastic Properties and Intrinsic Strength of Monolayer Graphene. *Science* **2008**, *321*, 385-388.
56. Huang, X.; Qi, X.; Boey, F.; Zhang, H., Graphene-based composites. *Chem Soc Rev* **2012**, *41*, (2), 666-86.
57. Hummers, W. S.; Offeman, R. E., Preparation of Graphitic Oxide. *Journal of the American Chemical Society* **1958**, *80*, (6), 1339-1339.
58. Sanchez, V. C.; Jachak, A.; Hurt, R. H.; Kane, A. B., Biological interactions of graphene-family nanomaterials: an interdisciplinary review. *Chem Res Toxicol* **2012**, *25*, (1), 15-34.
59. Yang, K.; Li, Y.; Tan, X.; Peng, R.; Liu, Z., Behavior and toxicity of graphene and its functionalized derivatives in biological systems. *Small* **2013**, *9*, (9-10), 1492-503.
60. Jastrzebska, A. M.; Kurtycz, P.; Olszyna, A. R., Recent advances in graphene family materials toxicity investigations. *J Nanopart Res* **2012**, *14*, (12), 1320.
61. Zhou, X.; Huang, X.; Qi, X.; Wu, S.; Xue, C.; Boey, F. Y. C.; Yan, Q.; Chen, P.; Zhang, H., In Situ Synthesis of Metal Nanoparticles on Single-Layer Graphene Oxide and Reduced Graphene Oxide Surfaces. *The Journal of Physical Chemistry C* **2009**, *113*, (25), 10842-10846.
62. Muszynski, R.; Seger, B.; Kamat, P. V., Decorating Graphene Sheets with Gold Nanoparticles. *The Journal of Physical Chemistry C* **2008**, *112*, (14), 5263-5266.
63. Zhu, Z.; Su, M.; Ma, L.; Ma, L.; Liu, D.; Wang, Z., Preparation of graphene oxide-silver nanoparticle nanohybrids with highly antibacterial capability. *Talanta* **2013**, *117*, 449-55.
64. Li, J.; Kuang, D.; Feng, Y.; Zhang, F.; Xu, Z.; Liu, M.; Wang, D., Green synthesis of silver nanoparticles-graphene oxide nanocomposite and its application in electrochemical sensing of tryptophan. *Biosens Bioelectron* **2013**, *42*, 198-206.
65. Vijay Kumar, S.; Huang, N. M.; Lim, H. N.; Marlinda, A. R.; Harrison, I.; Chia, C. H., One-step size-controlled synthesis of functional graphene oxide/silver nanocomposites at room temperature. *Chemical Engineering Journal* **2013**, *219*, 217-224.
66. Li, C.; Wang, X.; Chen, F.; Zhang, C.; Zhi, X.; Wang, K.; Cui, D., The antifungal activity of graphene oxide-silver nanocomposites. *Biomaterials* **2013**, *34*, (15), 3882-90.
67. Hassan, H. M. A.; Abdelsayed, V.; Khder, A. E. R. S.; AbouZeid, K. M.; Ternner, J.; El-Shall, M. S.; Al-Resayes, S. I.; El-Azhary, A. A., Microwave synthesis of graphene sheets supporting metal nanocrystals in aqueous and organic media. *Journal of Materials Chemistry* **2009**, *19*, (23), 3832.

68. Liu, J.; Fu, S.; Yuan, B.; Li, Y.; Deng, Z., Toward a universal "adhesive nanosheet" for the assembly of multiple nanoparticles based on a protein-induced reduction/decoration of graphene oxide. *J Am Chem Soc* **2010**, *132*, (21), 7279-81.
69. Du, J.; Lai, X.; Yang, N.; Zhai, J.; Kisailus, D.; Su, F.; Wang, D.; Jiang, L., Hierarchically ordered macro-mesoporous TiO<sub>2</sub>-graphene composite films: improved mass transfer, reduced charge recombination, and their enhanced photocatalytic activities. *ACS Nano* **2011**, *5*, (1), 590-6.
70. Hwang, J. O.; Lee, D. H.; Kim, J. Y.; Han, T. H.; Kim, B. H.; Park, M.; No, K.; Kim, S. O., Vertical ZnO nanowires/graphene hybrids for transparent and flexible field emission. *J. Mater. Chem.* **2011**, *21*, (10), 3432-3437.
71. Perreault, F.; Fonseca de Faria, A.; Elimelech, M., Environmental applications of graphene-based nanomaterials. *Chem Soc Rev* **2015**.
72. Guo, F.; Silverberg, G.; Bowers, S.; Kim, S. P.; Datta, D.; Shenoy, V.; Hurt, R. H., Graphene-based environmental barriers. *Environ Sci Technol* **2012**, *46*, (14), 7717-24.
73. Cohen-Tanugi, D.; Grossman, J. C., Water desalination across nanoporous graphene. *Nano Lett* **2012**, *12*, (7), 3602-8.
74. Hu, M.; Mi, B., Enabling graphene oxide nanosheets as water separation membranes. *Environ Sci Technol* **2013**, *47*, (8), 3715-23.
75. Lee, J.; Chae, H.-R.; Won, Y. J.; Lee, K.; Lee, C.-H.; Lee, H. H.; Kim, I.-C.; Lee, J.-m., Graphene oxide nanoplatelets composite membrane with hydrophilic and antifouling properties for wastewater treatment. *Journal of Membrane Science* **2013**, *448*, 223-230.
76. Ionita, M.; Pandeale, A. M.; Crica, L.; Pilan, L., Improving the thermal and mechanical properties of polysulfone by incorporation of graphene oxide. *Composites Part B: Engineering* **2014**, *59*, 133-139.
77. Choi, W.; Choi, J.; Bang, J.; Lee, J. H., Layer-by-layer assembly of graphene oxide nanosheets on polyamide membranes for durable reverse-osmosis applications. *ACS Appl Mater Interfaces* **2013**, *5*, (23), 12510-9.
78. Perreault, F.; Tousley, M. E.; Elimelech, M., Thin-Film Composite Polyamide Membranes Functionalized with Biocidal Graphene Oxide Nanosheets. *Environmental Science & Technology Letters* **2014**, *1*, (1), 71-76.
79. Goh, K.; Setiawan, L.; Wei, L.; Si, R.; Fane, A. G.; Wang, R.; Chen, Y., Graphene oxide as effective selective barriers on a hollow fiber membrane for water treatment process. *Journal of Membrane Science* **2015**, *474*, 244-253.
80. Hu, M.; Mi, B., Layer-by-layer assembly of graphene oxide membranes via electrostatic interaction. *Journal of Membrane Science* **2014**, *469*, 80-87.
81. Huang, L.; Zhang, M.; Li, C.; Shi, G., Graphene-Based Membranes for Molecular Separation. *J Phys Chem Lett* **2015**, *6*, (14), 2806-15.
82. McGinnis, R. L.; Elimelech, M., Energy requirements of ammonia-carbon dioxide forward osmosis desalination. *Desalination* **2007**, *207*, (1-3), 370-382.
83. Matin, A.; Khan, Z.; Zaidi, S. M. J.; Boyce, M. C., Biofouling in reverse osmosis membranes for seawater desalination: Phenomena and prevention. *Desalination* **2011**, *281*, 1-16.
84. Siddiqui, M. F.; Rzechowicz, M.; Oh, H.-S.; Saeidi, N.; Hui, L. J.; Winters, H.; Fane, A. G.; Chong, T. H., The efficacy of tannic acid in controlling biofouling by *Pseudomonas aeruginosa* is dependent on nutrient conditions and bacterial density. *International Biodeterioration & Biodegradation* **2015**, *104*, 74-82.

85. Cristiani, P.; Perboni, G., Antifouling strategies and corrosion control in cooling circuits. *Bioelectrochemistry* **2014**, *97*, 120-6.
86. D. Rana, T. M., Surface Modifications for Antifouling Membranes. *Chem. Rev* **2010**, *110*, 2448-2471.
87. Kang, G. D.; Cao, Y. M., Development of antifouling reverse osmosis membranes for water treatment: A review. *Water Res* **2012**, *46*, (3), 584-600.
88. Lu, X.; Romero-Vargas Castrillon, S.; Shaffer, D. L.; Ma, J.; Elimelech, M., In situ surface chemical modification of thin-film composite forward osmosis membranes for enhanced organic fouling resistance. *Environ Sci Technol* **2013**, *47*, (21), 12219-28.
89. Asatekin, A.; Olivetti, E. A.; Mayes, A. M., Fouling resistant, high flux nanofiltration membranes from polyacrylonitrile-graft-poly(ethylene oxide). *Journal of Membrane Science* **2009**, *332*, (1-2), 6-12.
90. Atar Adout , S. K., Ayse Asatekin, Anne M. Mayes and Menachem Elimelech Ultrafiltration Membranes Incorporating Amphiphilic Comb Copolymer Additives Prevent Irreversible Adhesion of Bacteria. *environmental Science & Technology* **2010**, *44*, (7), 2406–2411.
91. Nguyen, A.; Zou, L.; Priest, C., Evaluating the antifouling effects of silver nanoparticles regenerated by TiO<sub>2</sub> on forward osmosis membrane. *Journal of Membrane Science* **2014**, *454*, 264-271.
92. Gao, Y.; Hu, M.; Mi, B., Membrane surface modification with TiO<sub>2</sub>-graphene oxide for enhanced photocatalytic performance. *Journal of Membrane Science* **2014**, *455*, 349-356.
93. Vecitis, C. D.; Schnoor, M. H.; Rahman, M. S.; Schiffman, J. D.; Elimelech, M., Electrochemical multiwalled carbon nanotube filter for viral and bacterial removal and inactivation. *Environ Sci Technol* **2011**, *45*, (8), 3672-9.
94. P. Cristiani a, G. P. b., Antifouling strategies and corrosion control in cooling circuits. *Bioelectrochemistry* **2014**, *97*, 120-126.
95. Zhu, Y.; Murali, S.; Cai, W.; Li, X.; Suk, J. W.; Potts, J. R.; Ruoff, R. S., Graphene and graphene oxide: synthesis, properties, and applications. *Adv Mater* **2010**, *22*, (35), 3906-24.
96. Mi, B., Materials science. Graphene oxide membranes for ionic and molecular sieving. *Science* **2014**, *343*, (6172), 740-2.
97. Joshi, R. K.; Carbone, P.; Wang, F. C.; Kravets, V. G.; Su, Y.; Grigorieva, I. V.; Wu, H. A.; Geim, A. K.; Nair, R. R., Precise and ultrafast molecular sieving through graphene oxide membranes. *Science* **2014**, *343*, (6172), 752-4.
98. Celebi, K.; Buchheim, J.; Wyss, R. M.; Droudian, A.; Gasser, P.; Shorubalko, I.; Kye, J. I.; Lee, C.; Park, H. G., Ultimate permeation across atomically thin porous graphene. *Science* **2014**, *344*, (6181), 289-92.
99. Das, M. R.; Sarma, R. K.; Saikia, R.; Kale, V. S.; Shelke, M. V.; Sengupta, P., Synthesis of silver nanoparticles in an aqueous suspension of graphene oxide sheets and its antimicrobial activity. *Colloids Surf B Biointerfaces* **2011**, *83*, (1), 16-22.
100. de Faria, A. F.; Martinez, D. S.; Meira, S. M.; de Moraes, A. C.; Brandelli, A.; Filho, A. G.; Alves, O. L., Anti-adhesion and antibacterial activity of silver nanoparticles supported on graphene oxide sheets. *Colloids Surf B Biointerfaces* **2014**, *113*, 115-24.
101. Ocoy, I.; Paret, M. L.; Ocoy, M. A.; Kunwar, S.; Chen, T.; You, M.; Tan, W., Nanotechnology in Plant Disease Management: DNA-Directed Silver Nanoparticles on Graphene Oxide as an Antibacterial against *Xanthomonas perforans*. *ACS Nano* **2013**, *7*, (10), 8972-8980.

102. Thierry Cassagneau, J. H. F., Preparation and Layer-by-Layer Self-Assembly of Silver Nanoparticles Capped by Graphite Oxide Nanosheets. *J. Phys. Chem. B* **1999**, *103*, 1789-1793.
103. W.S. Hummers, R. E. O., Preparation of Graphitic Oxid. *J. Am. Chem. Soc.* **1958**, *80*, 1339.
104. Cath, T. Y.; Elimelech, M.; McCutcheon, J. R.; McGinnis, R. L.; Achilli, A.; Anastasio, D.; Brady, A. R.; Childress, A. E.; Farr, I. V.; Hancock, N. T.; Lampi, J.; Nghiem, L. D.; Xie, M.; Yip, N. Y., Standard Methodology for Evaluating Membrane Performance in Osmotically Driven Membrane Processes. *Desalination* **2013**, *312*, 31-38.
105. Wenzel, R. N., SURFACE ROUGHNESS AND CONTACT ANGLE. *J. Phys. Chem* **1949**, *53*, 1466-1467.
106. Hurwitz, G.; Guillen, G. R.; Hoek, E. M. V., Probing polyamide membrane surface charge, zeta potential, wettability, and hydrophilicity with contact angle measurements. *Journal of Membrane Science* **2010**, *349*, (1-2), 349-357.
107. Sharon L. Walker, S. B., Eric M. V. Hoek, and; Elimelech, M., A Novel Asymmetric Clamping Cell for Measuring Streaming Potential of Flat Surfaces. *Langmuir* **2002**, *18*, 2193-2198.
108. Lee, J. U.; Lee, W.; Yoon, S. S.; Kim, J.; Byun, J. H., Site-selective immobilization of gold nanoparticles on graphene sheets and its electrochemical properties. *Applied Surface Science* **2014**, *315*, 73-80.
109. Tian, J.; Liu, S.; Zhang, Y.; Li, H.; Wang, L.; Luo, Y.; Asiri, A. M.; Al-Youbi, A. O.; Sun, X., Environmentally friendly, one-pot synthesis of Ag nanoparticle-decorated reduced graphene oxide composites and their application to photocurrent generation. *Inorganic chemistry* **2012**, *51*, (8), 4742-6.
110. Eric M. Vrijenhoek, S. H., Menachem Elimelech, Influence of membrane surface properties on initial rate of colloidal fouling of reverse osmosis and nanofiltration membranes. *journal of Membrane Science* **2001**, *185*, 115-128.
111. Xu, W.-P.; Zhang, L.-C.; Li, J.-P.; Lu, Y.; Li, H.-H.; Ma, Y.-N.; Wang, W.-D.; Yu, S.-H., Facile synthesis of silver@graphene oxide nanocomposites and their enhanced antibacterial properties. *Journal of Materials Chemistry* **2011**, *21*, (12), 4593.
112. Li, Y.; Yuan, H.; von dem Bussche, A.; Creighton, M.; Hurt, R. H.; Kane, A. B.; Gao, H., Graphene microsheets enter cells through spontaneous membrane penetration at edge asperities and corner sites. *Proc Natl Acad Sci U S A* **2013**, *110*, (30), 12295-300.
113. Li, W. R.; Xie, X. B.; Shi, Q. S.; Zeng, H. Y.; Ou-Yang, Y. S.; Chen, Y. B., Antibacterial activity and mechanism of silver nanoparticles on Escherichia coli. *Appl Microbiol Biotechnol* **2010**, *85*, (4), 1115-22.
114. Ismail Ocsoy, M. L. P., Muserref Arslan Ocsoy, Sanju Kunwar, Tao Chen, Weihong Tan, Mingxu You,, Nanotechnology in Plant Disease Management: DNA-Directed Silver Nanoparticles on Graphene Oxide as an Antibacterial against Xanthomonas perforans. *ACS Nano* **2013**, *7*, (10), 8972-8990.
115. Romero-Vargas Castrillón, S.; Perreault, F.; de Faria, A. F.; Elimelech, M., Interaction of Graphene Oxide with Bacterial Cell Membranes: Insights from Force Spectroscopy. *Environmental Science & Technology Letters* **2015**, *2*, (4), 112-117.
116. MARK R. WIESNER, S. C., The promise of membrane technology. *Environ Sci Technol* **1999**, *33*, (17), 360A-366A.
117. Pendergast, M. M.; Hoek, E. M. V., A review of water treatment membrane nanotechnologies. *Energy & Environmental Science* **2011**, *4*, (6), 1946.

118. Ben-Sasson, M.; Zodrow, K. R.; Genggeng, Q.; Kang, Y.; Giannelis, E. P.; Elimelech, M., Surface functionalization of thin-film composite membranes with copper nanoparticles for antimicrobial surface properties. *Environ Sci Technol* **2014**, *48*, (1), 384-93.
119. Zhou, Z.; Calabrese, D. R.; Taylor, W.; Finlay, J. A.; Callow, M. E.; Callow, J. A.; Fischer, D.; Kramer, E. J.; Ober, C. K., Amphiphilic triblock copolymers with PEGylated hydrocarbon structures as environmentally friendly marine antifouling and fouling-release coatings. *Biofouling* **2014**, *30*, (5), 589-604.
120. Thanh, N. T.; Maclean, N.; Mahiddine, S., Mechanisms of nucleation and growth of nanoparticles in solution. *Chem Rev* **2014**, *114*, (15), 7610-30.
121. Liao, H. G.; Niu, K.; Zheng, H., Observation of growth of metal nanoparticles. *Chem Commun (Camb)* **2013**, *49*, (100), 11720-7.
122. Daer, S.; Kharraz, J.; Giwa, A.; Hasan, S. W., Recent applications of nanomaterials in water desalination: A critical review and future opportunities. *Desalination* **2015**, *367*, 37-48.
123. Chao Xu, X. W., and Junwu Zhu, Graphene-Metal Particle Nanocomposites. *J. Phys. Chem. C* **2008**, *112*, 19841–19845
124. Dreyer, D. R.; Park, S.; Bielawski, C. W.; Ruoff, R. S., The chemistry of graphene oxide. *Chem Soc Rev* **2010**, *39*, (1), 228-40.
125. Shaobin Liu, J. K., Tingying Helen Zeng, Chen Mario Hofmann, Ehdi Burcombe, Jun Wei, Rongrong Jiang, and Yuan, Antibacterial Activity of Graphite, Graphite Oxide, Graphene Oxide, and Reduced Graphene Oxide: Membrane and Oxidative Stress. *ASC NANO* **2011**, *5*, (9), 6971–6980.
126. Chen, J.; Peng, H.; Wang, X.; Shao, F.; Yuan, Z.; Han, H., Graphene oxide exhibits broad-spectrum antimicrobial activity against bacterial phytopathogens and fungal conidia by intertwining and membrane perturbation. *Nanoscale* **2014**, *6*, (3), 1879-89.
127. Mejias Carpio, I. E.; Santos, C. M.; Wei, X.; Rodrigues, D. F., Toxicity of a polymer-graphene oxide composite against bacterial planktonic cells, biofilms, and mammalian cells. *Nanoscale* **2012**, *4*, (15), 4746-56.
128. Zhang, D.; Liu, X.; Wang, X., Green synthesis of graphene oxide sheets decorated by silver nanoprisms and their anti-bacterial properties. *J Inorg Biochem* **2011**, *105*, (9), 1181-6.
129. de Faria, A. F.; Perreault, F.; Shaulsky, E.; Arias Chavez, L. H.; Elimelech, M., Antimicrobial Electrospun Biopolymer Nanofiber Mats Functionalized with Graphene Oxide-Silver Nanocomposites. *ACS Appl Mater Interfaces* **2015**, *7*, (23), 12751-9.
130. Soroush, A.; Ma, W.; Silvino, Y.; Rahaman, M. S., Surface modification of thin film composite forward osmosis membrane by silver-decorated graphene-oxide nanosheets. *Environ. Sci.: Nano* **2015**, *2*, (4), 395-405.
131. Eric M. Vrijen Hoek, S. H., Menachem Elimelech, Influence of membrane surface properties on initial rate of colloidal fouling of reverse osmosis and nanofiltration membranes. *Journal of Membrane Science* **2001**, *185*, 115-128.
132. Oss, C. J. v., *The Properties of Water and their Role in Colloidal and Biological Systems*. Academic Press: Amsterdam, 2008; Vol. vol. 16.
133. van Oss, C. J., Development and applications of the interfacial tension between water and organic or biological surfaces. *Colloids Surf B Biointerfaces* **2007**, *54*, (1), 2-9.
134. Franc-ois Perreault, A. F. d. F., Siamak Nejati, Menachem Elimelech, Antimicrobial Properties of Graphene Oxide Nanosheets: Why Size Matters. *ACS Nano* **2015**.

135. Agnihotri, S.; Mukherji, S.; Mukherji, S., Size-controlled silver nanoparticles synthesized over the range 5–100 nm using the same protocol and their antibacterial efficacy. *RSC Adv.* **2014**, *4*, (8), 3974-3983.